Evaluation and development of methods for measurement of penetration of filtering facepiece respirators

A THESIS
SUBMITTED TO THE FACULTY OF THE
UNIVERSITY OF MINNESOTA
BY

Swathi Satish

IN PARTIAL FULFILLMENT OF THE REQUIREMENTS
FOR THE DEGREE OF
MASTER OF SCIENCE

David. Y. Pui
David B. Kittelson

July 2015

ACKNOWLEDGEMENTS

The satisfaction and joy that accompany the successful completion of a project would be incomplete without the mention of the people who made it possible. I would like to express my gratitude to all the people who supported me during the course of this project.

First I thank my advisors, Professor David Pui and Professor David Kittelson for giving me the opportunity to work on this project and for advising me throughout the course the project. It has been a wonderful experience for me and have definitely learned a lot in last two years. I would like to thank Professor Jacob Swanson, who continuously guided me through every step of this project – his immense knowledge and patience helped me grow as a researcher.

I would like to thank 3M Company and the Center for Filtration Research at the University of Minnesota for supporting this project. I would also like to thank Kai Xiao for providing previously unpublished data, which helped to understand certain topics better in this project. I would also like to thank all my co-workers in the lab, who were always there to help me out with my queries.

Lastly I would like to thank for family for always being there for me.

Dedicated to my parents for their unconditional love and support, and my little sister to whom I hope to be a good role model.

ABSTRACT

Elevated concentrations of diesel exhaust have been linked to adverse health effects. Filtering facepiece respirators (FFRs) are widely used as a form of respiratory protection against diesel particulate matter (DPM) in occupational settings. The objective of this study was to evaluate NIOSH-certified R95 and P95 electret respirators challenged with Diesel exhaust and get a better understanding of the factors that influence penetration. Two techniques were employed for the measurement of penetration: (a) particle counting technique using a Scanning Mobility Particle Sizer (SMPS, TSI Inc.) which measures particle size distribution, and (b) Gravimetric analysis using polyfluortetraethylene (PTFE) and polypropylene (PP) filters.

Gravimetric measurements using PP filters were variable compared to SMPS measurements and biased high as a result of the adsorption of gas-phase semi-volatile material. Relatively inert PTFE filters adsorbed less semi-volatile material resulting in more accurate measurements. To attempt to correct for these artifacts associated with adsorption of semi-volatile material, primary and secondary filters were used in series upstream and downstream of the FFR. Correcting for adsorption by subtracting the secondary mass from the primary mass improved the result for both PTFE and PP filters but this correction is subject to "equilibrium" conditions that depend on sampling time and the concentration of particles and semi-volatile material. Overall, the results demonstrate that great care must be taken when using filters to determine filtration efficiency of FFRs challenged with diesel exhaust. Pure PTFE or other filters that minimize adsorption of semi-volatile artifacts and two filters should be used in tandem to allow correction for adsorbed artifacts.

Analysis of SMPS measurements indicated that the respirators behave differently for Diesel exhaust generated at light and heavy load on engine. At light load, the penetration of the R-95 and P-95 respirators showed a steep increase with time, exceeding the maximum allowed penetration of 5% after about 40 minutes. Whereas at heavy load, the respirators were found to have a relatively unchanging penetration (less than 5%) throughout the 90-minute test duration. This difference was attributed to the presence of a high concentration of organic carbon (OC) in Diesel exhaust which has a tendency to degrade the electric charges on the respirators, thus reducing the filtration enhancement from electrostatic attraction forces.

To account for the complex nature of DPM and its varying properties with changes in operating and sampling condition, an oxidation-dilution tunnel was designed to produce Diesel exhaust with a controlled set of properties: elemental carbon (EC) concentration, OC concentration, EC/OC ratio and volume flow rate. This device was used to evaluate R-95 and P-95 respirators for solid Diesel exhaust aerosol. The methodology proved to be effective in controlling the EC concentration and total volume flow rate. Results showed that the R-95 and P-95 respirators were more than 95% efficient for solid Diesel exhaust aerosol.

This thesis is divided into two parts. The first focuses on the measurement of penetration of FFRs for Diesel exhaust, the second on the development of a standard DPM generator for testing filtration systems.

TABLE OF CONTENTS

LIST OF TABLES

LIST OF FIGURES

LIST OF ABBREVIATIONS

CPC – Condensation particle counter

D_f – Fractal dimension

DMA – Differential mobility analyzer

DOC – Diesel oxidation catalyst

DOP – Dioctyl phthalate

DPM – Diesel particulate matter

EC – Elemental carbon

FFR – Filtering facepiece respirator

MPPS – Most penetrating particle size

NaCl – Sodium chloride

NIOSH – National Institute for Occupational Safety and Health

OC – Organic carbon

PM – Particulate matter

PP – Polypropylene

PTFE – Polytetrafluoroethylene

SMPS – Scanning mobility particle sizer

Part I

Evaluation of filtering facepiece respirators challenged with Diesel engine exhaust

Chapter 1
INTRODUCTION

1.1 Effects of exposure to Diesel exhaust

Diesel engines have been widely used for decades in various industrial sectors such as underground mining, construction, public transportation, ship loading in docks, agriculture, operation of machines and fire-fighting. In 2010, half of all newly registered cars were equipped with diesel engines (ACEA, 2010). Even though recent advances in diesel engine technology and in reformulation of diesel fuels have reduced the amount of diesel emissions, there are still a large number of automobiles with no or poor after-treatment systems. While most new cars in Europe have special filtration systems to reduce the number of particles emitted from diesel engines, a significant number of older cars do not have any sort of filtration system at all. This is also true for off-road applications of diesel engines for which after-treatment systems are not as advanced as for on-road applications. Even though the total number of off-road diesel engines is only a fraction of the number of on-road engines in most countries, the off-road sector contributes as much PM as the on-road sector, because off-road emission regulation has lagged behind on-road (Niemi et al., 2012). Emissions from diesel engines have been of great concern globally because of adverse effects on human health (Nel, 2005; Oberdorster, 2001; USEPA, 2002) and the environment (Hansen et al., 2000; Jacobson, 2001). Several studies have reported public health related problems such as airway inflammation and cellular inflammation on exposure to diesel exhaust fumes (Castranova et al., 2001; Garshick et al., 2004; Ohtoshi et al., 1998; Patel et al., 2011). International Agency for Research on Cancer classified (12 June 2012) diesel fumes as carcinogens to humans (Group 1). Exposure to diesel exhaust may also cause cardiovascular problems, asthma and hazardous allergies (Fujieda et al., 1998; Norris et al., 1999; Salvi and Frew, 1998). Boffetta et al. (1990) reported in an earlier study that railroad workers, heavy equipment operators, miners and truck drivers have higher mortality both for all causes and for lung cancer when compared with workers without exposure to diesel exhaust.

1.2 Particle size distribution and filter penetration

(a) Particle size distribution

Particle size distribution is an index that quantifies the amount of particles present for different sizes of particles in a sample. Typically, the amount of particles are quantified based on number, surface area, volume or mass. In this study, we will only deal with number-based and mass-based particle size distributions.

(b) Penetration and filtration efficiency

Penetration (P) of a filter is defined as the fraction of incident particles that exit or penetrate the filter. It is typically expressed as a percentage. Filtration efficiency is the fraction of incident particles that is captured by the filter.

$$\mathrm{P}\ (\%) = \frac{\text{number or mass of particles downstream of filter}}{\text{number or mass of particles upstream of filter}} * 100 \quad \text{(1-a)}$$

$$\mathrm{FE}\ (\%) = 100 - \mathrm{P} \quad \text{(1-b)}$$

1.3 Composition, morphology and size distribution of Diesel exhaust

Diesel exhaust is a complex mixture of constituents in either a gas or particle form. Gaseous components of Diesel exhaust include hydrocarbons (HCs), oxides of nitrogen (NO_x), oxides of carbon (carbon monoxide (CO) and carbon dioxide (CO_2)), water vapor, oxygen and other sulfur and nitrogen compounds. Hydrocarbons vary in volatility and are found in both gaseous and particle phase. The particles present in Diesel exhaust or Diesel particulate matter (DPM) vary in size, shape and composition depending on engine type, speed, load, air/fuel ratio, temperature, fuel and many other factors. DPM is defined by EPA regulations and sampling procedures as all compounds collected on a pre-conditioned filter in diluted diesel exhaust gases at a maximum temperature of 47±5 ºC. Diesel exhaust particles typically comprise of agglomerated solid carbonaceous material and ash, and volatile organic and sulfur compounds. The size of primary particles in these agglomerates range from 10 nm to 80 nm. Figure 1.1 illustrates the morphology of DPM.

DPM consists of particles that can mainly be classified into elemental carbon (EC), organic carbon (OC), sulfur compounds and ash. EC is typically solid, non-volatile residual carbon that is formed from combustion in localized rich regions of the cylinder. OC consists of semi-volatile adsorbed or condensed hydrocarbons, i.e. carbonaceous matter resulting from incomplete combustion of fuel and lube oil in the cylinder. OC is also referred to as soluble organic fraction (SOF) and contains polycyclic aromatic compounds containing oxygen, nitrogen, and sulfur (Kittelson,1998; Farrar-Khan et al., 1992). The relative magnitudes of total elemental carbonaceous material and organic carbon are characterized by the EC/OC ratio. Since hydrocarbons formed from incomplete combustion have a wide range of volatilities, they are found in both, gaseous and particulate phases. In addition to EC and OC, Diesel exhaust also includes a minor fraction of non-volatile, non-carbonaceous, inorganic components referred to as metal PM or ash PM. Ash PM is of sub-micrometer size and is thus inhalable. Ash consists primarily of species formed chemically from combustion of lubricating oil metal additives including metal oxides, sulfate, and phosphate compounds of mainly Ca, Mg, and Zn (Bardasz et al., 2005; Sappok and Wong, 2007; Vaaraslahti et al., 2005).

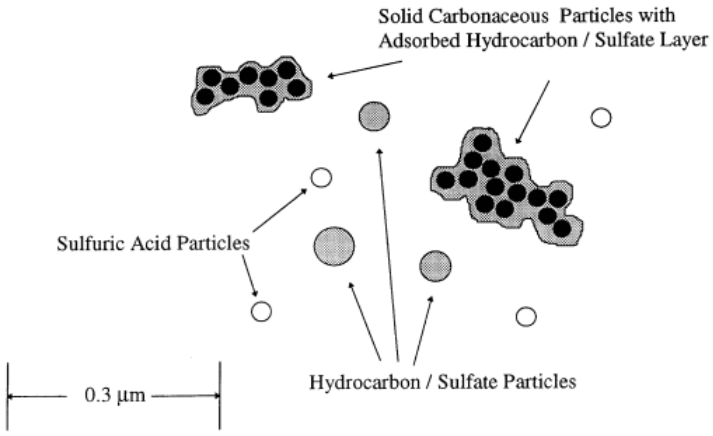

Figure 1.1 Composition of Diesel particulate matter (DPM)

The size distribution of diesel exhaust generally displays three modes, namely, course mode, accumulation mode and nucleation mode (Kittelson, 1998). A lognormal curve is used to fit the size distribution of Diesel exhaust particles. Figure 1.2 shows the typical number-based and mass-

based size distributions for Diesel exhaust. The course mode consists of particles approximately larger than 500 nm and contains 5 – 20% of the particulate mass. These particle are mostly accumulation mode particles that were previously deposited on the cylinder walls or exhaust system surfaces. Accumulation mode particles consist of solid carbonaceous agglomerates with adsorbed and condensed semi-volatile species. The accumulation mode in diesel exhaust is not sensitive to dilution conditions (Kittelson et al., 2002; Maricq et al., 2002) and consists of particles with diameter ranging from 50 to 500 nm. This mode holds a majority of particle mass in Diesel exhaust. Particles in the nucleation mode have diameter ranging from 5 to 50 nm. Solid nucleation mode particles consist primarily of carbonaceous particles, metallic compounds while semi-volatile nucleation mode particles consist of water, semi-volatile organic and sulfur compounds. Nucleation mode particles form during dilution and cooling of exhaust gas (Kittelson, 1998; Tanaka and Shimizu, 1999). Thus the formation is sensitive to dilution parameters such as dilution ratio, temperature and relative humidity of the dilution air, and the exact development of temperature and instantaneous partial pressures of vapors during dilution. Within the tailpipe, a majority of the volatile material present in Diesel exhaust are in the gas phase because of high temperatures. As the exhaust enters the atmosphere, it is diluted and cooled, and processes such as nucleation, condensation and adsorption transform volatile material to solid and liquid particulate matter (Kittelson, 1998). The amount of material that adsorb or condense onto existing particles, or nucleate to form new particles is highly dependent on the dilution conditions (Abdul-Khalek et al., 1999). The tendency of nucleation has been connected with high sulfur or high hydrocarbon content in exhaust gas (Vaaraslahti et al., 2004). Therefore, the formation of nucleation mode particles also depends indirectly on engine parameters, fuel and lubricant oil properties, and after-treatment systems.

Examination of the influence of engine load on size distribution of DPM indicates that at light load, the engine exhaust is mostly composed of nucleation mode particles and there is a high concentration of semi-volatile material (unburned hydrocarbon, etc.) in the vapor-phase (Abdul-Khalek et al., 2000). At medium/heavy load, the cylinder and exhaust temperatures are much higher, thus most of the volatile materials are burned. Therefore, the soot concentration is higher and most of the exhaust particles belong to the accumulation mode, while the vapor-phase concentration of semi-volatile material is much lower. Previous research using a John Deere engine (Kittelson et al. 2010) determined that the light load condition contained a bimodal distribution

consisting of an easily identifiable nucleation mode and an accumulation mode, while the medium load condition had a unimodal (the accumulation mode) size distribution consisting of 80% EC and 20% OC. Typically, EC/OC ratio is a function of load on the engine and is higher for heavier loads.

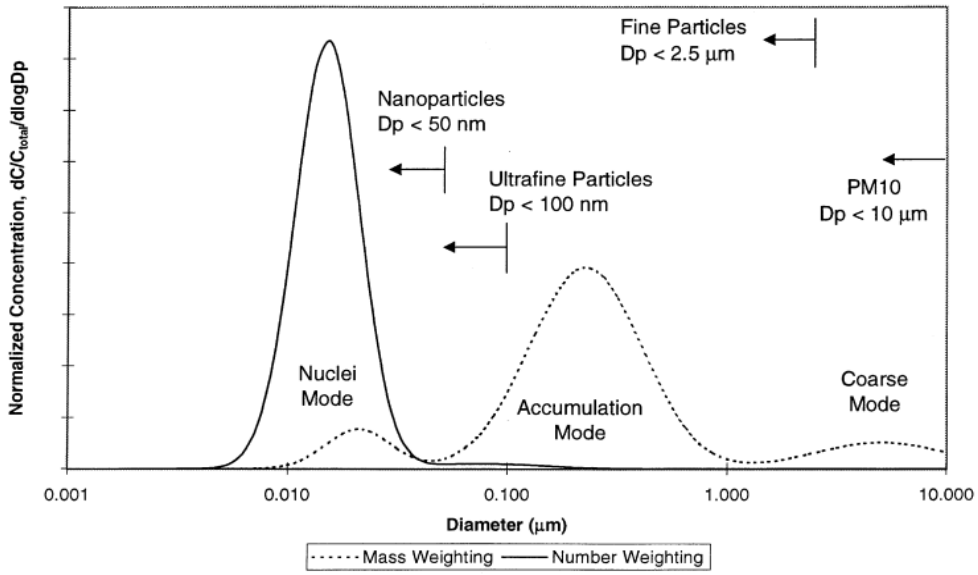

Figure 1.2 Typical Diesel exhaust size distribution

1.4 Respiratory protection against Diesel exhaust

To reduce the inhalation of particles, respiratory protection is required in occupational settings where engineering and administrative controls are not feasible or not yet implemented. Particulate half-masks, also referred to as filtering facepiece respirators (FFRs) are the most widespread form of respiratory protection due to their versatility, price, convenience of use, and lightness (Huang et al., 2007). Standards for testing and certifying respirators are different in Europe and in the USA (Rengasamy et al., 2009). Currently in the USA, the National Institute for Occupational Safety and Health (NIOSH) certifies respirators in accordance with Title 42 of the U.S. Code of Federal Regulations, section 84 (42 CFR 84). Certification ensures that respirators meet the prescribed performance criteria so as to ensure a minimum level of user protection. Certification also results in an explicit categorization of respirator types and classes that aid users in selecting a level of protection appropriate for a specific hazard. Respirator filtration efficiency is tested and certified for 95%, 99%, or 99.97% removal of the challenged particles. These respirators are labeled as 95,

99, or 100 class efficiency respectively. Respirators are further classified as N, R, or P based on the type of aerosol used for testing. N-type filters are intended to protect workers from solid particulate matter and are tested against a polydisperse sodium chloride (NaCl) aerosol with a count median diameter (CMD) of 75 nm ± 20 nm. R and P-type filters demonstrate resistance to oil particles in addition to solid particles and are tested against a polydisperse distribution of dioctylphthalate (DOP) particles with a CMD of 185 nm ± 20 nm. The certification tests are conducted at a flow rate of 85 L/min. The European Norm (EN 149:2004) classifies filtering facepiece respirators as FFP1, FFP2, and FFP3 with minimum filtration efficiencies of 80%, 94% and 99% respectively. The certification test flow rate is set at 30 or 95 L/min, and products are tested separately with both NaCl and paraffin oil aerosols. Moyer and Bergman (2000) reported that the initial penetration levels of NaCl for three models of N-95 FFRs were less than 5%. R and P-type respirators show similar high performance (Martin and Moyer, 2000; Richardson et al., 2006; Eninger et al., 2008a; Rengasamy et al., 2008b).

Respirators that were tested in this study consisted of electret filter material, which includes a permanent electric charge of the filter fibers. Polarized fibers create internal electric fields which significantly increase filtration efficiency due to increased deposition of particles on charged filter fibers (Janssen et al., 2003). Stability of the electrical charge is important because filters can lose their efficiency when loaded with some aerosols such as DOP (Barrett and Rousseau, 1998; Tennal et al., 1991). Certain use patterns or aerosol exposure can increase filter penetration of electrostatic filter media (Tennal et al., 1991; Baumgartner and Loffler, 1986; Kanaoka et al., 1984; Blackford et al., 1986; Fissan et al., 1984). Barrett and Rousseau (1998) demonstrated that the magnitude of the electrostatic charge has a significant effect on the filtration efficiency of the filters. For measurements with a DOP aerosol, a high level of electrostatic charge leads to improved initial efficiency but a more rapid increase in penetration with increased aerosol loading. They hypothesized that this behavior can be due to the spreading of oily liquid aerosol droplets over filter fibers, reducing the filtration enhancement from electrostatic charge on the filter fibers.

Few evaluations of electret media (Barrett and Rousseau, 1998) have used diesel exhaust as the challenge aerosol. Berardinelli et al. (2001) reported the changes in laboratory penetration before and after DPM exposure and found that diesel exhaust degrades the laboratory performance of electret filters. They also found that NIOSH R- and P-series filters performed well at DPM loading up to 50 mg. Janssen and Bidwell (2006) found that the penetration of some of the R-95 filters

exposed for 8 hours (continuously or intermittently) resulted in mean laboratory penetration greater than 5% at DPM loads above 60 mg. Conversely, the P-95 filters were not impacted by loading. Panconek et al. (2012) evaluated the filtration efficiency of FFRs (approved in accordance with the European Norm) during 40-min in-use conditions of exposure to diesel exhaust fumes generated from an idling diesel engine. It was reported that the filtration efficiencies were lower than the minimum standard filtration efficiency required by the European standards, questioning the utility of these respirators as protective devices against diesel particulate matter. The authors used polypropylene (PP) fibrous analytical filters and gravimetric analysis to determine mass penetrations. However, the use of PP filters may not be appropriate for DPM measurements because these filters are known to adsorb low-volatility gases (Wei et al., 2003; Teas et al., 2001) that are ubiquitous in diesel exhaust. Material collected on PP filters may not represent true "particulate matter," rather, an adsorbed artifact that results in an over-estimation of the particulate mass collected by the filter. This effect is observed routinely during DPM and ambient measurements using TX40 and relatively inert PTFE filters (Chase et al., 2004; Swanson and Kittelson, 2009, Swanson et al., 2010, Liu et al., 2012).

1.5 Objectives

This study aims to determine the true efficacy of commercially available NIOSH-certified R- and P-95 respirators for protection against Diesel exhaust. The objectives of this study are:

(a) To evaluate R- and P-95 respirators for standard test aerosols NaCl and DOP, as a precursor to the experiments with DPM.
(b) To measure the penetration of R- and P-95 respirators for DPM continuously during the loading process using a Scanning Mobility Particle Sizer (SMPS) to record particle size and mass distributions. Since a majority of previous literature on filter penetration for DPM provide only the initial and final penetration values of the respirators, this study will give us a better understanding of the loading process.
(c) To compare the results from (a) to gravimetric analysis to determine the limitations of the gravimetric method.
(d) To determine changes in respirator penetration with increasing loading time, or more importantly, with increasing mass loaded on to the respirators.

(e) To evaluate the effect of engine load on the number-based and mass-based penetration of respirators.

(f) To analyze the influence of engine test condition and loading time on particle size-based penetration.

Chapter 2
MATERIALS AND APPARATUS

2.1 Atomizer

TSI Oil Droplet Generator Model 9307 was used as an atomizer in this study to generate sodium chloride (NaCl) and dioctylphthalate (DOP) aerosols. It utilizes the Laskin nozzle principle (see Figure 2.1) to generate droplets. Pressurized air flows down a tube and exits through four radial holes. Just above these holes, there is a ring which is secured with four adjacent holes. This arrangement is immersed in the fluid to be atomized. As the compressed air flows at high velocity out of the radial holes, the liquid is drawn in to the airflow and into the small air bubbles created, which then grow and move to the surface of the liquid where they burst, therefore releasing the generated droplets they contain into the air above the liquid. An internal impactor plate prevents larger droplets from exiting the atomizer, therefore generating particles with a reasonably narrow size distribution.

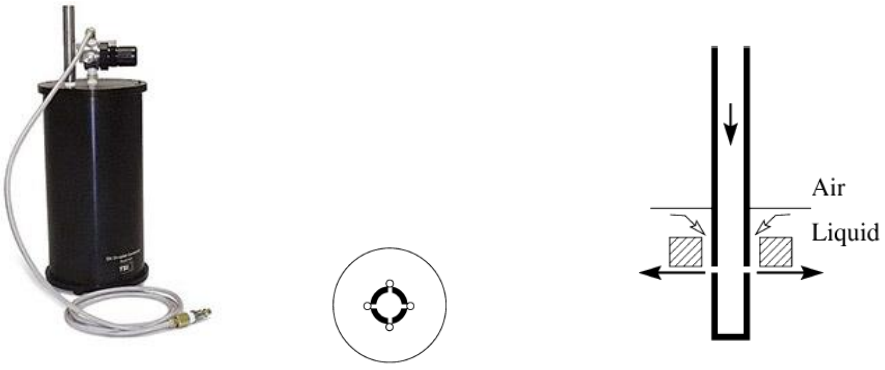

Figure 2.1 TSI Oil Droplet generator and principle of a Laskin nozzle

2.2 Engine

Three different engines were used in this study to generate Diesel exhaust aerosol. B0 or commercial ultra-low sulfur Diesel (ULSD) with zero biodiesel content was used as the fuel for all the engines.

(a) *Engine 1 (small generator engine, high OC emissions)* – A clone of the Yanmar L100V6 model year 2009 engine, All-power APG3201N – a single-cylinder, 0.435 L, 6.5 kW (at 3600 rpm) engine. It is an air-cooled, direct injection, non-CARB compliant diesel engine. Tests were conducted at light load = 2.8 Nm at 2400 rpm (15% of full engine load) and heavy load = 13.5 Nm at 2400 rpm (75% of full engine load).

(a) (b)

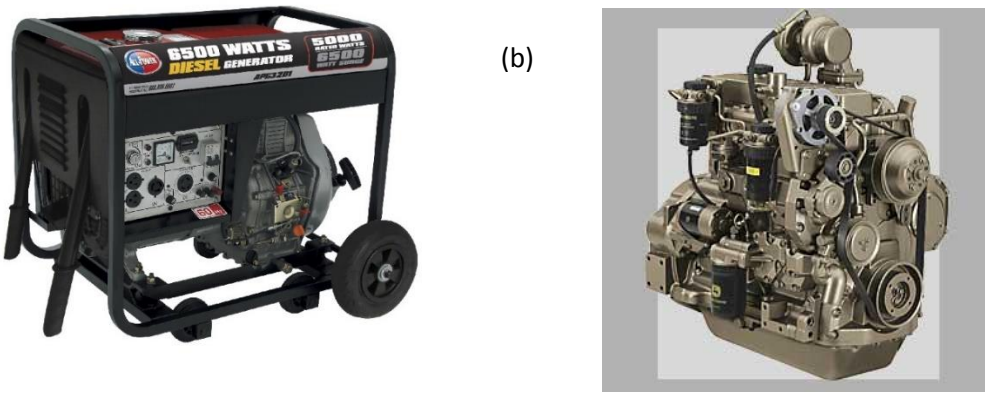

Figure 2.2 (a) Engine 1- small generator engine, (b) Engine 2– modern off-road engine

(b) *Engine 2 (modern off-road engine)* - A 4-cylinder, 4.5 L, 129 kW (at 2400 rpm), model year 2005, John Deere 4045H - a turbocharged, aftercooled engine with common rail fuel injection but without exhaust gas recirculation. It has tier 2 certification for off-highway applications. Tests were conducted at light load = 50 Nm at 1400 rpm (10% of full engine load) and heavy load = 250 Nm at 1400 rpm (50% of full engine load).

(c) *Engine 3 (modern off-road engine)* - A 4-cylinder, 4.5 L, 86 kW (at 2400 rpm), model year 2010, John Deere 4045H – Similar to Engine 2, but with interim Tier 4 emissions certification. Tests were conducted at light load = 45 Nm at 1400 rpm (10% of full engine load) and medium load = 155 Nm at 1400 rpm (35% of full engine load).

2.3 Critical flow orifice

Critical or choked flow orifices are used in this study to maintain constant flow rates through various lines. It works on the principle that when the pressure downstream of the orifice is less than

the critical flow pressure, the flow rate through the orifice becomes independent of the downstream pressure but is directly proportional to upstream pressure and inversely proportional to the square root of upstream temperature.

2.4 Dilution system

One of the important factors to take into consideration while generating Diesel exhaust for laboratory tests is the transformation of Diesel exhaust particles when they enter the atmosphere. An ejector dilution system is used in this study to simulate atmospheric dilution conditions for Diesel exhaust particles. The ejector dilutor consists of a vacuum inlet, compressed air inlet, and an outlet. It is described in detail elsewhere (Abdul-Khalek et al., 1998). Figure 2.3 shows a schematic of a typical 2-stage ejector dilutor system.

Engine exhaust flows through a critical orifice into the primary ejector dilutor (AIR-VAC model TD260H). The diluted exhaust then flows into a residence chamber which facilitates nucleation and condensation of particles. The residence time depends on the flow rate of the aerosol entering the chamber and the dimensions of the chamber. The transformed Diesel exhaust aerosol is then diluted a second time when it flows through the secondary ejector dilutor to freeze further changes in the aerosol.

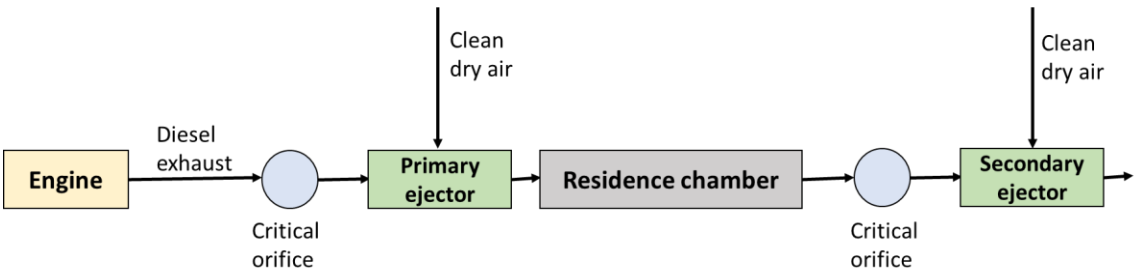

Figure 2.3 Schematic of a two-stage ejector dilutor system

2.5 Filtering facepiece respirators

Commercially available NIOSH certified facepiece particulate respirators were evaluated in this study. These respirators are made from electrostatically charged microfibers and their filtering capability is based on the permanent electric charge on the filter fibers. In addition to mechanical particle collection mechanisms such as impaction, interception and diffusion, electrostatic attraction plays a major role in particle deposition on to the filter fibers. Polarized fibers create internal electric fields which significantly increase the deposition of aerosol particles on filter fibers. Thus a relatively high removal efficiency can be achieved at a moderate flow resistance level as these respirators have a lower packing density compared to mechanical respirators. Two types of respirator models, namely, the R-95 and P-95 respirators from a manufacturer were chosen for this study (Figure 2.4). These respirators are rated to have a filtration efficiency of at least 95% against solid and liquid aerosols including oils. The R-95 respirator has a recommended service life of 8 hours (continuous or intermittent use) while the P-95 respirator has a recommended service life of 40 hours or 30 days (the lesser of the two). This is obviously assuming that the respirator is not damaged or that the breathing resistance does not go beyond the comfortable limit of the user during its period of use. Unlike the R95 respirator, the P95 respirator has a one-way exhalation valve.

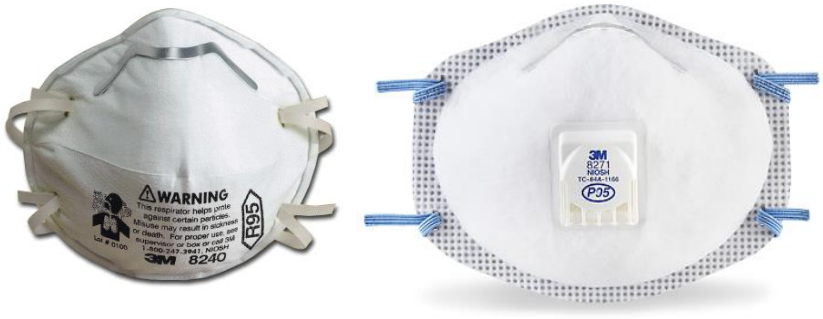

Figure 2.4 R-95 and P-95 test respirators evaluated in this study

2.6 Respirator test chamber

A rectangular acrylic plate with a circular cut-out at the center was used to hold the test respirator. The respirator was glued on to the plate using a dental adhesive (3M ESPE) and the plate was

placed in the respirator test chamber. The dimensions of the plate and hole are 25 cm X 19 cm (length X width) and 3 cm (radius) respectively (refer to Appendix II for picture). The respirator test chamber consists of an inlet diverging cone followed by a diverging duct and an outlet converging duct. These are circular to rectangular ducts, with the rectangular sides facing one another. Figure 2.5 shows a two dimensional sketch of the respirator chamber with dimensions (not to scale). The narrow end of the inlet diverging cone has a diameter of 2.5 cm and the wide end of the cone has diameter of 9 cm. The rectangular end of the ducts have a length of 30 cm and a width of 23 cm. The plate with the respirator is sandwiched between the rectangular sides of the duct along with gaskets on either side of the plate. This chamber was ensured to be air-tight and leak-proof.

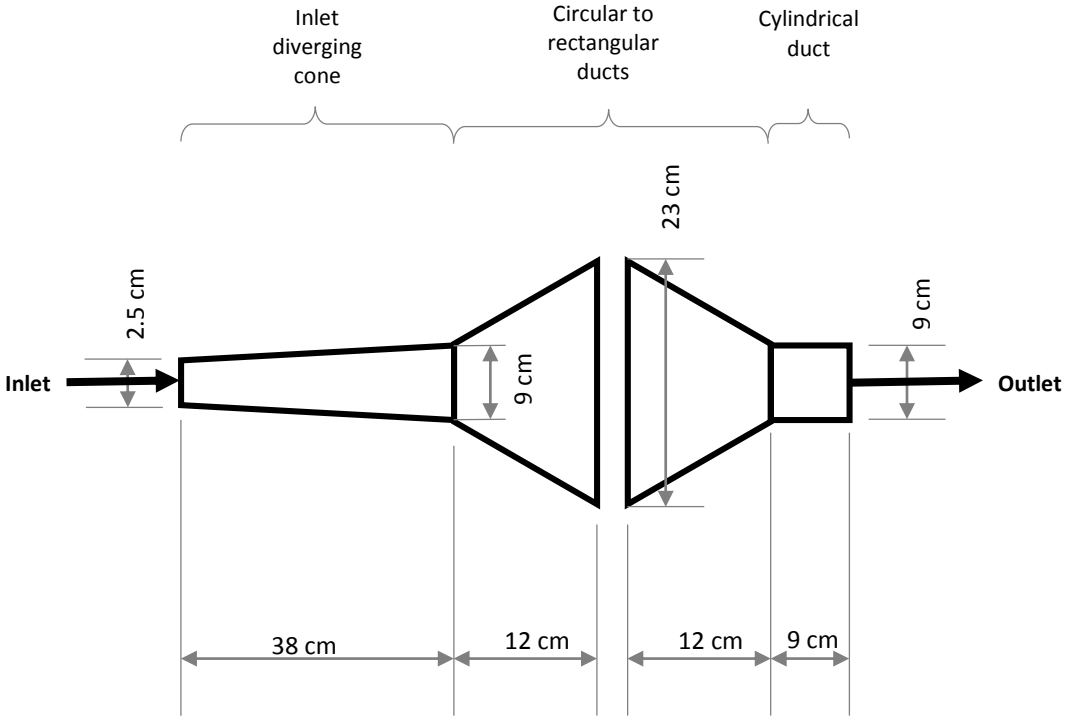

Figure 2.5 Two dimensional sketch of the respirator test chamber

2.7 Scanning Mobility Particle Sizer (SMPS)

The SMPS consists of a TSI 3081 differential mobility analyzer (DMA) which classifies particles according to their electrical mobility, and a TSI 3776 condensation particle counter (CPC) which

counts the number of particles with selected mobility classified by the DMA. The particles enter the DMA where they are allowed to migrate into a clean sheath air flow under the influence of an electric field (Figure 2.7). The rate of migration depends on the electrical mobility of the particles, and mobility, in turn, depends on both the size and electrical charge of the particle. If all the particles have the same charge, then particles of a given mobility will all be of the same size. Since the particles migrate at different rates, they are spread out through the sheath air according to mobility. Withdrawal of a portion of the sheath air flow separates a narrow range of particle mobility from the rest of the aerosol. In an SMPS the voltage on the DMA is varied at a controlled rate to scan through the selected range of mobilities and corresponding mobility diameters. These size-selected particles then flow into the CPC where their concentration is measured.

Figure 2.6 TSI Scanning Mobility Particle Sizer (SMPS)

As shown in Figure 2.7, upon entering the CPC the aerosol stream is saturated with alcohol (typically butanol) vapor. As the mixture is cooled in the condenser tube, the vapor becomes supersaturated and condenses on particles. As a result, the particles grow to a larger diameter, allowing for optical detection and counting. The voltage on the DMA is varied after fixed intervals of time over a specific range to size-select particles within a certain range of mobility diameter, which are then counted by the CPC. The SMPS is widely used as a standard method for measuring airborne particle size distributions.

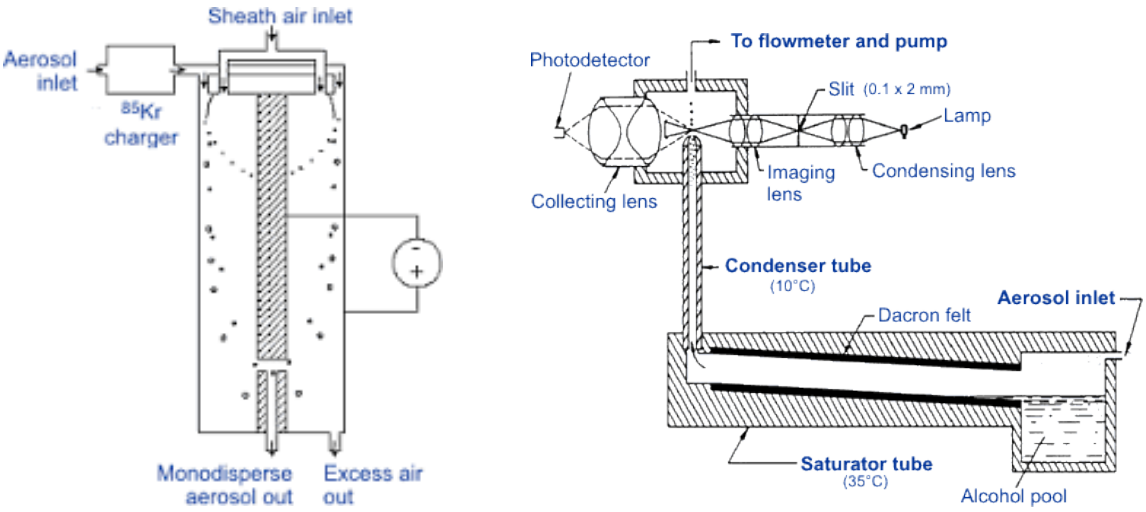

Figure 2.7 Working principle of a (a) DMA, (b) CPC – Images from Hinds (1999)

2.8 Analytical filters for gravimetric analysis

Two types of analytical filters are used in this study for making gravimetric measurements.

(a) Polypropylene (PP) fibrous filters

(b) Polytetrafluoroethylene (PTFE) fibrous filters

Both types of filters used in this study have a thickness of 2 µm and diameter of 37 mm or 47 mm, depending on the test condition. The filters are rated to be 99.99% efficient for 0.5 µm, 1 µm and 2 µm particles, and 99.97% efficient for 3 µm particles.

Chapter 3
EXPERIMENTAL SETUP AND PROCEDURE

3.1 Experiments with NaCl and DOP

A schematic of the test setup for measurement of penetration of respirators challenged with NaCl and DOP aerosols is shown in Figure 3.1. NaCl and DOP solutions were atomized using a TSI Oil Droplet Generator model 9307. For experiments with NaCl, 2% by volume NaCl in distilled water was used. For experiments with DOP, 0.01% by volume DOP in isopropanol (IPA) was used. Compressed air was fed into the atomizer at a pressure of 206.8 kPa. The compressed air flow rate was controlled using a rotameter. The aerosol exiting the atomizer was diluted using an ejector dilutor. This facilitates the evaporation of water or isopropanol droplets in the aerosol, leaving behind only NaCl or DOP particles in the aerosol. The resulting diluted aerosol was then made to flow into the respirator test chamber. The flow rate of the aerosol through the respirator was controlled at 85 L/min using a rotameter downstream of the respirator test chamber. A high efficiency particulate air (HEPA)

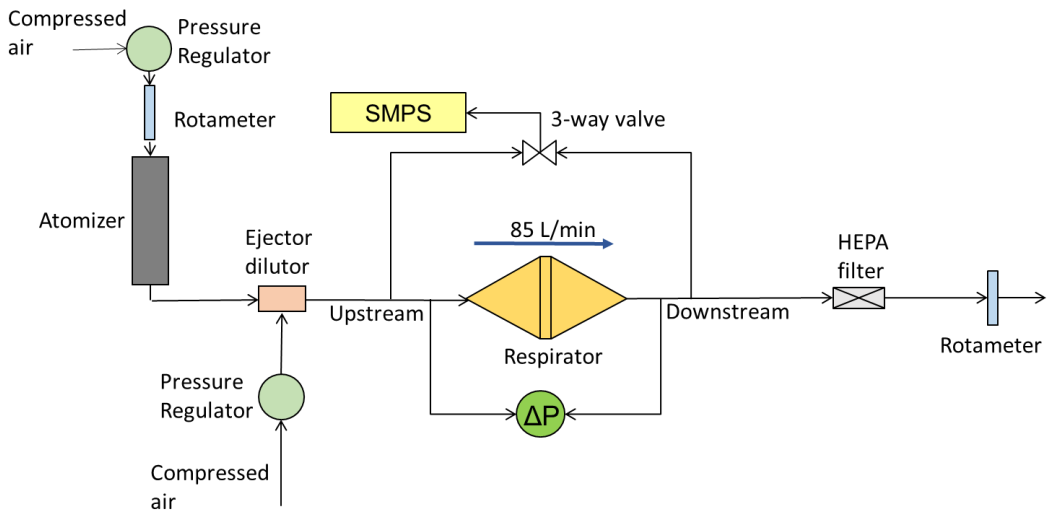

Figure 3.1 Schematic of experimental setup for tests with NaCl and DOP

filter ensured that clean air flowed into the rotameter. The pressure drop across the respirator was monitored using a differential pressure gauge. The SMPS was used to measure particle size distributions upstream and downstream of the respirator, using a 3-way valve to switch between upstream and downstream samples. The SMPS was configured to measure particle size distributions in the mobility size range 7.64 nm – 278.7 nm using a 60 s upscan, a 30 s downscan and a 30 s interval between two scans. The DMA aerosol and sheath flow rates were 1.5 L/min and 10 L/min respectively. Penetration through the respirator is calculated as the ratio of downstream to upstream particle concentration. Table 3.1 shows the test matrix for this setup.

Table 3.1. Test conditions for experiments with NaCl (2%) and DOP (0.01%)

Test aerosol	**Test respirator**	**Atomizer inlet flow rate (L/min)**	**Tests**
NaCl	R-95	20	1,2,3
NaCl	P-95	20	1,2,3
DOP	R-95	20	1
DOP	P-95	20	1
DOP	P-95	11	2,3

3.2 Experiments with Diesel exhaust aerosol

3.2.1 Experimental setup

A schematic of the test apparatus for the measurement of filtration efficiency of respirators challenged with Diesel exhaust from Engine 1 (small diesel generator) and Engine 2 (off-road diesel engine) is shown in Figure 3.2. While the testing process is similar using the two engine aerosol generators, the respective test setups are slightly different from one another.

For experiments with Engine 1, the engine exhaust aerosol sample was extracted from the exhaust pipe and diluted using a single-stage ejector dilution system. The secondary ejector dilutor was removed to ensure that analytical filters collect sufficient mass so that accurate mass measurements can be made for gravimetric analysis. This results in a test aerosol with a particle concentration

much higher than typical occupational exposure limits. However, in the presence of a secondary dilutor, the time taken for sufficient mass to be collected on the analytical filters becomes unreasonably long. Therefore for respirator penetration measurements using gravimetric analysis, there is a trade-off between particle concentration of the test aerosol and the test duration.

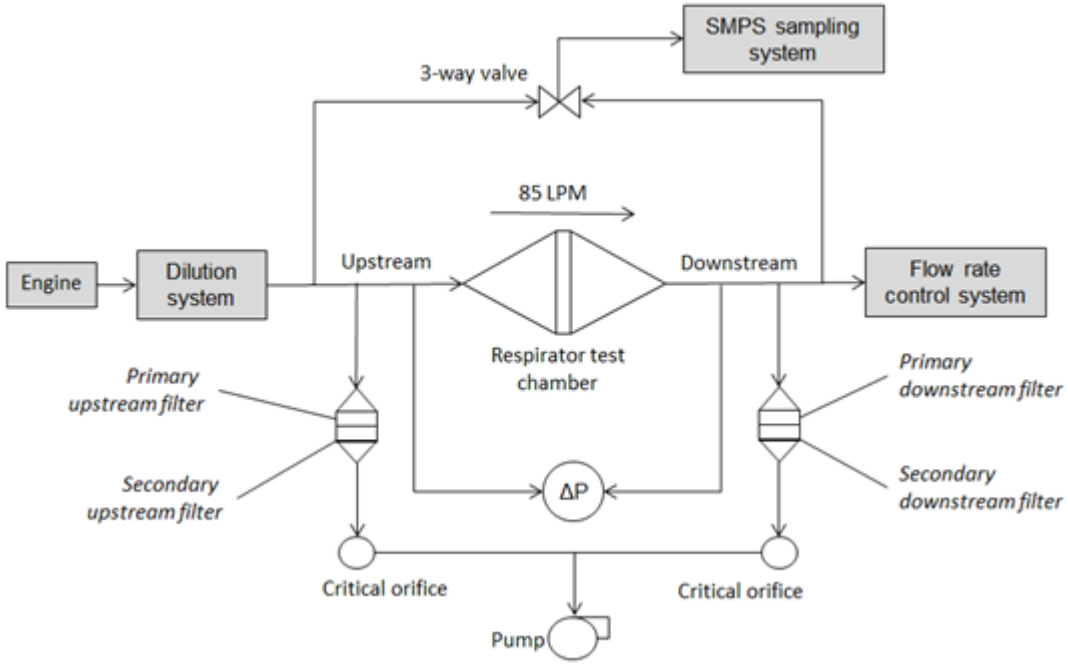

Figure 3.2 Schematic of the experimental setup for experiments with Diesel exhaust aerosol

The aerosol at the outlet of the residence chamber was divided into seven parts using an end cap with seven outlets. This was done with the intention of achieving a flow rate as high as 85 L/min through the respirator without the use of a pump downstream of the respirator. The aerosol was made to flow from the end cap into a circular manifold through conductive silicone tubes to minimize particle transport losses. The circular manifold consists of twelve inlets and one outlet. The test aerosol flowed into the manifold through seven inlets, while four out of the remaining five inlets were plugged. A differential pressure gauge was attached to the last inlet to monitor the pressure inside the manifold with respect to atmospheric pressure. Aerosol exiting from the circular manifold was used to challenge the respirator. For experiments with Engine 2 as aerosol generator,

a two-stage ejector dilution system was used. The aerosol obtained after secondary dilution was used as the final test aerosol for evaluation of the respirators.

The test respirators were placed in an air-tight and leak-proof test chamber consisting of an inlet diverging cone and outlet converging cone (refer to section 2.6). The test aerosol flowrate was 85 L/min. A differential pressure gauge was used to monitor the pressure drop across the respirator for each test.

With Engine 1 as the aerosol generator, the flow rate through the respirator was maintained at 85 L/min using a rotameter (of range 0 – 100 L/min) downstream of the respirator. Whereas with Engine 2, the flow rate through the respirator is maintained using a flowmeter (TSI 4043) and a vacuum pump downstream of the respirator test chamber. The absence of a vacuum pump downstream of the respirator (in the case of experiments with Engine 1) gives a better simulation of realistic scenarios with regard to upstream and downstream pressures.

3.2.2 Measurement methods

In this study, R-95 and P-95 respirators were evaluated using two techniques.

(i) Gravimetric analysis

PP or PTFE filters (refer to section 2.8) were located upstream and downstream of the respirators under test. The filters were weighed before and after particle collection in an environmentally controlled room that was maintained at 30% ± 3% RH and 22°C ± 2°C. The filters were equilibrated for 24 hours before being weighed three times using a microbalance (CAHN C-31) with a resolution of 1 µg. The filters were neutralized prior to weighing to reduce electrostatic charge effects. A blank reference filter was placed in the weighing room for background correction. All filter measurements are background corrected. Penetration (P) of the test respirator from gravimetric analysis is calculated as follows:

$$P\ (\%) = \frac{M_D/Q_D}{M_U/Q_U} * 100 \qquad (3\text{-a})$$

Where M_D and M_U are the mass collected on the analytic filter downstream and upstream of respirator respectively, and Q_D and Q_U are the sampling flow rates for the downstream and upstream filters.

(ii) Particle counting and sizing using a Scanning Mobility Particle Sizer (SMPS, TSI Inc.)

The SMPS was used to measure particle size distributions upstream and downstream of the respirator, using a three-way valve to switch between the upstream and downstream samples. For experiments with Engine 1, the aerosol passed through a secondary dilution system before entering the SMPS. This is necessary as the low primary dilution ratio used in this setup produces a test aerosol with a number concentration that exceeds the detection limit of the CPC. The SMPS was configured to measure particle size distributions in the mobility size range 7.64 nm – 278.7 nm using a 60 s upscan, a 30 s downscan and a 30 s interval between two scans. This SMPS size range captured more than 99 % of particle number and 94% particle mass, and was deemed to be adequate for this experiment. The DMA aerosol and sheath flow rates were 1.5 and 10 L/min respectively. Size distributions were converted to mass distributions using a particle effective density method (Park et al., 2003; Swanson et al., 2010). Penetration through the respirator is calculated as the ratio of downstream to upstream particle mass concentration.

3.2.3 Data collection and analysis

(i) Engine 1 (small diesel generator)

Penetration of the respirators with Engine 1 was measured by gravimetric method using PP filters with and without an "artifact" correction and these results were compared to SMPS measurements. Measurements using the three techniques were conducted in parallel with one another and the penetration values shown are averaged over 90 min. Error bars were calculated from three sets of measurements for each technique. The adsorbed vapor artifact correction consists of secondary filters placed behind the primary filters both upstream and downstream of the respirator. To estimate the adsorbed mass on the PP filters, the secondary filter mass (i.e. only adsorbed vapor) is

subtracted from the primary filter mass (particulate matter + adsorbed vapor). Penetration using tandem upstream and downstream filters is calculated as follows:

$$P = \frac{(M_{D1} - M_{Da})/Q_D}{(M_{U1} - M_{Ua})/Q_U}, \quad \text{(3-b)}$$

where M_{D1} is the total mass collected on the primary downstream filter and M_{U1} the total mass on the primary upstream filter; M_{Da} is the mass of the adsorbed material collected on the secondary downstream filter while M_{Ua} is the mass of the adsorbed material collected on the secondary upstream filter; and Q_D and Q_U are the sampling flow rates for the downstream and upstream filters.

(ii) Engine 2 (John Deere off-road engine)

Respirator penetration measurements were performed using gravimetric method with PP filters (with and without artifact correction as described in the Engine 1 section) and the SMPS. PTFE filters were evaluated as an alternative to PP filters in a limited number of evaluations of the P95 respirator.

Chapter 4
RESULTS AND DISCUSSION

4.1 Experiments with NaCl and DOP

4.1.1 Challenge aerosol size distributions

Figure 4.1 shows the number-based size distributions of the NaCl and DOP test aerosols used in this study. DOP 1 was used for test 1 with the R-95 respirator and test 1 with the P-95 respirator. DOP 2 was used for tests 2 and 3 with the P-95 respirator (refer to Table 3.1).

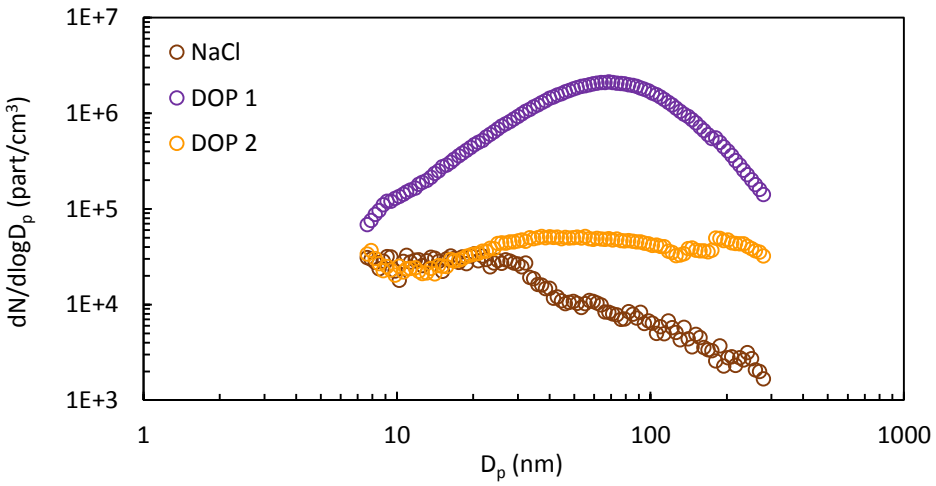

Figure 4.1 Number-based size distributions of NaCl and DOP test aerosols

4.1.2 Results – NaCl aerosol

(i) Particle concentrations upstream and downstream of the respirators

The SMPS was used to measure particle size distributions upstream and downstream of the test respirators. The upstream aerosol is the test NaCl aerosol generated using the atomizer and challenged on to the respirators at 85 L/min. The sample flow into the SMPS is 1.5 L/min and matches the flow out of the SMPS to the CPC. The downstream concentration is basically the

concentration of particles in the filtered aerosol. In Figures 4.2 and 4.3, the solid points represent the upstream concentrations and the hollow points represent the downstream concentrations. Figures 4.2 and 4.3 represent the variation of number-based and mass-based particle concentrations with the time durations for which the respirators are loaded. The points represent the average of measurements from three tests and the error bars represent the standard deviation. The number-based and mass-based particle concentrations upstream of the test respirators remain stable with loading time. For the R-95 respirator, the time-averaged number-based and mass-based upstream particle concentrations are 8.23e+4 #/cm^3 and 78.0 µg/m^3 respectively. Similarly for the P-95 respirator, the time-averaged number-based and mass-based upstream particle concentrations are 8.36e+4 #/cm^3 and 72.0 µg/m^3 respectively. Table 4.1 shows the time-averaged upstream particle concentrations for each of the three tests conducted for the R-95 and P-95 respirators. The average upstream concentrations for all tests are stable with time, with maximum standard deviation of 10%. From Figures 4.2 and 4.3, note that the downstream particle concentrations are less than the upstream concentrations by more than two orders of magnitude for all cases. The downstream concentrations do not seem to follow an increasing or decreasing trend and are reasonably constant with loading time, with slight fluctuations at certain points. Although the upstream particle concentrations are similar for both R-95 and P-95 test respirators, the particle concentrations downstream of the respirator are greater in the case of the R-95 respirator when compared to the P-95 respirator, indicating that the P-95 respirator has a better collection efficiency compared to the R-95 respirator.

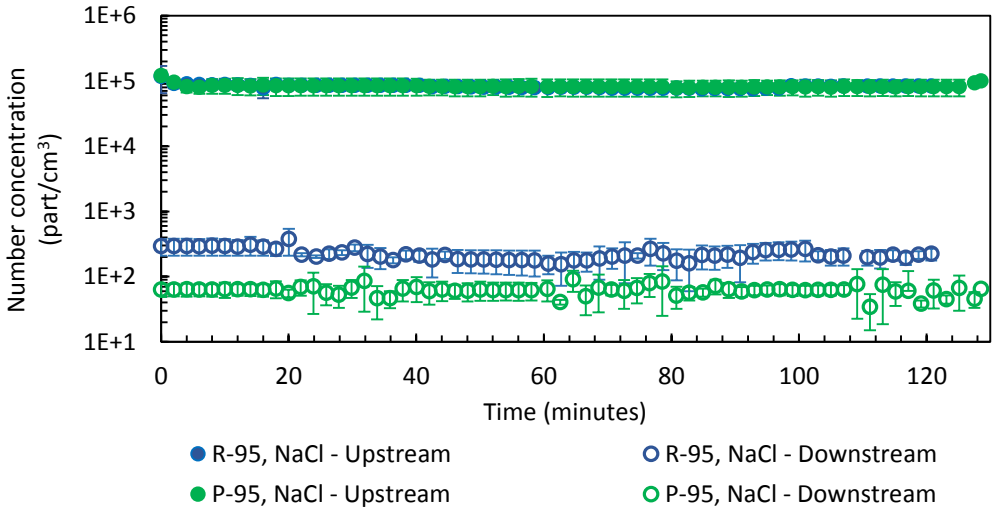

Figure 4.2 Number-based upstream and downstream particle concentrations for the R-95 and P-95 respirators

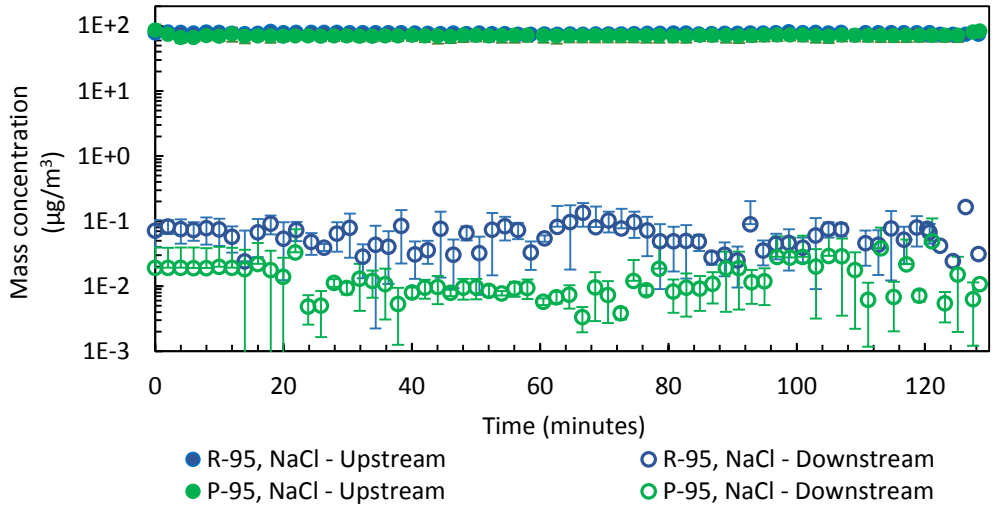

Figure 4.3 Mass-based upstream and downstream particle concentrations for the R-95 and P-95 respirators

Table 4.1 Upstream number-based and mass-based concentrations for individual tests with NaCl aerosol

NaCl	**Test 1**		**Test 2**		**Test 3**	
	average	standard deviation (%)	average	standard deviation (%)	average	standard deviation (%)
			R-95			
Number concentration (#/cm3)	8.18E+4	10.8	7.99E+4	10.1	8.28E+4	7.18
Mass concentration (µg/m3)	77.3	6.23	78.9	6.28	78.5	4.29
			P-95			
Number concentration (#/cm3)	9.83E+4	6.71	9.33E+4	5.64	5.57E+4	3.66
Mass concentration (µg/m3)	82.3	5.01	77.3	4.41	55.6	7.32

(ii) Number-based penetration

Figure 4.4 represents the variation of number-based penetration with mass loaded on to the respirator for the R-95 and P-95 respirators when tested with NaCl aerosol. Number-based penetrations are calculated as the percentage of downstream number-based particle concentration to the upstream number-based particle concentration. Mass loaded on to the respirator is calculated as:

$$\text{Mass loaded (mg)} = [\text{average upstream particle concentration } (\mu g/m^3)\ /1000 * \text{test aerosol flow rate } (m^3/min) * \text{loading time (min)}] \quad (4\text{-a})$$

We observed in the previous section that for similar upstream particle number concentrations, the downstream particle number concentrations were greater for the R-95 respirator when compared to the P-95 respirator. This leads to the data shown in Figure 4.4 – Number-based penetration of the R-95 respirator is greater than that of the P-95 respirator. The data points in the figure represent the average of measurements over three tests and the error bars represent the standard deviation.

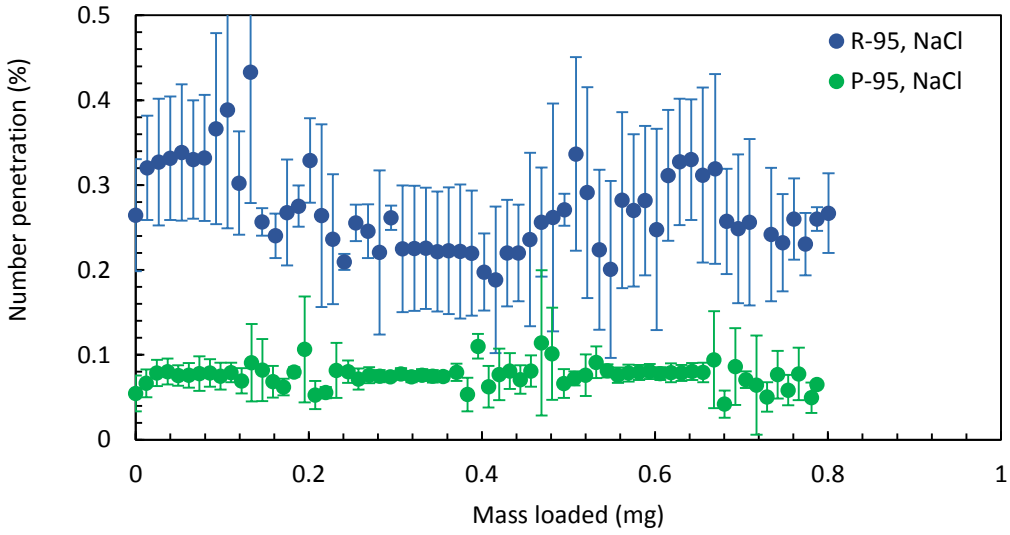

Figure 4.4 Number-based penetration results with NaCl test aerosol

The number-based penetration for the R-95 respirator varies from 0.19 ± 0.08% to 0.43 ± 0.15% within a testing duration of 120 minutes. The average number-based penetration was found to be 0.27 ± 0.07%, implying that the R-95 respirator has a filtration efficiency of 99.73 ± 0.07%. For the P-95 respirator, the number-based penetration varies from 0.04 ± 0.01% to 0.11 ± 0.08% in 120 minutes. The average number-based penetration was 0.07 ± 0.02% for the P-95 respirator, implying that the P-95 respirator has a filtration efficiency of 99.93 ± 0.02%. Even though the maximum penetration of the R-95 respirator is about four times that of the P-95 respirator, both respirators have number-based less than 5%, which is the maximum allowed penetration.

(iii) Mass-based penetration

Figure 4.5 represents the variation of mass-based penetrations with mass loaded on to the respirator for the R-95 and P-95 respirators. Mass-based penetration is calculated as a percentage of downstream mass-based particle concentration to upstream mass-based particle concentration. The data points shown in the figure are averaged over measurements from three tests and the error bars represent the standard deviation.

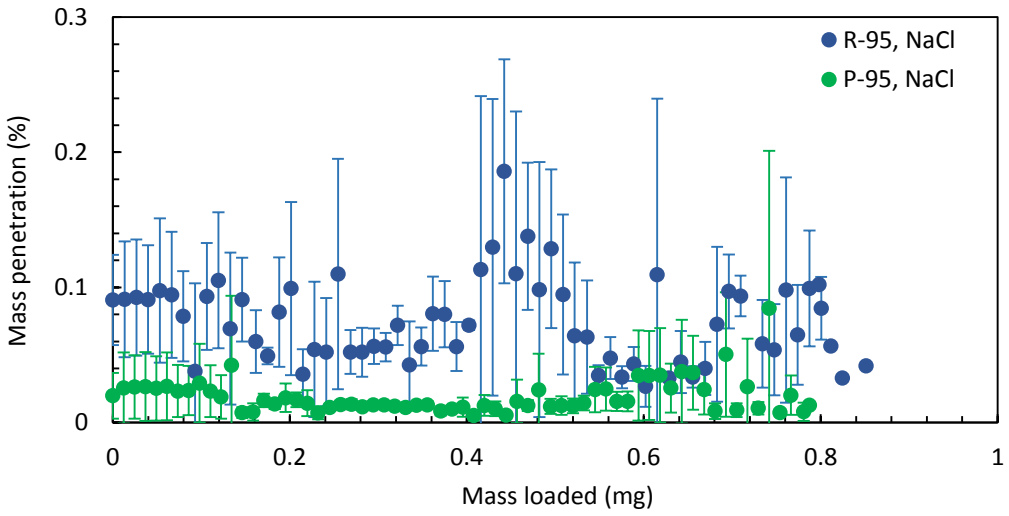

Figure 4.5 Mass-based penetration results with NaCl test aerosol

The mass-based penetration for the R-95 respirator varies within a range of 0.03 ± 0.01% to 0.19 ± 0.08% during 120 minutes of loading. The average number-based penetration was found to be 0.07

± 0.04%, implying that the R-95 respirator has a filtration efficiency of 99.93 ± 0.04%. For the P-95 respirator, the number-based penetration varies from 0.005% to 0.084% in 120 minutes. The average number-based penetration was 0.02 ± 0.01% for the P-95 respirator, implying that the P-95 respirator has a filtration efficiency of 99.98 ± 0.01%. Results indicate that the P-95 respirator is more efficient that the R-95 respirator for NaCl aerosol. However both respirators have a filtration efficiency greater than 95% certification limit.

(iv) Size-based penetration

Figure 4.6 shows the average penetration of the R-95 and P-95 respirators on the y-axis and particle size or mobility diameter on the x-axis. The data points represent the average value of penetration from three tests and the error bars represent the standard deviation. The size-based penetration results helps us gauge the collection efficiency of the test respirators for different sized particles. From Figure 4.6, it is evident that the P-95 respirator is more efficient than the R-95 respirator for all particle sizes.

Filters are also rated in terms of most penetrating particle size (MPPS). It is the particle size for which the filter is most susceptible to particles passing through it. The MPPS of a filter is a function of filter type and construction, aerosol density and face velocity. When challenged with NaCl aerosol, the R-95 respirator was found to show an MPPS of 31 nm and the P-95 respirator was found to show an MPPS of 34 nm. This leads to the elucidation of the difference in the number-based penetration and the mass-based penetration results discussed in the previous sections. Number-based penetration is greater for both R-95 and P-95 respirators compared to mass-based penetration. From the size-based penetration results, it was observed that most particles that penetrate the respirators have size ranging from 20 to 60 nm. These particles, though present in relatively larger numbers, make up only a small percentage of the total mass, most of the mass is found in larger particles. Therefore, number-based penetration for the R-95 and P-95 respirators is greater than mass-based penetration.

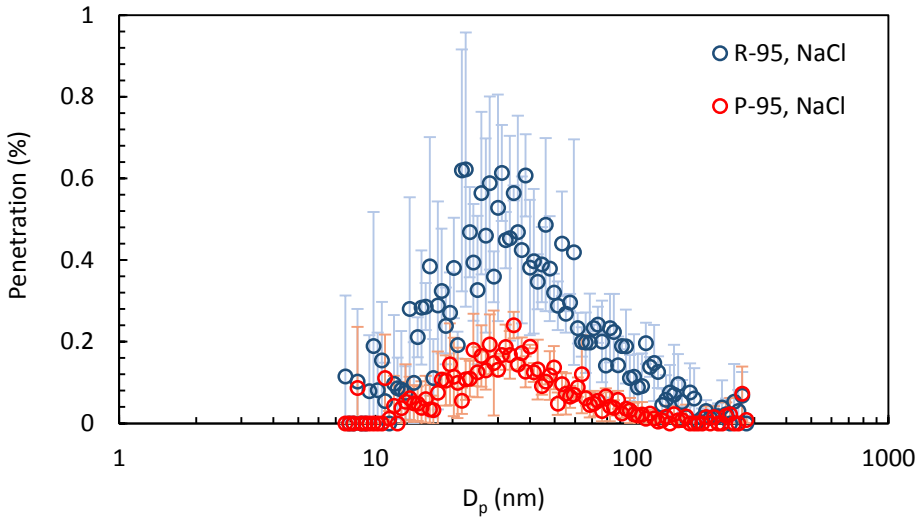

Figure 4.6 Size-based penetration results with NaCl as test aerosol

4.1.3 Results – DOP aerosol

(i) Particle concentrations upstream and downstream of the respirators

Similar to measurements with NaCl as test aerosol, the SMPS was used to measure particle size distributions upstream and downstream of the test respirator. Figures 4.7 and 4.8 represent the variation of number-based and mass-based particle concentrations with loading time. Referring back to the test conditions for measurements with DOP aerosol, a single test was performed on the R-95 respirator for a duration of 80 minutes. Whereas for the P-95 respirator, a single test was performed at one test condition and two more tests at a different test condition, both for a duration of 120 minutes. In Figures 4.7 and 4.8, upstream 1 and downstream 1 represent results from test 1 with the P-95 respirator and will be referred to as case 1 from here on. Upstream 2 and downstream 2 represent results averaged from tests 2 and 3, and will be referred to as case 2.

The upstream number-based and mass-based particle concentrations were found to be stable with loading time for all tests. For the R-95 respirator, the time-averaged number-based and mass-based upstream particle concentrations are 1.22e+6 #/cm^3 and 643 µg/m^3 respectively. Similarly for the P-95 respirator, the time-averaged number-based and mass-based upstream particle concentrations for case 1 are 1.43e+6 #/cm^3 and 805 µg/m^3 respectively, and for case 2 are 5.72e+4 #/cm^3 and

65.0 µg/m^3 respectively. Thus the upstream mass concentration for case 2 was less than that for case 1 by a factor of 12. Table 4.2 shows the time-averaged upstream particle concentrations for each test conducted for the R-95 and P-95 respirators with DOP as the test aerosol. The upstream concentrations for all tests are stable with time, with maximum standard deviation of 11%. From Figures 4.7 and 4.8, note that the downstream particle concentrations are less than the upstream concentrations by more than two orders of magnitude for all cases. Particle concentration downstream of the respirator is greater in the case of the R-95 respirator when compared to the P-95 respirator. Particle concentration is lower for case 2 of P-95 respirator compared to case 1 due to lower particle concentration of the test aerosol measured upstream of the respirator.

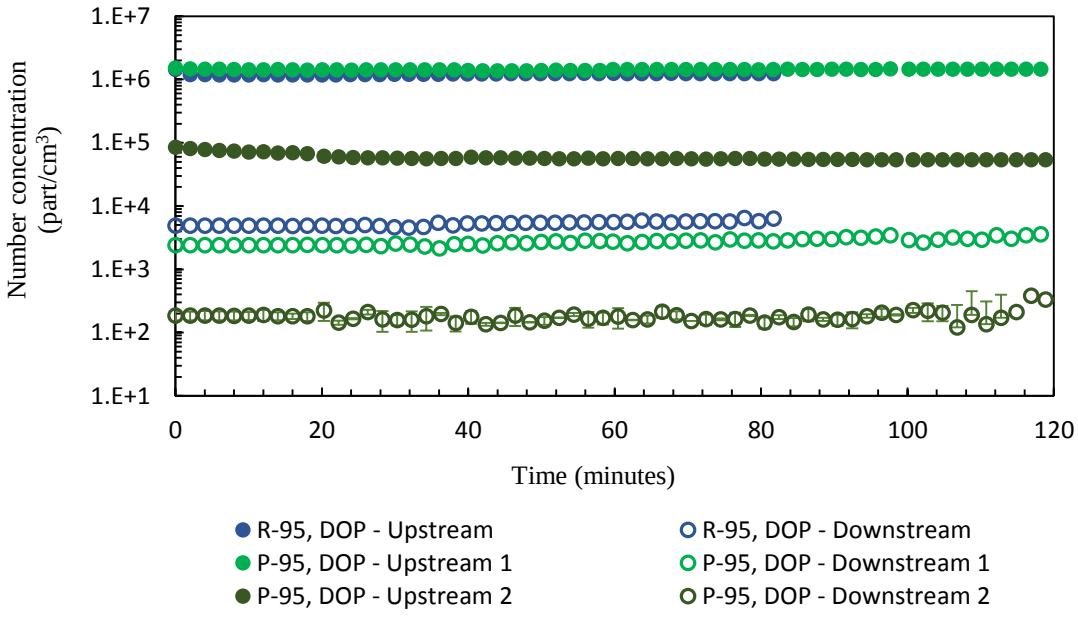

Figure 4.7 Number-based upstream and downstream particle concentration in DOP aerosol

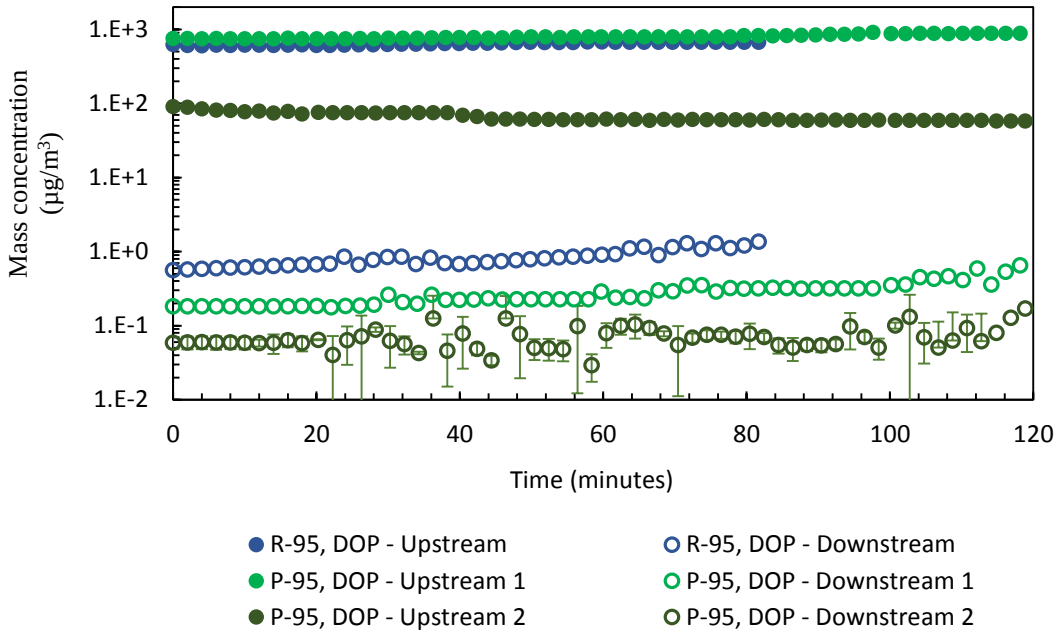

Figure 4.8 Number-based upstream and downstream particle concentration in DOP aerosol

Table 4.2 Upstream number-based and mass-based particle concentrations for individual tests with DOP aerosol

DOP	**Test 1**		**Test 2**		**Test 3**	
	average	standard deviation (%)	average	standard deviation (%)	average	standard deviation (%)
	R-95					
Number concentration (#/cm3)	1.22E+6	2.08	n/a	n/a	n/a	n/a
Mass concentration (µg/m3)	643	4.15	n/a	n/a	n/a	n/a
	P-95					
Number concentration (#/cm3)	1.43E+6	1.72	5.60E+4	7.00	5.85E+4	9.50
Mass concentration (µg/m3)	805	6.07	64.9	8.47	65.1	11.6

(ii) Number-based penetration

Number-based penetration is calculated in the same manner as mentioned in the case of tests with NaCl. It is the percentage of downstream particle number concentration to upstream particle number concentration. In Figure 4.9, the y-axis represents number-based penetration of R-95 and P-95 test respirators challenged with DOP; the x-axis represents the mass loaded on the respirators during testing. For the R-95 respirator, the total mass loaded on to the respirators in 80 minutes was 4.46 mg. The total mass loaded on to the P-95 respirator in 120 minutes for case 1 was 8.05 mg and the average total mass loaded on to the P-95 respirator for case 2 was 0.67 mg. These are relatively low compared to 200 mg, which is the maximum allowed mass deposition on the R-95 and P-95 respirators.

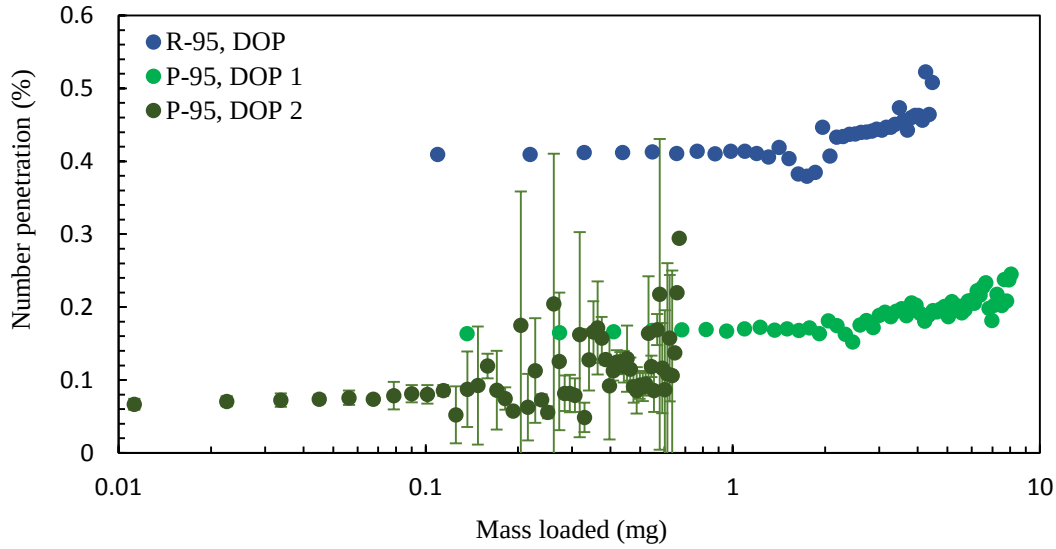

Figure 4.9 Number-based penetration results with DOP aerosol

Penetration results with NaCl as test aerosol did not follow any specific trend with increasing mass loaded on to the respirators. However, with DOP as the test aerosol, we observe a clearly increasing penetration with increasing mass loaded on to the respirators (Figure 4.9). The number-based penetration for the R-95 respirator increases from 0.34% to 0.52% within a testing duration of 80 minutes. For the P-95 respirator, the number-based penetration increases from 0.15% to 0.25% in 120 minutes for case 1 and from 0.22 ± 0.02% to 0.71 ± 0.38% for case 2. Even though the increase

in number-based penetration of the respirators for DOP is relatively less compared to the maximum allowed penetration of 5%, the difference in behavior of the respirators for NaCl and DOP is worth being noted.

(iii) Mass-based penetration

Figure 4.10 shows the mass-based penetration of R-95 and P-95 test respirators when challenged with DOP aerosol. For the R-95 respirator, the mass-based penetration increases from 0.09% to 0.20% during the 80 minute loading duration. For case 1 of the P-95 respirator, mass-based penetration increases from 0.06% to 0.29% during the 120 minute test duration. For case 2 of the P-95 respirator, mass-based penetration increases from 0.02 ± 0.01% to 0.07 ± 0.04% during the 120 minute test duration. Similar to number-based penetration results with DOP aerosol, we observe a clearly increasing trend in mass-based penetration with increasing mass loaded on to the respirator for all tests. Mass-based penetration of the P-95 respirator becomes greater for case 2 compared to case 1 even though the downstream mass-based particle concentration is lower for case 2. This is because the upstream mass-based particle concentration for case 2 is lower than that of case 1 by about a factor of 12. Therefore the mass-based downstream concentration needs to be considered relative to the mass-based upstream concentration. This is reflected in the mass-based penetration results as penetration is calculated as a ratio of downstream to upstream concentration.

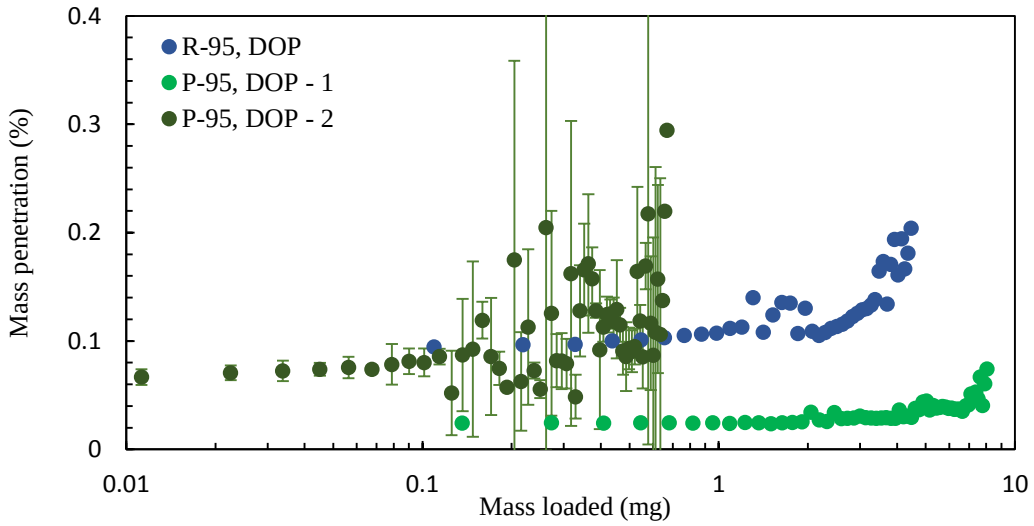

Figure 4.10 Mass-based penetration results with DOP aerosol

(iv) Size-based penetration

Figure 4.11 shows the penetration of the R-95 and P-95 respirators for particles of different sizes in a certain size range when challenged with DOP aerosol. Most penetrating particle size (MPPS) for the R-95 respirator challenged with DOP was found to be 31 nm with a maximum penetration of 0.83 ± 0.08%. For the P-95 respirator, the MPPS was found to be 38 nm with a maximum penetration of 0.55 ± 0.23%.

The penetration curves of the R-95 and P-95 respirators challenged with DOP aerosol are similar to those with NaCl aerosol. However, the penetration of the respirators at their MPPS is higher with DOP test aerosol. In the case of NaCl, the maximum penetration for the R-95 respirator at 31 nm was 0.61 ± 0.11% and that for the P-95 respirator at 34 nm was 0.24 ± 0.03%. Referring to previous literature on testing of electret filters and respirators with DOP aerosol (see section 1.4), it can be hypothesized that DOP aerosol forms an oily layer on the respirators and in the process covers the electric charges on the filter fibers. This leads to a decrease in collection efficiency due to electrostatic attraction, causing an increase in penetration as more DOP particles are loaded on to the test respirators.

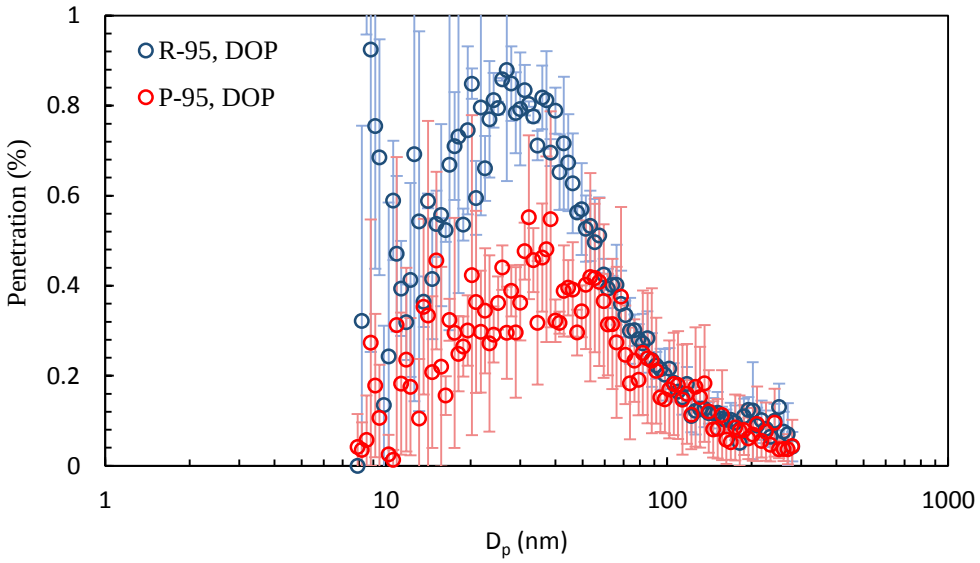

Figure 4.11 Size-based penetration results with DOP aerosol

4.2 Experiments with Diesel exhaust aerosol

4.2.1 Challenge aerosol size distributions

Figure 4.12 shows the averaged SMPS particle number and mass distributions measured upstream of the respirator after primary dilution, grouped by engine and load. There is a substantial difference in the nucleation and accumulation modes of the four distribution curves. Engine 1 at light and heavy load and Engine 2 at light load both show prominent nucleation modes, indicating the strong presence of semi-volatile material. Results from previous EC/OC measurements of both of these engines (Kittelson et al., 2010; Swanson et al., 2015) show that Engine 1 is an extremely high emitter of OC, while Engine 2 emits EC and OC in roughly similar proportions. Exhaust from Engine 1 was found to contain greater than 90% OC at light and heavy load at concentrations >10 mg/m^3. Engine 2 was found to produce exhaust with 1.2 mg/m^3 OC and 1.4 EC/OC ratio at light load and 2.0 mg/m^3 OC and 0.3 EC/OC ratio at heavy load.

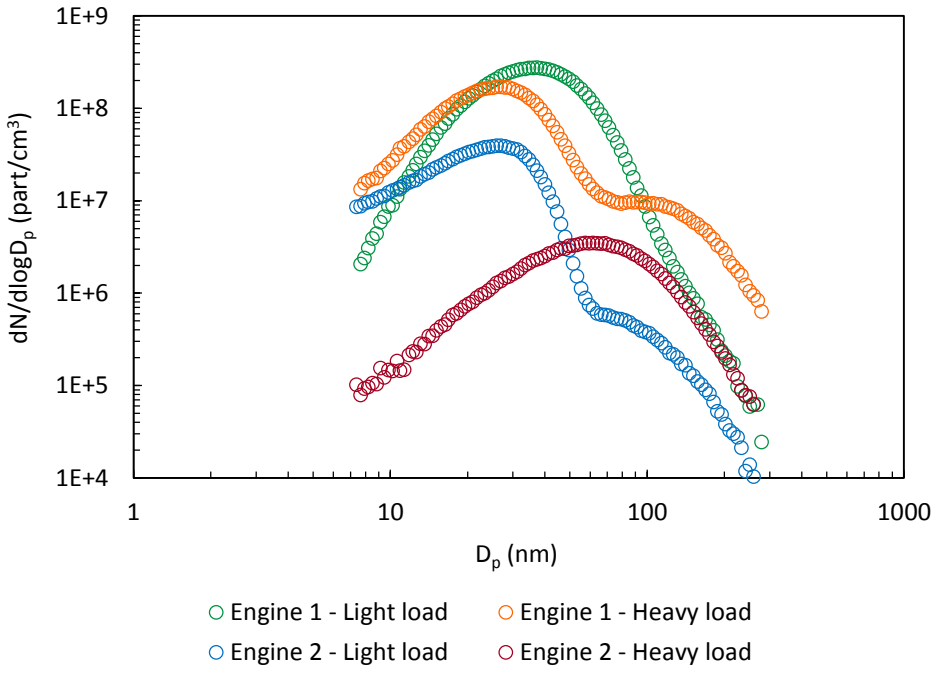

Figure 4.12 Number-based particle size distributions of Diesel test aerosol from Engine 1 and Engine 2

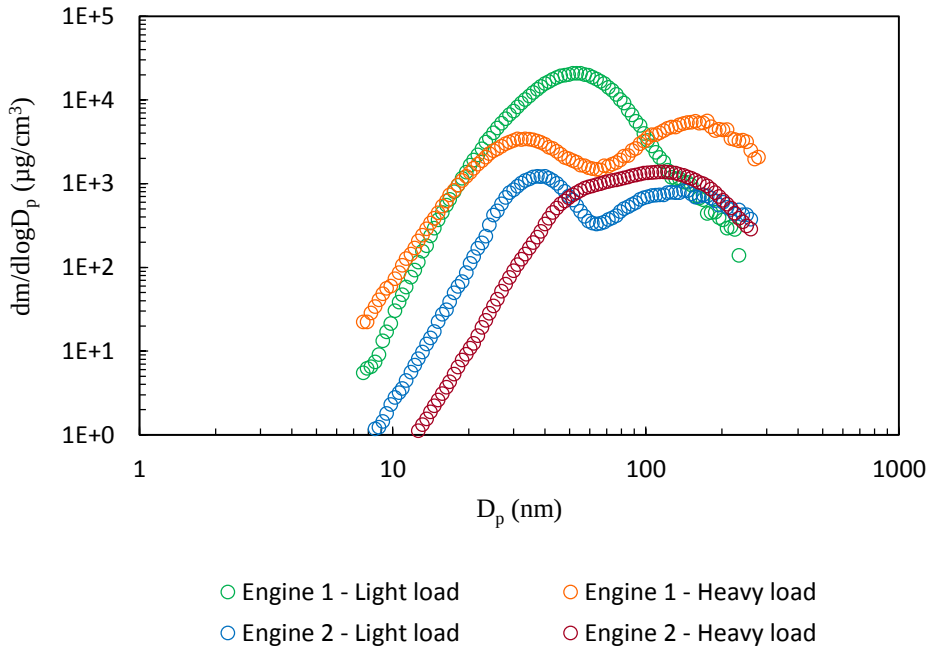

Figure 4.13 Mass-based particle size distributions of Diesel test aerosol from Engine 1 and Engine 2

4.2.2 Results – Engine 1 (small Diesel generator)

(i) Particle concentrations upstream and downstream of the respirators

Particle concentrations upstream and downstream of the respirators were measured using the SMPS continuously over a test duration of 90 minutes. A 3-way valve was used before the SMPS inlet to switch between upstream and downstream aerosols every 3 samples. Figures 4.14 – 4.17 show the variation of number-based and mass-based particle concentrations for the R-95 and P-95 respirators with loading time. The data points represent the average of measurements over three tests and the error bars represent the standard deviation. The upstream particle concentrations for all tests were stable during loading. For the R-95 respirator at light load, the time-averaged upstream particle number and mass concentrations are 1.70e+8 #/cm^3 and 8701 µg/m^3 respectively. At heavy load, the upstream particle number and mass concentrations are 8.61e+7 #/cm^3 and 3937 µg/m^3 respectively. For the P-95 respirator at light load, the time-averaged upstream particle number and mass concentrations are 1.19e+8 #/cm^3 and 9929 µg/m^3 respectively. At heavy load, the upstream particle number and mass concentrations are 7.87e+7 #/cm^3 and 3321 µg/m^3 respectively. Table

4.3 shows the time-averaged upstream number-based and mass-based concentrations for each test conducted. The maximum standard deviation was 17%. Engine-out concentrations were not as stable as atomizer concentrations.

The variation of downstream particle concentrations with loading time is different for light load and heavy load. At light load, the downstream concentration increases rapidly with loading time. For the R-95 respirator, the downstream number concentration increases from 2.54e+6 #/cm^3 to 1.86e+8 #/cm^3 and the mass concentration increases from 60.4 µg/m^3 to 1193 µg/m^3 during the course of the test. Similarly for the P-95 respirator, the downstream number concentration increases from 1.01e+6 #/cm^3 to 8.85e+6 #/cm^3 and the mass concentration increases from 55.1 µg/m^3 to 569 µg/m^3 in 90 minutes.

It was observed that the respirators behave differently when challenged with Diesel exhaust generated from heavy load. For the R-95 respirators tested at heavy load, the average particle number concentration downstream of the respirator decreases from 1.54E+6 to 0.96e+06. The downstream mass concentration increases negligibly from 31.4 µg/m^3 to 41.9 µg/m^3. Similarly for the P-95 respirator at heavy load, the downstream number concentration increases by a small factor from 5.20E+5 to 7.91e+06. The downstream mass concentration increases from 9.5 µg/m^3 to 22.6 µg/m^3.

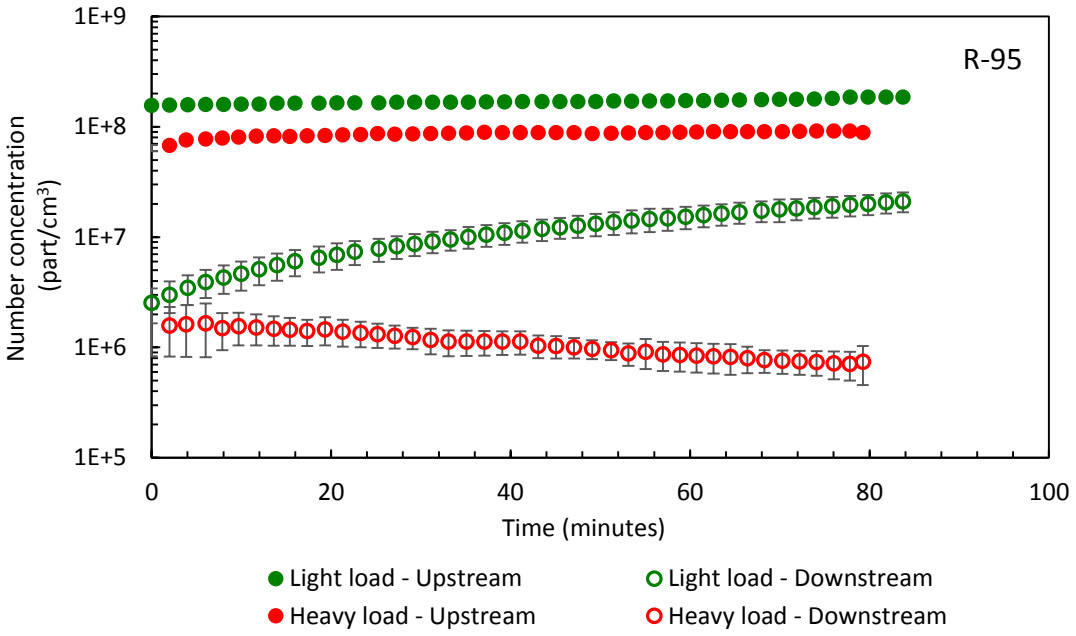

Figure 4.14 Number-based particle concentrations upstream and downstream of the R-95 respirator

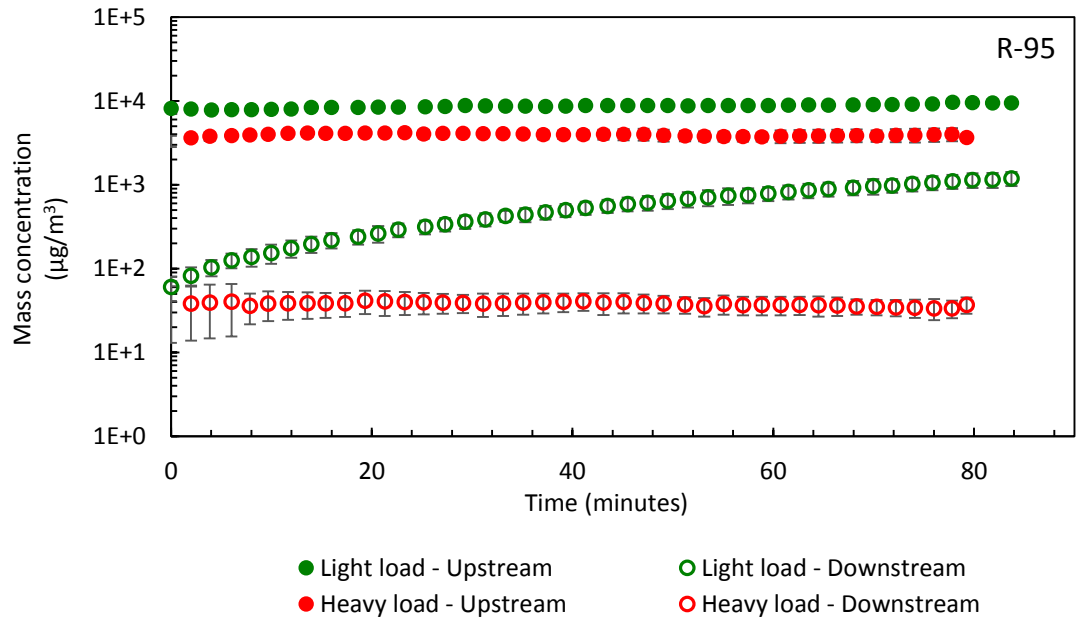

Figure 4.15 Mass-based particle concentrations upstream and downstream of the R-95 respirator

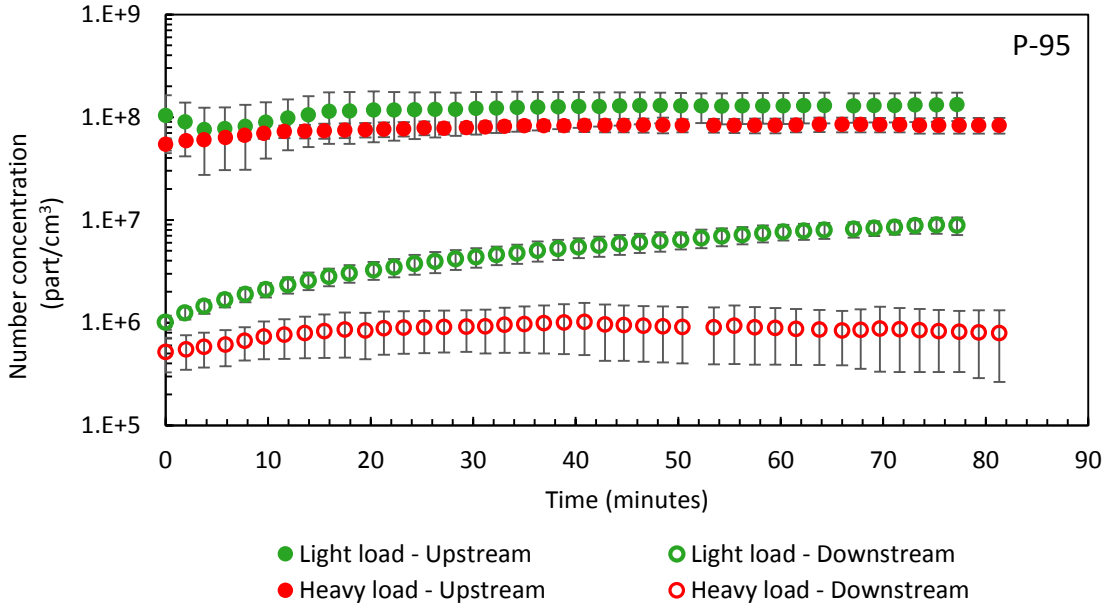

Figure 4.16 Number-based particle concentrations upstream and downstream of the P-95 respirator

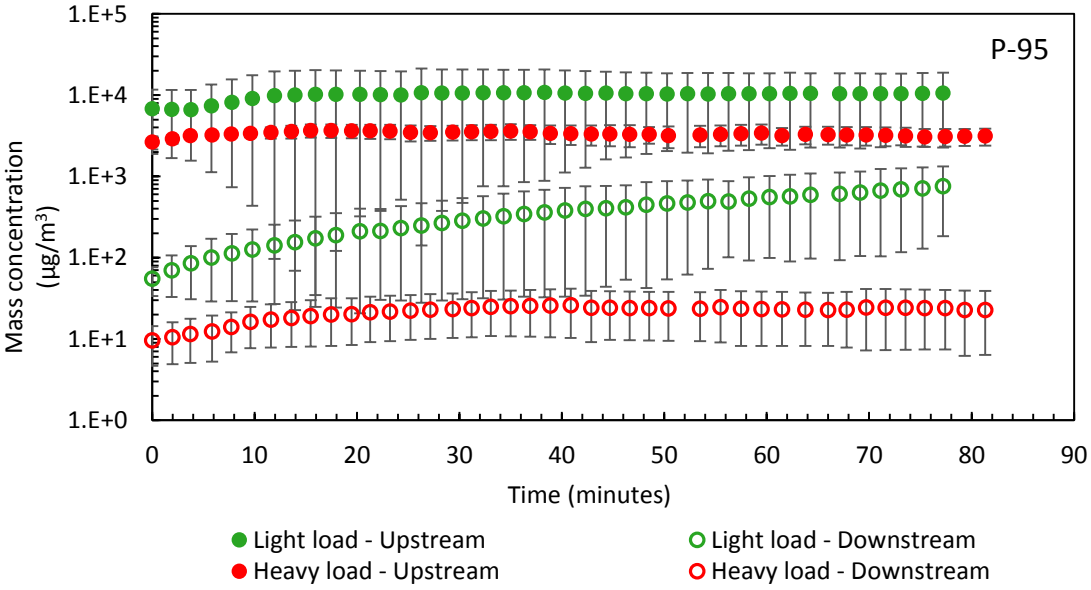

Figure 4.17 Mass-based particle concentrations upstream and downstream of the P-95 respirator

Table 4.3 Number-based and mass-based particle concentrations of Diesel exhaust aerosol for individual tests performed with Engine 1

Diesel exhaust aerosol	**Test 1**		**Test 2**		**Test 3**	
	average	standard deviation (%)	average	standard deviation (%)	average	standard deviation (%)
	R-95, Light load					
Number concentration (#/cm3)	1.67E+8	5.8	1.83E+8	4.6	1.60E+8	3.8
Mass concentration (µg/m3)	8944	5.8	9042	7.2	8118	4.1
	R-95, Heavy load					
Number concentration (#/cm3)	8.39E+7	6.8	8.42E+7	7.0	9.03E+7	8.1
Mass concentration (µg/m3)	3950	6.5	3542	9.2	4319	7.7
	P-95, Light load					
Number concentration (#/cm3)	6.43E+7	17.8	1.44E+8	10.1	1.48E+8	5.1
Mass concentration (µg/m3)	3673	17.1	19743	5.2	6373	6.7
	P-95, Heavy load					
Number concentration (#/cm3)	6.76E+7	6.4	8.10E+7	13.4	8.76E+7	12.5
Mass concentration (µg/m3)	2699	13.2	3241	4.9	4022	12.2

(ii) Number-based penetration

Number-based penetration is calculated as the percentage of number-based particle concentration downstream of the respirator to that upstream of the respirator. The R-95 and P-95 respirators are certified to have penetration less than 5% for solid and oily aerosols. In Figure 4.18, y-axis represents number penetration of the respirators and x-axis represents mass loaded on to the respirators. Mass loaded is calculated as shown in equation 4-a.

The test aerosol flow rate is 85 L/min and is common for all the respirators. Mass loaded on to the respirators after 90 minutes at is 60 to 70 mg at light load and 20 to 30 mg at heavy load. This is

dependent on the particle concentration of the aerosol challenged on to the respirators. The upstream aerosol concentration at light load is greater than that at heavy load (refer to section 4.2(b)(i)).

We can observe from Figure 4.18 that the number-based penetration of the R-95 and P-95 respirators increase rapidly with mass loaded on to the respirators at light load. Whereas at heavy load, the number penetration of the respirators remains relatively unchanging during the 90 minute loading duration. For the R-95 respirator at light load, the number penetration increases from 1.62 ± 0.54% to 11.3 ± 1.5% and at heavy load, the number penetration decreases from 2.11 ± 1.49% to 0.98 ± 0.38%. Similarly for the P-95 respirator at light load, the number penetration increases from 1.37 ± 1.06% to 6.99 ± 1.70% and at heavy load, the number penetration slightly decreases from 0.95 ± 0.29% to 0.89 ± 0.51%

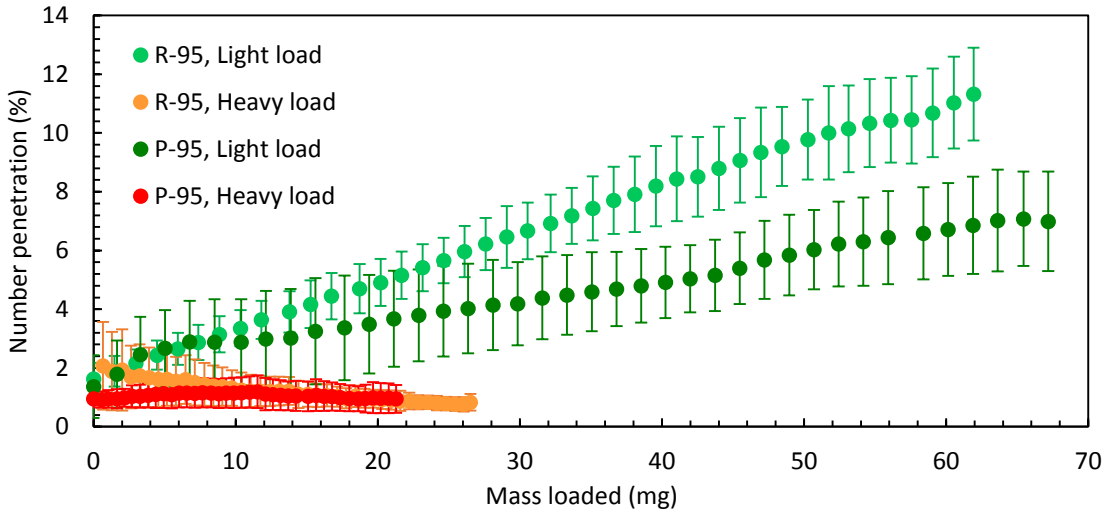

Figure 4.18 Number-based penetration at light and heavy load with Engine 1

(iii) Mass-based penetration

Mass-based penetration is calculated as the percentage of downstream mass concentration to the upstream mass concentration. Figure 4.19 shows the variation of mass-based penetration with mass loaded on to the respirators at light and heavy load. The mass-based penetration trends are similar

to those of number-based penetration. For the R-95 respirator at light load, the mass-based penetration increases from 0.77 ± 0.34% to 12.6 ± 1.7% and at heavy load, mass penetration increases only slightly from 1.08 ± 0.60% to 0.87 ± 0.29%. Similarly for the P-95 respirator at light load, the mass penetration increases from 0.97 ± 0.32% to 7.24 ± 0.20% and at heavy load, there is only a minor increase in mass penetration from 0.38 ± 0.19% to 0.70 ± 0.49%. Results indicate that amongst the two models of test respirators, the P-95 respirator is more efficient for Diesel exhaust.

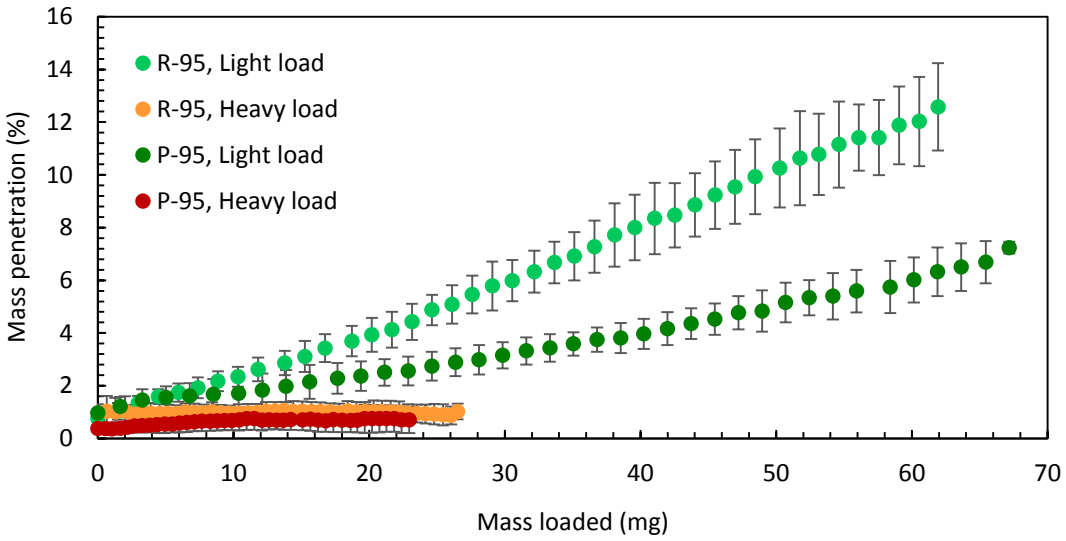

Figure 4.19 Mass-based penetration at light and heavy load with Engine 1

(iv) Size-based penetration

Figure 4.20 shows size-based penetration for the R-95 respirator, with penetration on the y-axis and particle mobility diameter on the x-axis. For respirators challenged with NaCl and DOP aerosols, we observed that the size-based penetration curves were unchanging during the 120 minute loading test. However, that is not the case for respirators challenged with Diesel exhaust. The size-based penetration curves change considerably with time. In Figure 4.20, initial and final size-based penetration curves are shown for the R-95 respirator challenged with Diesel exhaust at light and heavy load. Refer to Appendix I for more detailed size-based penetration curves for each test condition. At light load, the final penetration is greater than initial penetration for all particle

sizes. There is a shift in the MPPS of the respirator from 24 nm to 45 nm. The peak penetration also increases from 4.2 ± 0.8% to 13.1 ± 1.7%. Whereas at heavy load, the size-based penetration curve is much more flat - penetration decreases for particles with size less than 60 nm and increases for particles with size greater than 60 nm. The peak penetration decreases from 4.0 ± 0.8% to 1.8 ± 1.0% and MPPS increases from 35 nm to 55 nm.

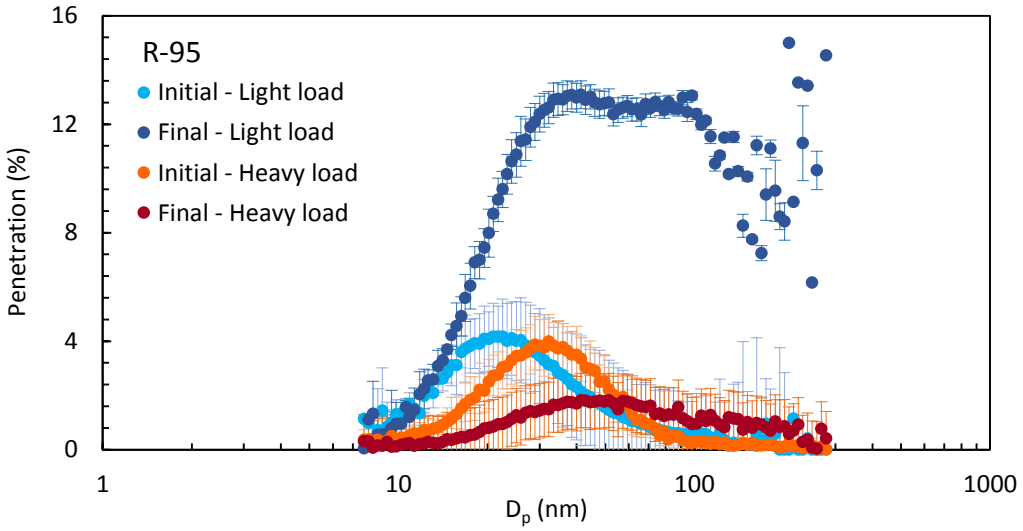

Figure 4.20 Size-based penetration results for the R-95 respirator tested with Diesel exhaust from Engine 1

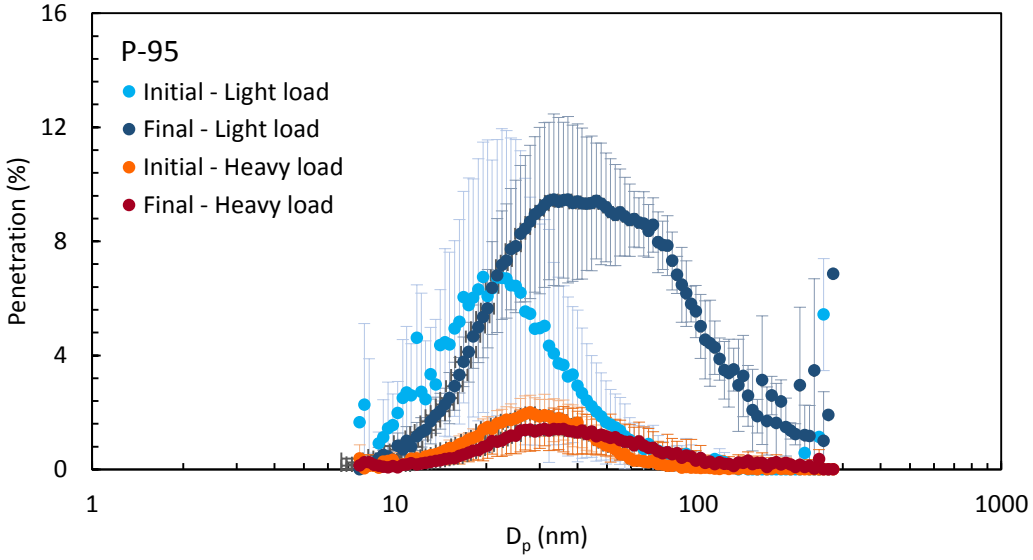

Figure 4.21 Size-based penetration results for the R-95 respirator tested with Diesel exhaust from Engine 1

The behavior of P-95 respirators at light and heavy load is similar to that of the R-95 respirator. At light load, the penetration increases with loading time for all particle sizes (Figure 4.20). The MPPS shifts towards the right, from 24 nm to 40 nm. The peak penetration increases from 6.7 ± 5.2% to 9.4 ± 2.9%. At heavy load, penetration decreases for particles with size less than 47 nm and increases for particles with size greater than 47 nm. The MPPS shifts from 30 nm to 38 nm after 90 minutes of loading, and the peak penetration decreases from 2.0 ± 0.6% to 1.4 ± 0.8%.

Results shown above highlight the difference in behavior of the test R-95 and P-95 respirators at light and heavy load on the engine. This can be attributed to the difference in composition of Diesel exhaust at light and heavy load. Engine 1 has a lower EC/OC ratio at light load compared to heavy load. Results from Swanson et al. (2015) show that exhaust from Engine 1 has an extremely high OC/EC ratio and is not comparable to typical OC/EC ratios which are in the range of 1.25 at heavy load to 2.5 at light load. The engine exhaust at light load is mostly composed of nucleation mode particles. This is likely associated with a high concentration of semi-volatile material in the gas phase. At heavy load, the cylinder and exhaust temperatures are much higher and some of the semi-volatile material is burned, although the total OC concentration still remains high. A clear accumulation mode appears at heavy load and the soot particles will adsorb some OC, further reducing the concentration of OC vapor. It can be hypothesized that the high concentration of OC vapor present at light load degrades the respirator by removing the electric charges on the respirator. Thus, it results in a reduction in the particle collection efficiency of the respirators due to weakening of electrostatic forces that aid particle deposition. However, Engine 1 at heavy load also produces a large quantity of OC in the form of particles, which would remove the electric charges on the respirator according to our hypothesis and lead to an increase in penetration with loading time. This was not observed in our experimental results at heavy load. On the contrary, the number penetration of the test respirators decreased with loading time. A probable reason for this is that condensed OC and vapor-phase OC have different effects on the respirator, due to a difference in the mechanism of interaction of particles and vapors with filter fibers. The mechanism of organic vapor interaction with respirators that leads to removal of electret charges on the filter fibers are not completely understood. Rengasamy et al. (2010) found that electret N95 and P100 respirators are degraded when exposed to isopropanol vapor, but remain unaffected when exposed to xylene vapor. Results from previous literature also found that electret respirators showed no significant increase in penetration when exposed to vapors of xylene, toluene and ethyl benzene (Jasper et al., 2005; Jasper

et al., 2006; Jasper et al., 2007). The difference in behavior of electret respirators to isopropanol vapor and other organic vapors was attributed to the difference in the interaction mechanism of the organic vapors with the filter fibers, possibly due to the isopropanol being polar. For organic vapors, sorption and diffusion processes occur at different time scales, with diffusion typically being the rate limiting step. However, it was suggested that isopropanol vapors diffuse rapidly and interact with the electric charges in the filter fibers.

It is possible that a similar process is taking place with vapor-phase OC in Diesel exhaust. The R-95 and P-95 test respirators used in this study are certified to be more than 95% efficient for all particulate matter, including semi-volatile particles. This is made possible due to a manufacturing technique which incorporates a shielding effect to retain the electric charges on the fibers. However, this shielding effect need not be applicable for semi-volatile vapors present in the challenged test aerosol. Even though previous results indicate that similar electret respirators are efficient for certain organic vapors, it appears that the R-95 and P-95 respirators are not suitable to be used for Diesel exhaust with high vapor-phase OC concentration. All in all, results show that the efficiency of the R-95 and P-95 respirators is highly dependent on the engine and operating conditions.

(v) Gravimetric analysis

Gravimetric measurements were performed simultaneously with SMPS measurements. For gravimetric measurements with Engine 1, PP analytical filters were used – measurements were made with single upstream and downstream PP filters as well as tandem upstream and downstream PP filters. Figure 4.22 shows a comparison of particle mass penetration of R95 and P95 respirators for diesel exhaust generated from Engine 1 from both SMPS and gravimetric analysis. The penetration measurements from gravimetric analysis without artifact correction ('Single PP filter' in Figure 4.22) are higher than SMPS measurements in all cases. Percent penetration of the R95 respirator without artifact correction exceeds the percent penetration obtained from SMPS measurements by factors of 1.5 and 2.9 for light and heavy engine load respectively. Similarly, percent penetration of the P95 respirator without artifact correction exceeds the percent penetration obtained from SMPS measurements by factors of 1.4 and 5.5 for diesel exhaust from light and heavy engine load respectively. Especially in the heavy engine load case, these results show the propensity for PP filters to adsorb gas phase material – a positive filter artifact. Given the OC

concentration is similar for both load cases, the reason for the difference between the SMPS-based mass penetration and filter-based mass penetration could be due to the presence of vapor-phase organic carbon in Diesel exhaust.

Particle mass penetration varied considerably with engine load. At light engine load, average penetration of the R95 and P95 respirators obtained using the SMPS was 6.81% and 4.49% respectively and at heavy engine load, average penetration of the R95 and P95 respirators was 1.00% and 0.64%, respectively.

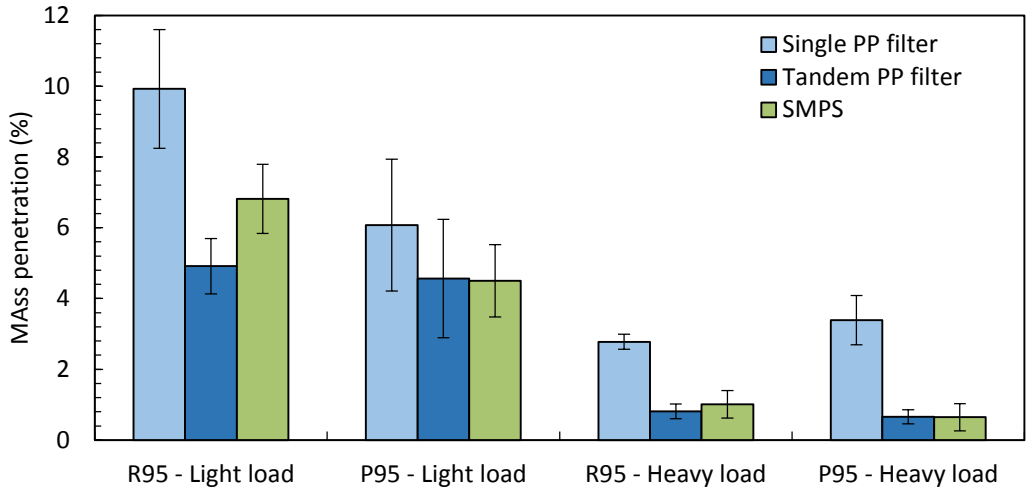

Figure 4.22 Mass penetration of diesel exhaust through R95 and P95 respirators measured using gravimetric analysis with single PP filter, gravimetric analysis with tandem PP filter, and SMPS

Tandem PP filters were used to make a positive artifact correction. Figure 4.22 shows penetration measurements with the artifact correction agree more closely with SMPS results. The differences between penetration values obtained from SMPS measurements and from gravimetric analysis with tandem PP filters were not statistically significant. Thus it appears the artifact correction is a potential means to improve gravimetric measurements in these cases.

Figure 4.23 shows the mass collected by the upstream and downstream (and primary and secondary) PP filters for light and heavy engine load. For the case of the upstream sample, secondary filter, light load condition, the mass collected was 14 mg. This is a tremendous amount of gas phase semi-volatile material – and it must be gas phase because the primary filter captures

almost all of the particles. The downstream filter captures much less but this is possibly the result of the respirator adsorbing much of the low-volatility OC vapor just as the filters do. The secondary filters for the heavy load case collected significantly less mass than secondary filters for the light load case, confirming that the mass collected by the secondary filters correlates to the concentration of gas phase OC in the challenged aerosol. The amount of semi-volatile material being collected on upstream and downstream filters is not in proportion to the total concentration of OC, which suggests there are other indefinite factors impacting the result. If this is the case, it is unlikely the secondary filter artifact correction will be particularly robust. The correct is only valid if the primary and secondary filters are in "equilibrium," or that the mass of adsorbed semi-volatile material on each filter is the same.

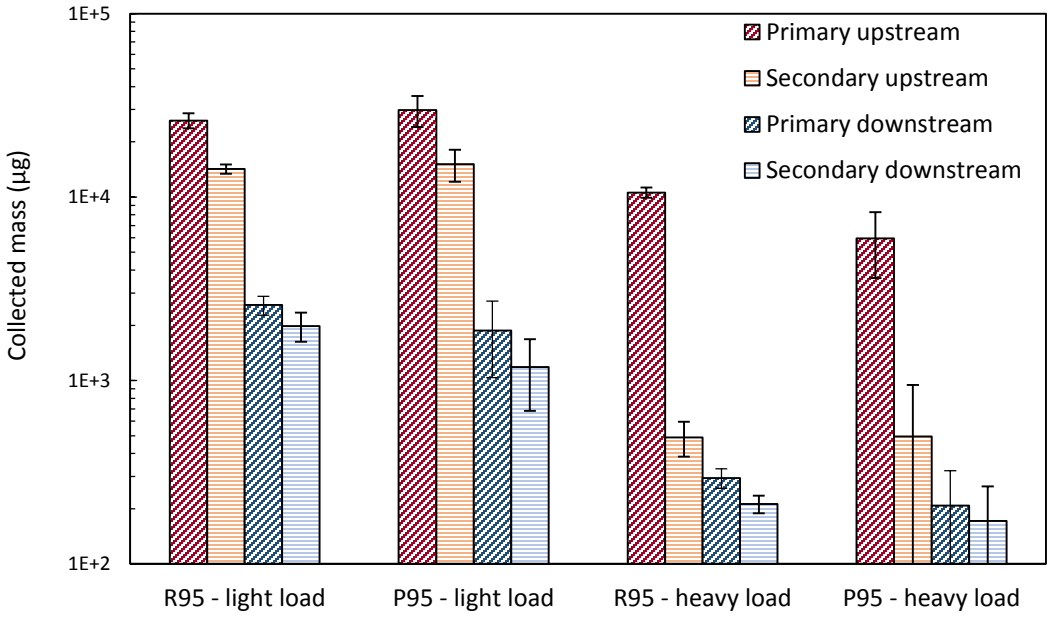

Figure 4.23 Mass collected on the tandem PP filters using with Engine 1 as the aerosol source.

Adsorption of semi-volatile material on the filters depends on temperature, relative humidity, pressure drop and surface area of particle deposition, among other parameters (Chase et al., 2004; Turpin et al., 2000; Mader et al., 2001). Increased particle deposition implies availability of more particle surface area for adsorption of semi-volatile material, which results in greater adsorption on the primary filters compared to the secondary filters. Because there is no standard protocol for

challenging respirators with diesel exhaust, none of these variables are controlled in these tests nor particularly well-understood. Nevertheless, these results were repeatable as demonstrated by low experimental variability (typically <10%).

4.2.3 Results – Engine 2 (off-road Engine)

Figure 4.24 shows the penetration measurements with Engine 2 at light load for the P-95 respirator from gravimetric analysis with PTFE and PP filters. Similar to gravimetric measurements with Engine 1, measurements were made with singular upstream and downstream filters as well as with tandem upstream and downstream filters. Average penetration of the respirator determined by gravimetric analysis with singular upstream and downstream PP filters was 10.90% and penetration determined by gravimetric analysis with PTFE filters was found to be 1.03%. The significant difference between penetrations obtained using PP filters and PTFE filters can be attributed to the fact that the PTFE filters, being relatively inert, collect mostly particles while PP filters collect particulate matter as well as a significant amount of semi-volatile material. The average penetration calculated using singular and tandem gravimetric analysis setup with PTFE filters were 1.03% and 0.99% respectively. Average penetration measured using single and tandem PP filters were 10.90% and 3.23% respectively, still underestimating the effect of artifacts on penetration. This substantial difference of 7.67% in percent penetration demonstrates again that the adsorption of semi-volatile material on PP filters leads to inaccurate estimate of mass penetration. Another observation that can be noted from Figure 4.24 is that the percent penetration measured with tandem PP filters is 3.26 times that measured with tandem PTFE filters. Again, the secondary filter artifact correction is only accurate if the mass of adsorbed vapor is the same on the primary and secondary filter (i.e. they are in "equilibrium"). Because there is no *in-situ* method for determining if the equilibrium adsorption criteria is met, the validity of the artifact correct will never be known without a secondary measurement such as the SMPS.

Figure 4.25 shows a comparison of the mass collected on the PP and PTFE filters. The mass collected on the secondary PTFE filters as a fraction of the mass collected on the primary PTFE filters was 0.006 upstream of the respirator and 0.05 downstream of the respirator. On the other hand, mass collected on the secondary upstream and downstream PP filters as a fraction of the mass collected on the primary upstream and downstream PP filters was 0.06 and 0.72 respectively. These

values are considerably high in comparison to the fraction of mass on secondary PTFE filters, further confirming that the adsorption of semi-volatile material is significant for PP filters.

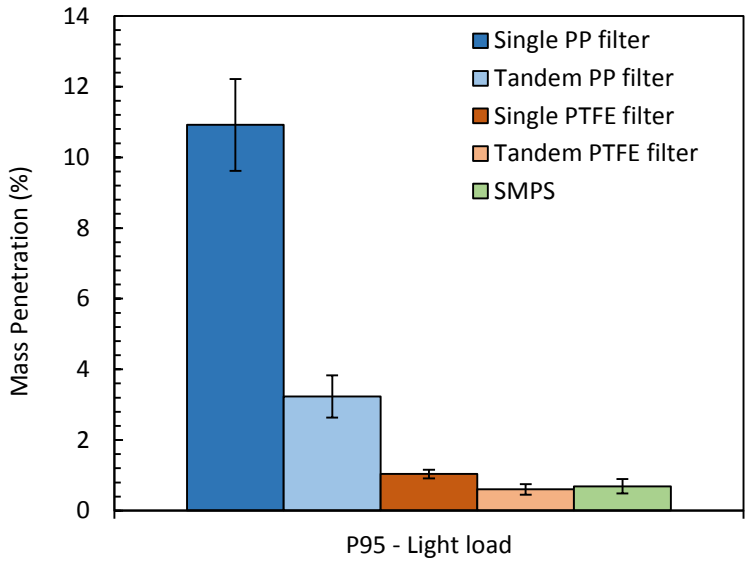

Figure 4.24 Mass penetration of P95 respirator measured at light load (Engine 2) using (a) gravimetric method with and without artifact correction, and (b) SMPS

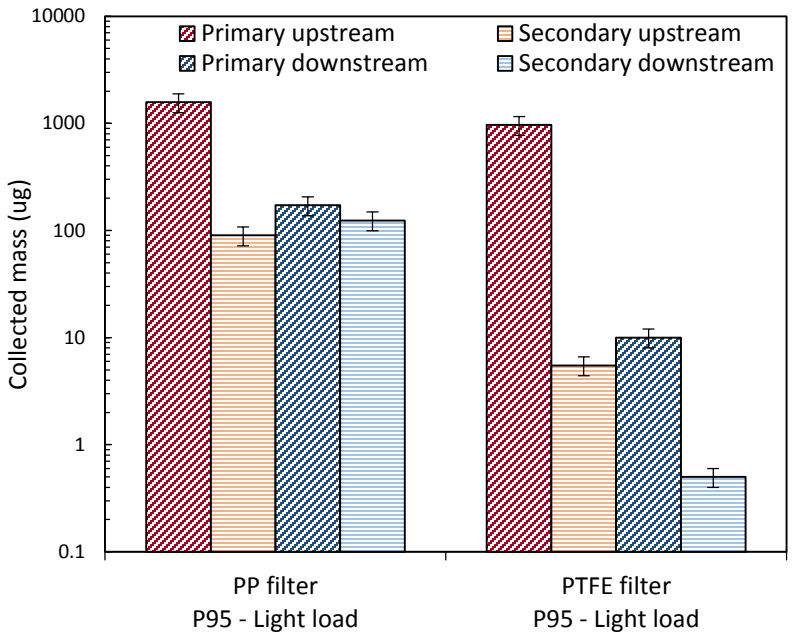

Figure 4.25 Mass collected on PP and PTFE filters with Engine 2 at light load as the aerosol source.

4.2.4 Limitations of gravimetric analysis for penetration measurement

(i) Gravimetric measurements with analytical filters requires a minimum amount of mass to be collected on the filters for accurate mass measurements using a microbalance. Mass collected on the filters is dependent on the aerosol concentration and the collection time. In order for the mass collected to be greater than the minimum required for accurate mass measurements, either the aerosol concentration, the collection time, or both should be sufficiently high. If we choose a high aerosol concentration, it will not be representative of the occupational exposure limits for that aerosol. If we increase the collection time, laboratory tests become unreasonably long. Therefore, gravimetric measurements involve a trade-off between aerosol concentration and collection time.

(ii) Gravimetric analysis is highly sensitive to the composition of the test aerosol. As we observed in the previous section, the presence of semi-volatile material in the test aerosol adversely affects gravimetric measurements due to filter artifacts, producing to inaccurate penetration results.

(iii) Gravimetric measurements do not take into consideration the size of particles in the test aerosol.

(iv) Gravimetric analysis cannot be used to monitor the penetration of respirators continuously for a certain period of time. It can be used to measure only the average penetration for a test.

All in all for gravimetric analysis, PTFE or similar filters should be used with precautions taken to check for filter artifacts.

Part II

Development and testing of a standard method to generate Diesel exhaust for the evaluation of filters and respirators

Chapter 5
CONCEPT, DESIGN AND EXPERIMENTAL SETUP

5.1 Concept

The previous chapter emphasizes the difference in the behavior of respirators when challenged with Diesel exhaust generated at different engine operating conditions. We also observed that the behavior of respirators with Diesel exhaust is different from that with NaCl or DOP aerosols. Figure 5.1 shows that mass penetration of R-95 and P-95 respirators for DOP is much less than that for Diesel exhaust generated from Engine 1 at light load.

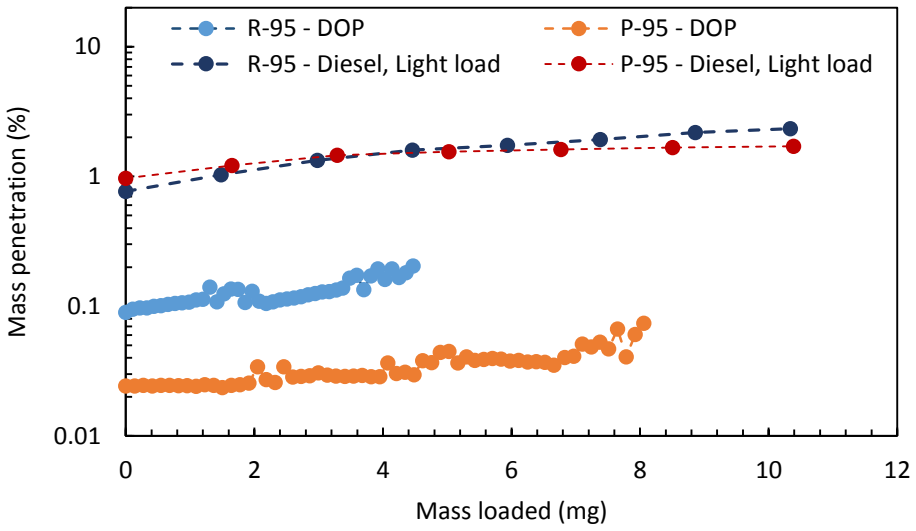

Figure 5.1 Comparison of mass penetration of R-95 and P-95 FFRs for DOP and Diesel exhaust at light load from Engine 1

The current NIOSH standard testing procedure for evaluating the filtration efficiency of air-purifying respirators recommends using the TSI model 8130 Automated Filter Tester or equivalent instrument with NaCl and DOP as the test aerosols. However, this method is not easily adaptable to evaluate the filtration efficiency of respirators challenged with Diesel exhaust. In the previous

chapter, we also observed that the filtration efficiency of electret respirators is strongly influenced by the EC/OC ratio in Diesel exhaust, with a maximum when the OC concentration was minimum. With engine 1 at light load with high OC and no soot mode evident in the size distribution, penetration increased with filter loading and exceeded 5% with moderate loading. On the other hand at heavy load where a soot mode was evident in the size distribution, the penetration stayed nearly constant at around 1%. There is a need for a "standard" Diesel exhaust aerosol that can be used to test various types of filters and respirators. With this goal in mind, the methodology outlined below was conceptualized. The following method accounts for the complex nature of diesel exhaust and provides a realistic exposure but yet standardizes many components of the measurement to make it easily replicable.

DPM has characteristics that depend on operating and sampling conditions in complex ways. These characteristics have the potential to significantly impact the measurement of filtration efficiency if not fully controlled or understood. Some of these are listed below.

(a) EC to OC ratio (roughly the ratio of solids to semi-volatile material) in diesel exhaust – This is dependent on engine design, fuel, and engine load. Biodiesel fuels tend to produce a lower EC to OC ratio while higher engine loads generally have a higher EC to OC ratio.

(b) Particle size distribution – The dilution ratio and residence time influence the partitioning of semi-volatile materials between formation of nucleation mode particles, adsorption onto existing solid accumulation mode particles, or remaining in the gas phase.

(c) Particle morphology – The formation of solid carbon aggregates depends on engine technology (fuel-air temperature, composition, time history) and operating conditions (e.g., speed, load, EGR rate) while the formation of spherical nucleation particles depends on sampling conditions and the presence of semi-volatile materials from the fuel and the lubricating oil, and the ratio of semi-volatile material to the amount of soot in the accumulation mode.

The methodology outlined here enables us to achieve a high degree of control over the characteristics of engine out particles described above. By controlling the EC to OC ratio in the exhaust, the dilution ratio and the residence time, diesel particulate matter (DPM) with a specific set of properties can be obtained nearly independently of the diesel engine used to generate exhaust.

The following procedure is aimed to be replicable with most commercially available diesel engines which may differ in power rating and capacity. Since it is not feasible to obtain the required EC to

OC ratio in diesel exhaust from different engines at the same (load, rpm) engine set points, known concentrations of EC and OC aerosols will be generated separately and combined at a later stage to form the test aerosol.

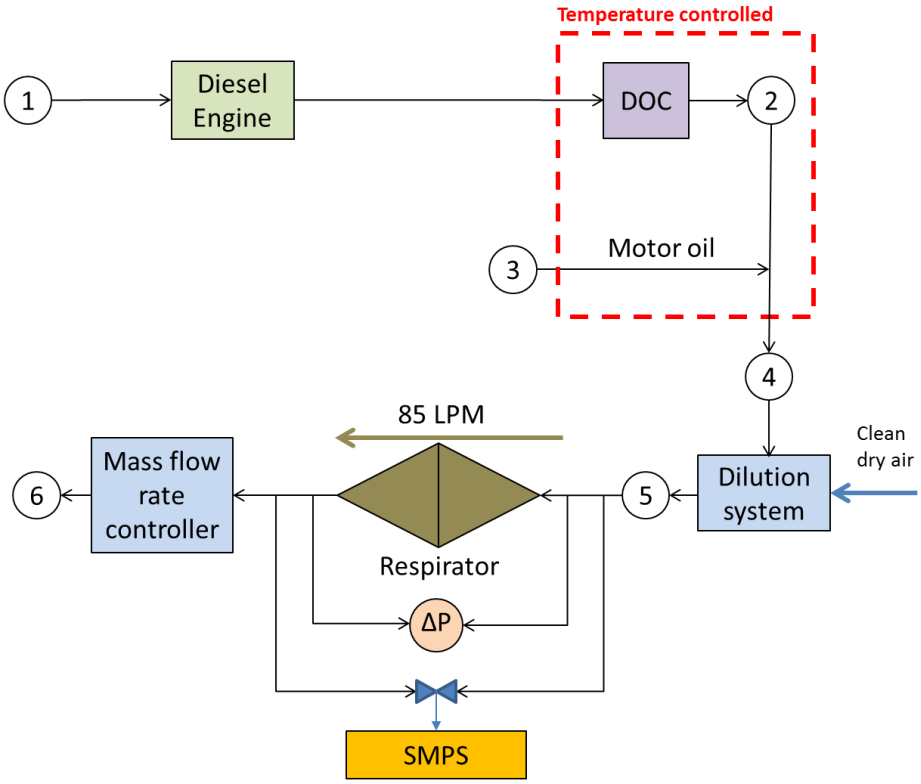

Figure 5.2 Conceptual schematic diagram for generating Diesel exhaust with required properties

A modern Diesel engine with low lube oil consumption is used as the source of EC, assuming that most modern Diesel engine produce carbon aggregates of a similar size (60 – 80 nm). Exhaust from the engine is treated with an oversized diesel oxidation catalyst (DOC), which is designed to oxidize all of the organic compounds in the exhaust. The aerosol flowing out of the DOC will consist mainly of dry black carbon particles which is later mixed with a known quantity of organic carbon. This enables us to control the EC/OC ratio in the test aerosol effectively. The mixture of EC aerosol and OC vapor is made to pass through a dilution system which facilitates adsorption or condensation of OC vapors onto the surface of soot particles, to create the required test aerosol. To

ensure that the adsorption of OC is independent of the dilution air temperature, an OC compound with low volatility is chosen for the test so that nearly all the OC will be in the particle phase. The extent of dilution or the dilution ratio depends on the EC mass concentration and EC/OC required in the test aerosol. This test aerosol is then used to challenge respirators. The penetration of respirators is determined by using the SMPS to measure particle size distributions upstream and downstream of the respirators.

5.2 Design and operation

The system described below is an oxidation-dilution tunnel designed by Trevor Edgeworth, Keith Koppen, Robert Mclean and Brandon Sohn, students of Minnesota State University, Mankato. It was designed with the objective of converting exhaust from a Diesel engine to the required test aerosol with a controlled EC concentration, mass flow rate and EC/OC ratio. Figure 5.3 shows the prototype design and Figure 5.4 shows a two dimensional view of the longitudinal cross-section of the device.

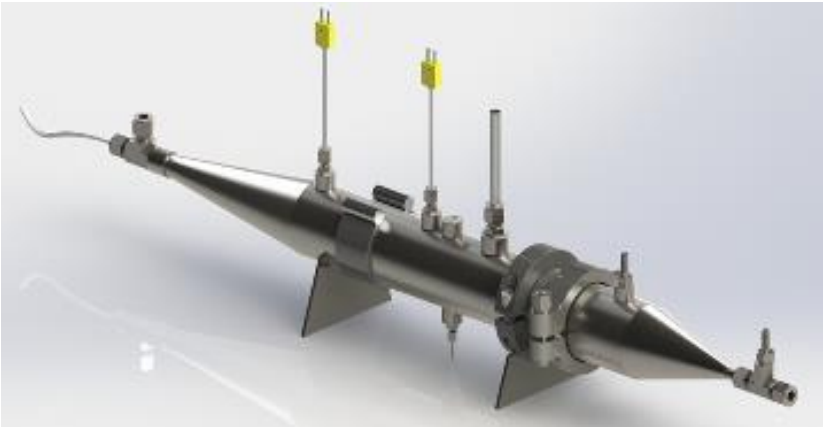

Figure 5.3 Design of the oxidation-dilution tunnel

The oxidation-dilution tunnel is a hollow cylindrical device of about 1.3 m in length, 0.1 m diameter resting on two support legs (Figure 5.3). It consists of an entrance cone of approximately 15^{o} in angle, with an inlet for Diesel exhaust near the narrow end. Inside the entrance cone is a cartridge heater to preheat the sampled exhaust. The cartridge heater has the following specifications: power rating 525 W, length 18 cm, diameter 0.635 cm. It is controlled by a temperature controller that

receives feedback from the primary thermocouple. Following that is a diesel oxidation catalyst (DOC) to remove semi-volatile material from Diesel exhaust. The temperature of the DOC is maintained sufficiently high by a band heater (clamped externally on the device) for complete oxidation of semi-volatile material in Diesel exhaust. The temperature of a band heater is controlled by a temperature controller that receives feedback from the secondary thermocouple. Downstream of the DOC, there is an inlet for adding an external source of OC to the oxidized Diesel exhaust aerosol. Following this, there is an inlet for clean, dry air to dilute the mixture to facilitate the condensation of OC and to obtain the required flow rate for the test aerosol. Pressure taps at the ends of the exit cone enable measurement of pressure drop and its correlation to flow rate.

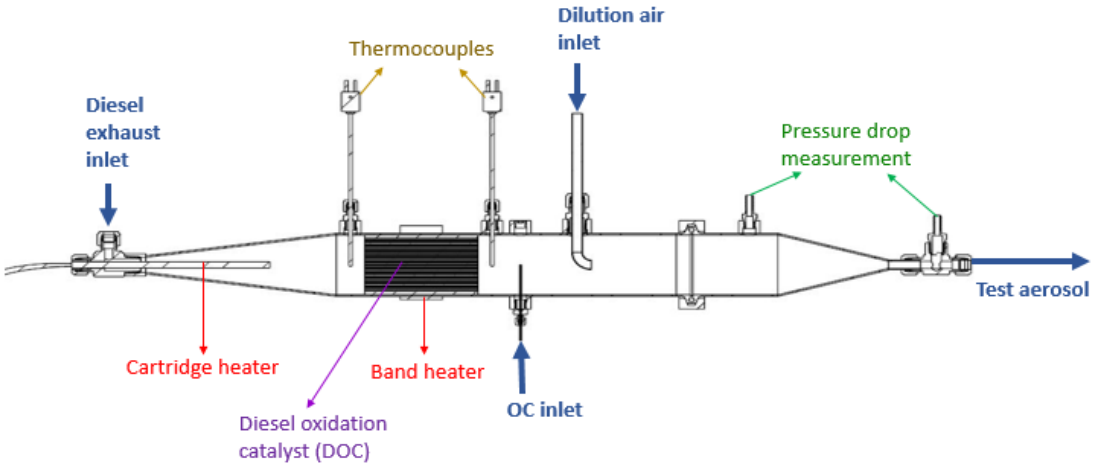

Figure 5.4 Cross-sectional outline view of the oxidation-dilution tunnel

5.3 Experimental setup and procedure

The experiments conducted in this part of the study consist of measurements with solid Diesel exhaust aerosol only.

5.3.1 Calibration of flow rate

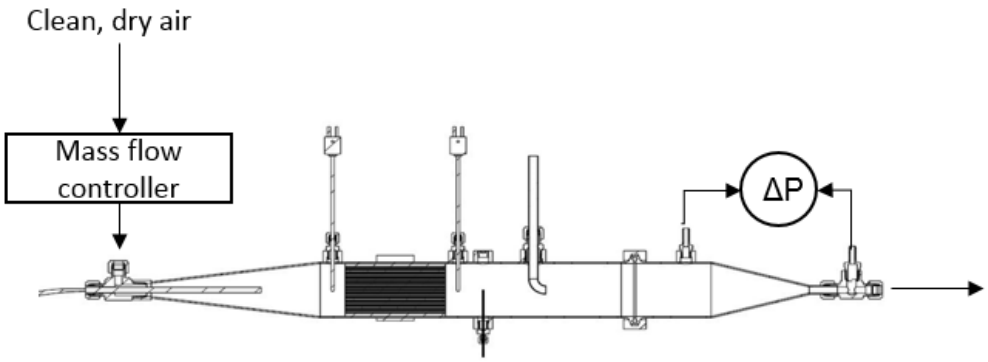

Figure 5.5 Experimental setup for flow calibration in the oxidation-dilution tunnel

Flow rate through the device was calibrated with clean, dry air. A known flow rate of air controlled using a mass flow controller (Alicat Scientific MCR-250SLPM) was connected to the inlet of the device (Figure 5.5). Pressure drop near the exit of the device was recorded using a differential pressure gauge, with the OC inlet and dilution air inlet closed. This was performed for air flow rates from 20 L/min to 130 L/min. Pressure drop was plotted against volume flow rate of air.

5.3.2 Calibration of EC concentration

Once the pressure gauge near the exit is calibrated for volume flow rate, the reading on the pressure gauge is maintained at the value corresponding to a flow rate of 85 L/min. Calibration of the system for EC concentration involves using the SMPS to measure particle concentration at the exit of the device. Figure 5.6 shows a schematic of the experimental setup for EC calibration. Exhaust from the Diesel engine (Engine 3 – see section 2.2) enters the device and is preheated by the cartridge heater. The temperature of the heater is maintained at 250 C using a temperature controller attached to the primary thermocouple through a feedback mechanism. The pre-heating stage is followed by the oxidation of semi-volatile material in the exhaust by the DOC. The temperature of the DOC is maintained at 350 C using a band heater which is controlled by a temperature controller connected to a feedback thermocouple downstream of the DOC. The resulting aerosol is then diluted by a

controlled flow rate of clean dry air. The SMPS draws a sample of the diluted aerosol at the exit of the device. Downstream of the device, there is a gate valve and a vacuum pump. The valve opening is adjusted so that the differential pressure gauge reading near the exit of the device corresponds to a flow rate of 85 L/min. To obtain the required EC concentration at the exit of the device, the dilution air flow rate is set to a certain value using the mass flow controller such that the SMPS reading indicates a total particle mass concentration of around 176 µg/m^3. This value was chosen keeping in mind the permissible exposure limit (PEL) for EC in underground mines according to the Mining Safety and Health Administration (MSHA). Different values of EC concentration could also be chosen according to the application for which filters or respirators are being evaluated. The device is calibrated for three engine conditions: light, medium and heavy load.

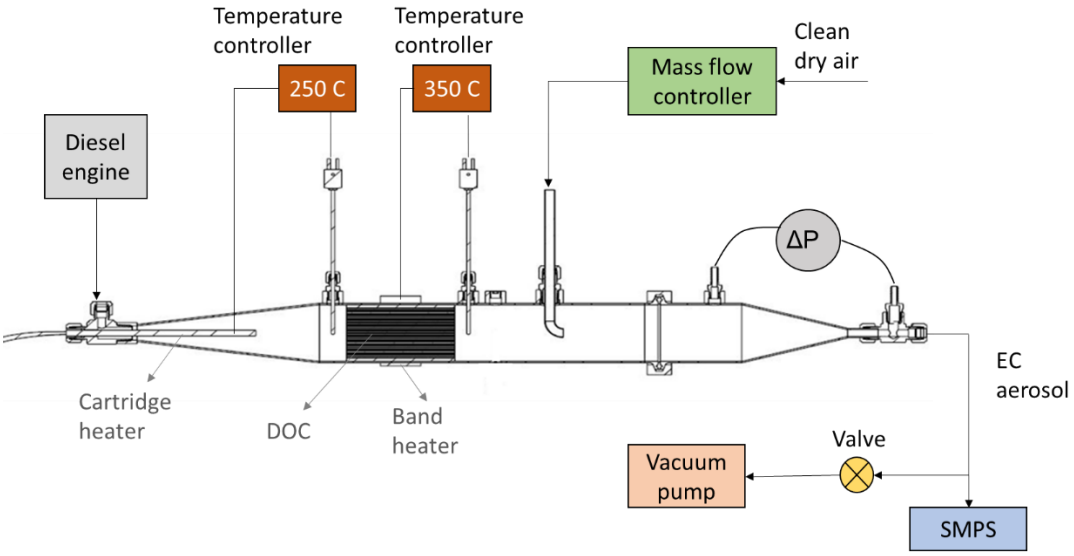

Figure 5.6 Experimental setup for calibration of EC at the exit of the dilution tunnel

5.3.3 Measurement of penetration

Figure 5.7 shows a schematic of the experimental setup for the measurement of penetration (refer to Appendix III for images). It is similar to the setup for calibration of EC concentration, with the inclusion of the respirator test chamber downstream of the device. The test EC aerosol with a controlled flow rate and particle mass concentration was challenged on to the respirator. Particle

size distributions were measured upstream and downstream of the respirator with an SMPS. The aerosol and sheath flow rates were 1.5 L/min and 10 L/min respectively. The size distribution measurement range was set to 7.23 nm to 294.24 nm with a 90 s upscan and a 20 s downscan. A 3-way valve was used to switch between upstream and downstream aerosol measurements. Three tests were conducted for the R-95 and P-95 respirators at both light and medium load conditions. Each test lasted for a duration of 60 minutes.

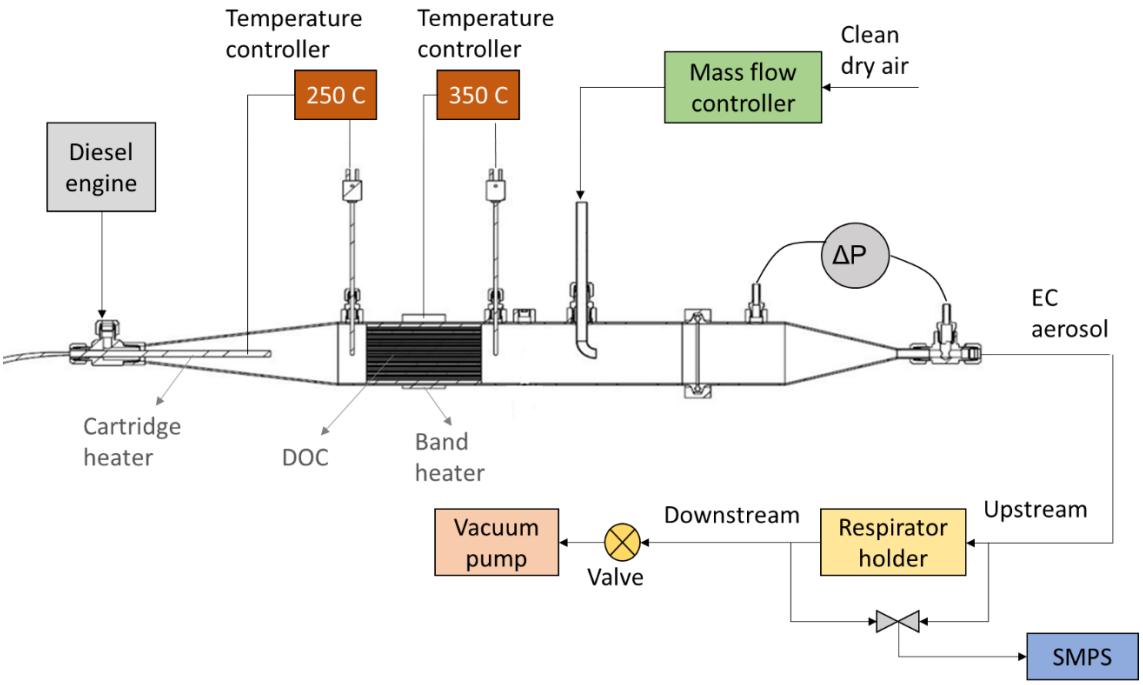

Figure 5.7 Experimental setup for measurement of penetration with Diesel exhaust from Engine 3

Chapter 6
RESULTS AND DISCUSSION

6.1 Calibration results

6.1.1 Flow rate calibration results

Figure 6.1 shows a plot of pressure drop near the exit of the oxidation device versus volume flow rate of air flowing through the device. The equation on the plot represents the curve fit for the experimental calibration result. From the plot, the pressure drop corresponding to a flow rate of 85 L/min was found to be 2.6 in H2O.

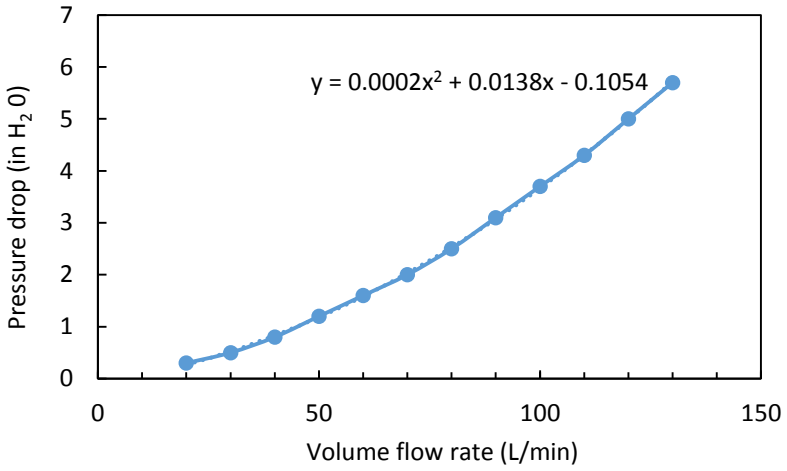

Figure 6.1 Flow calibration curve

6.1.2 EC concentration calibration results

Table 6.1 shows the total EC mass concentrations at the exit of the oxidation device when calibrated at light, medium and heavy load. The values shown are density corrected using a correction method described elsewhere (Park et al., 2003; Swanson et al., 2010). At light load, raw exhaust from the engine has a relatively low particle concentration and the dilution ratio required to obtain the required EC concentration is also lower. Whereas at higher loads, particle concentration in raw

exhaust is much higher. Therefore, higher dilution ratios are used to obtain the required EC particle concentration in the test aerosol. Figure 6.2 shows the number-based size distributions of the test aerosol obtained at the exit of the oxidation device at light, medium and heavy loads. The data points represent average measurements over three samples and the error bars represent standard deviation. The total number-based particle concentration of the test aerosol obtained at the exit of the oxidation-dilution tunnel at light, medium and heavy loads is shown in Table 6.1. From Figures 6.2 and 6.3, we observe that the size distributions of the aerosol at the outlet of the dilution tunnel at light, medium and heavy load overlap closely. The R-95 and P-95 respirators were evaluated at light and medium load conditions.

Table 6.1 Calibrated EC concentrations in the test aerosol and corresponding dilution parameters

Load on engine	EC mass concentration ($\mu g/m^3$)	EC number concentration ($part/cm^3$)	Exhaust flow rate (L/min)	Dilution air flow rate (L/min)	Total flow rate (L/min)	Dilution ratio
Light	137.43	3.38E+06	20	65	85	4.25
Medium	124.4	2.85E+06	17.5	67.5	85	4.86
Heavy	128.72	1.79E+06	14.5	70.5	85	5.86

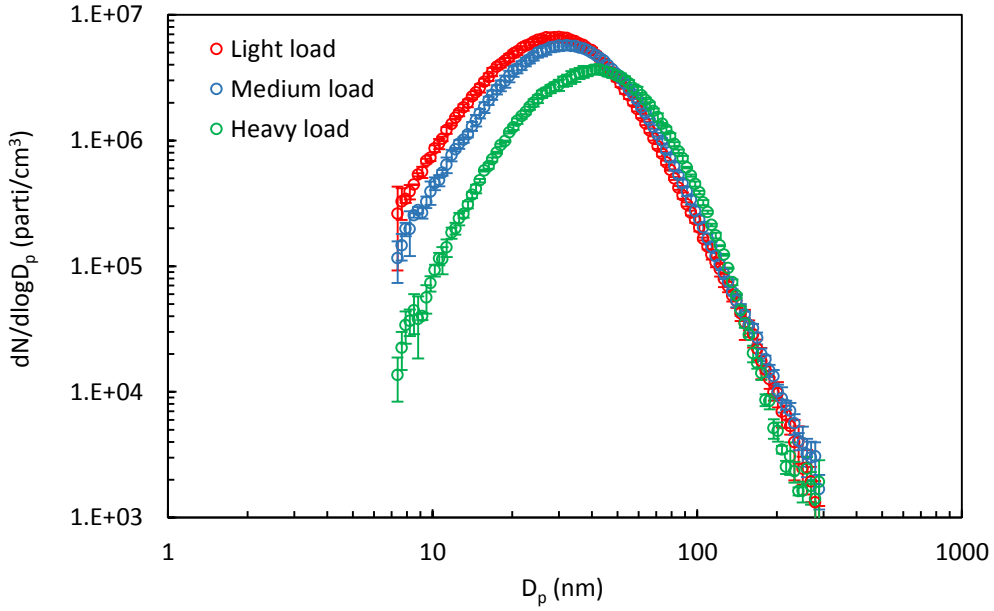

Figure 6.2 Number-based size distribution of solid Diesel exhaust aerosol

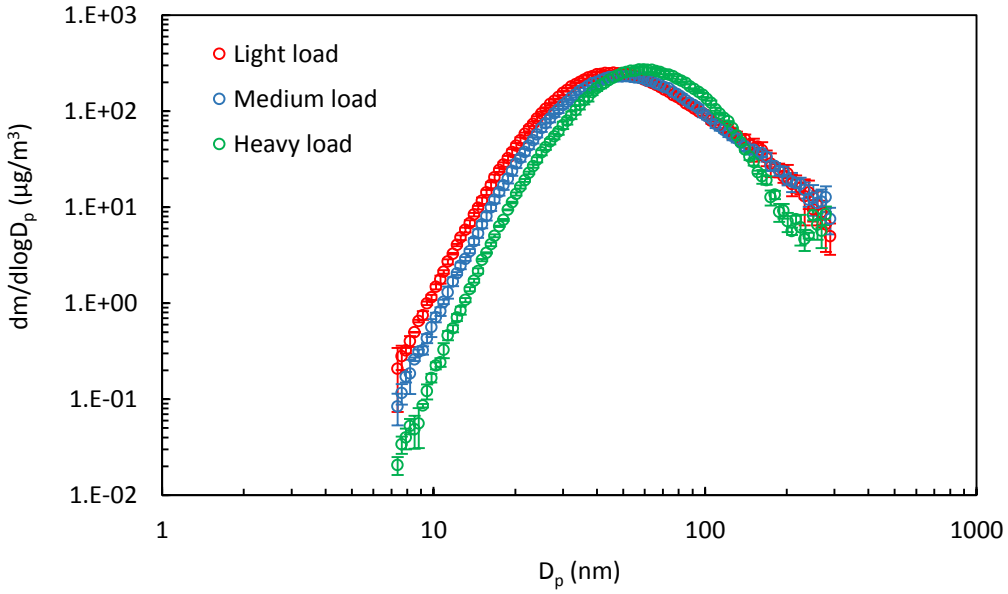

Figure 6.3 Mass-based size distribution of solid Diesel exhaust aerosol

6.2 Particle concentrations upstream and downstream of the respirators

R-95 and P-95 respirators were loaded with the test aerosol for a duration of 60 minutes. Particle concentrations upstream and downstream of the test respirators were measured with an SMPS. Three tests were conducted for each type of respirator at light and medium load. Figure 6.4 shows the variation of number-based particle concentrations upstream and downstream of the R-95 respirator at light and medium load. At light load, fluctuations in the upstream concentration were found to be much higher compared to medium load condition. Table 6.2 shows the upstream number-based and mass-based concentrations for each test conducted. For the R-95 respirator at light load, the maximum standard deviations for the upstream number-based and mass-based concentrations were found to be 9.4% and 18.4% respectively. This is relatively higher compared to the maximum standard deviation in upstream particle concentrations at medium load for measurements with R-95 respirator. At medium load, the upstream concentration was found to be more stable during the course of the tests. The maximum standard deviation in upstream number-based and mass-based concentrations were 9.4% and 5.1% respectively.

Similarly for the P-95 respirator tested at light load, the maximum standard deviations in upstream number-based and mass-based particle concentrations were 33.7% and 39.7%. These are considerably high compared to the standard deviation in upstream particle concentration at medium load. At medium load, the maximum standard deviations observed in upstream number-based and mass-based concentrations were 7.9% and 6.9%. This behavior is typical for Diesel engines running at light load.

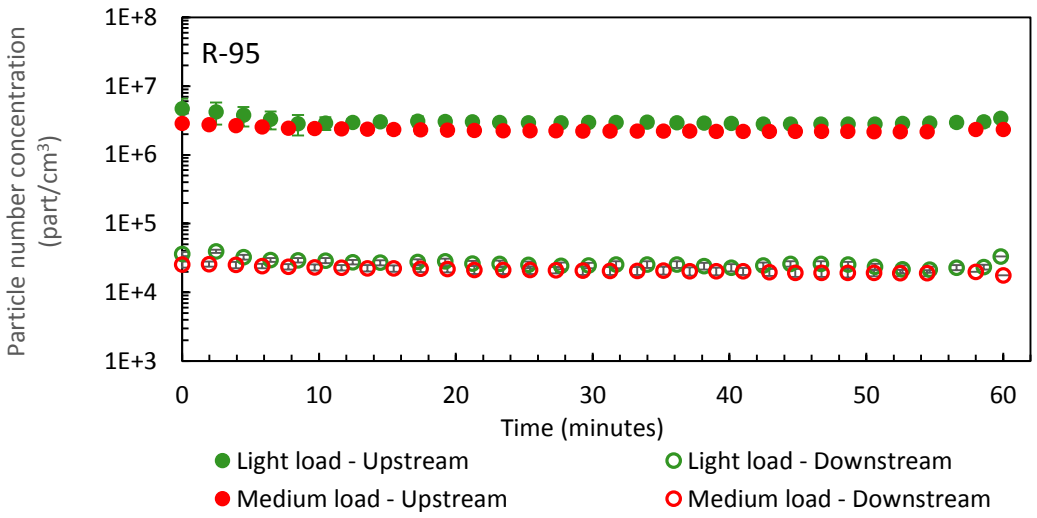

Figure 6.4 Number-based upstream and downstream particle concentrations for R-95 respirator

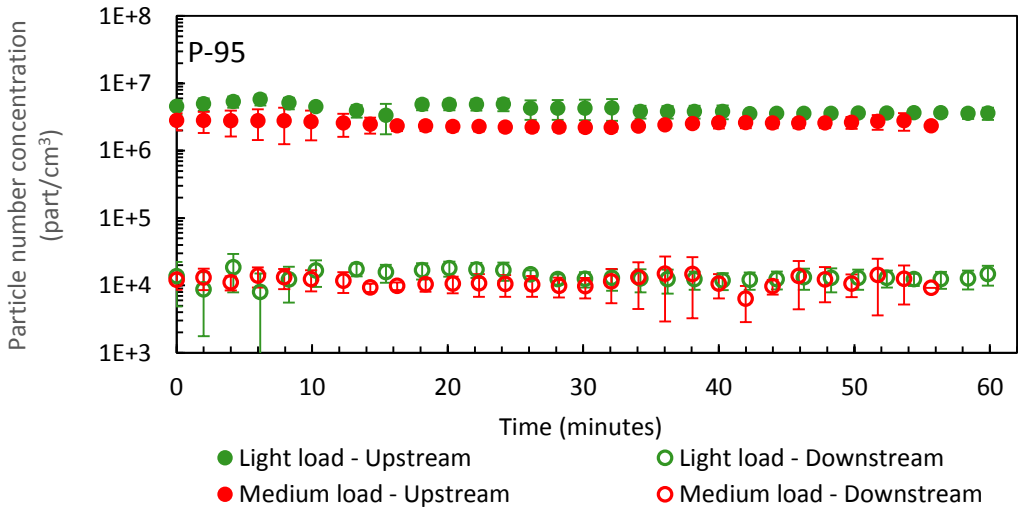

Figure 6.5 Number-based upstream and downstream particle concentrations for the P-95 respirator

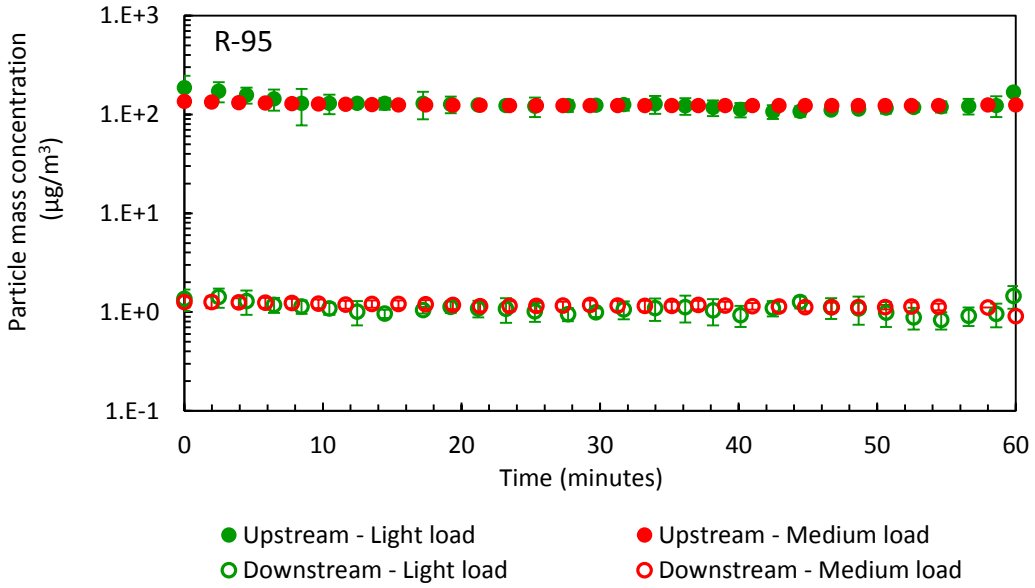

Figure 6.6 Mass-based upstream and downstream concentrations for the R-95 respirator

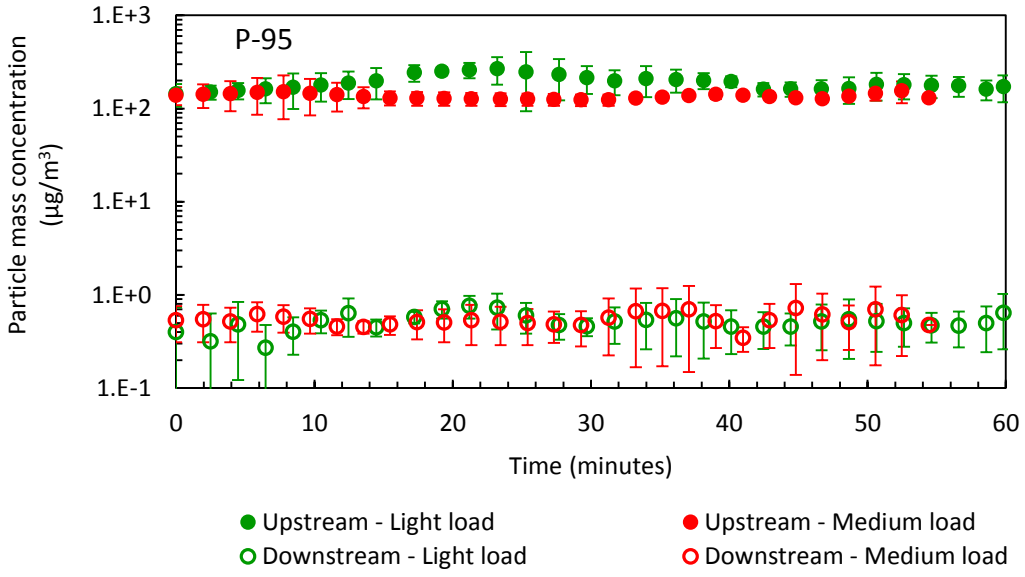

Figure 6.7 Mass-based upstream and downstream particle concentrations for the P-95 respirator

Table 6.2 Number-based and mass-based particle concentrations of solid Diesel exhaust test aerosol

solid Diesel exhaust aerosol	**Test 1**		**Test 2**		**Test 3**	
	average	standard deviation (%)	average	standard deviation (%)	average	standard deviation (%)
			R-95, Light load			
Number concentration (#/cm3)	3.05E+6	9.42	3.23E+6	9.41	2.99E+6	8.31
Mass concentration (µg/m3)	133	18.2	125	18.4	124	15.2
			R-95, Medium load			
Number concentration (#/cm3)	2.55E+6	5.48	2.09E+6	9.36	2.31E+6	7.87
Mass concentration (µg/m3)	125	0.84	116	5.09	133	4.04
			P-95, Light load			
Number concentration (#/cm3)	4.21E+6	8.80	4.17E+6	31.7	4.16E+6	25.5
Mass concentration (µg/m3)	209	22.7	201	39.7	166	24.2
			P-95, Medium load			
Number concentration (#/cm3)	2.28E+6	7.89	2.41E+6	7.25	2.82E+6	6.27
Mass concentration (µg/m3)	117	6.87	135	3.90	152	5.62

The particle concentrations downstream of the respirator remain almost unchanging with time for all cases. For both R-95 and P-95 respirators, the downstream particle concentrations were similar for light and medium load conditions. For the R-95 respirator, the time-average downstream particle mass concentrations at light and medium load were 1.08 µg/m3 and 1.16 µg/m3. For the P-95 respirator, the time-averaged mass-based particle concentrations downstream of the respirator at light and medium load were 0.51 µg/m3 and 0.55 µg/m3 respectively.

6.3 Number-based penetration

Number-based penetration was calculated as the percentage of downstream number-based particle concentration to the upstream number-based particle concentration. In Figure 6.8, number

penetration of the R-95 and P-95 respirators are shown on the y-axis, with mass loaded on to the respirators on the x-axis. Mass loaded is calculated as shown in equation (4-a).

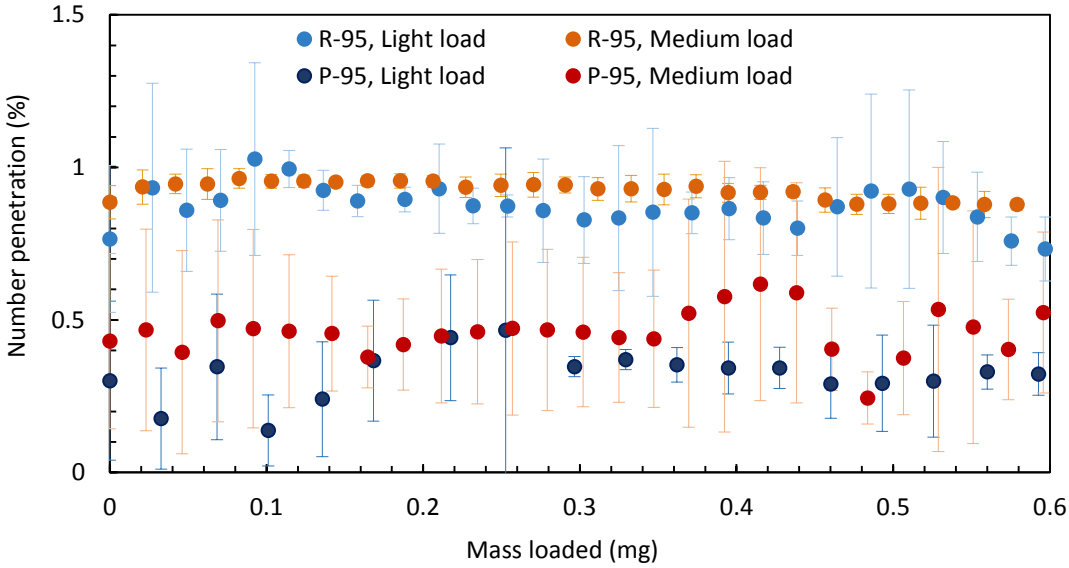

Figure 6.8 Number-based penetration results for the R-95 and P-95 respirators

Number-based penetration was found to be fairly constant during the course of the test, and less than 1% for all cases, with a few fluctuations. The time-averaged number-based penetration of the R-95 respirator was 0.86 ± 0.18% at light load and 0.91 ± 0.05% at medium load. For the P-95 respirator, the time-averaged number penetration at light and medium load were 0.32 ± 0.12% and 0.45 ± 0.22% respectively. Thus the P-95 respirator is more efficient for solid Diesel exhaust aerosol than the R-95 respirator.

6.4 Mass-based penetration

Mass-based penetration was calculated as the percentage of mass-based particle concentration downstream of the test respirators to the mass-based particle concentrations upstream of the respirators. Results were found to be similar to number-based penetration results. The time-averaged mass-based penetrations of the R-95 respirator were 0.85 ± 0.15% and 0.94 ± 0.03% at light and medium load respectively. For the P-95 respirator, the time-averaged mass-based

penetration at light and medium load were 0.25 ± 0.12% and 0.40 ± 0.25% respectively (Figure 6.9).

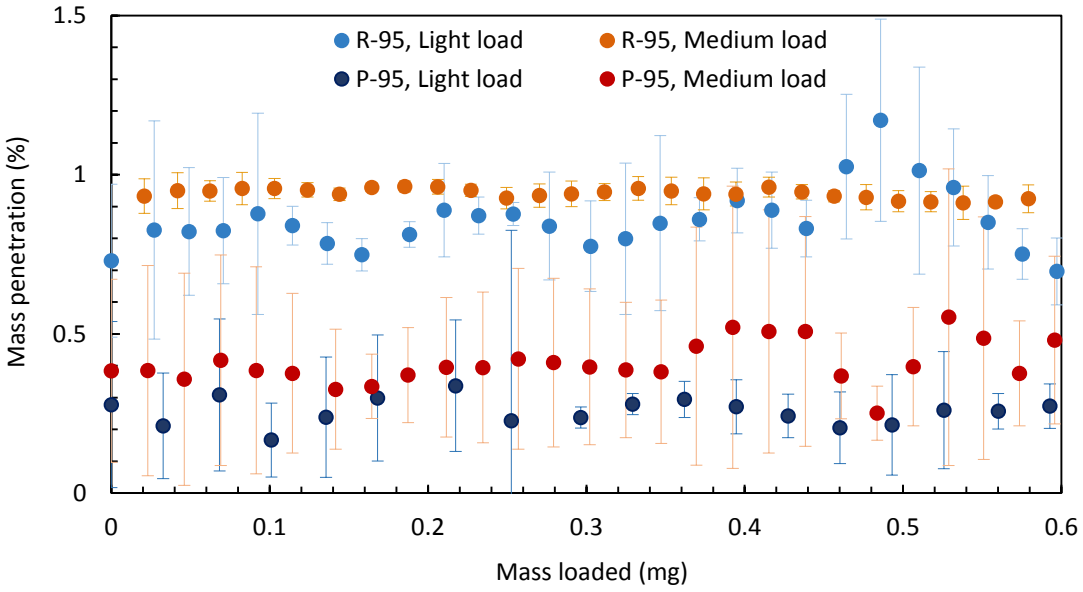

Figure 6.9 Mass-based penetration results for the R-95 and P-95 respirators

6.5 Size-based penetration

Figure 6.10 shows the size-based penetration curves for the R-95 and P-95 respirators at light and medium load, with penetration on the y-axis and particle mobility diameter on the x-axis. Size-based penetration curves were different for the R-95 and P-95 respirators. In the case of the R-95 respirator, the MPPS was found to be 30 nm and 41.4 nm at light and medium loads with a maximum penetration of 1.14 ± 0.13% and 1.19 ± 0.04% respectively. For the P-95 respirator, the MPPS was found to be much lower: 10.9 nm and 11.8 nm at light and medium loads with a maximum penetration of 0.49 ± 0.21% and 0.63 ± 0.35% respectively. Unlike the size penetration curve for the R-95 respirator, the size-based penetration curve for the P-95 respirator is almost flat, implying that particles of all sizes have similar penetration in the case of the P-95 respirator. It should also be noted that the size penetration curves for both R-95 and P-95 respirator shift slightly towards the right at medium load. This could be due to differences in particle density and morphology at light and medium load.

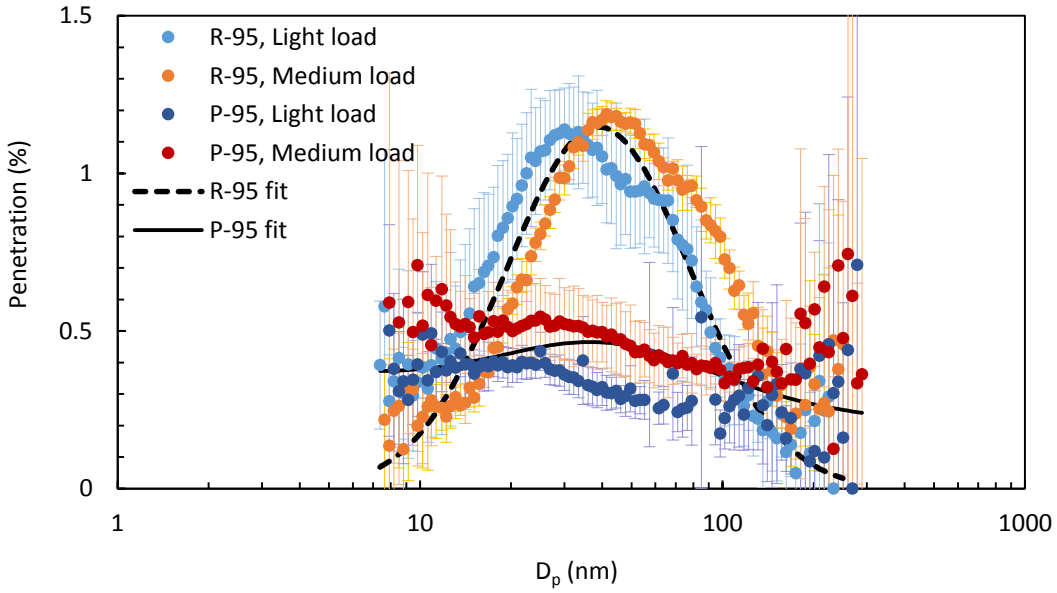

Figure 6.10 Size-based penetration results for the R-95 and P-95 respirators

Implications

Figure 6.10 also shows the curve fits for the size-based penetration curves of the R-95 and P-95 respirators. The curve equation is lognormal and was obtained by trial and error to get the best fit for the average of the size-based penetration curves at light and medium load conditions. This was used to estimate the variability in penetration of the respirators due to the influence of certain uncontrolled factors.

In our experiments, the controlled parameters of Diesel exhaust test aerosol were EC concentration and total flow rate. The methodology used in this study can be replicated easily to produce solid Diesel exhaust from most commercially available engines. An important assumption for this was that most modern engines have a size distribution with a geometric mean diameter (D_g) of 30 nm – 70 nm. In order to test the sensitivity of penetration, let us assume that D_g for solid Diesel exhaust aerosol varies in the range of 10 nm – 100 nm. Figure 6.11 shows possible number-based size distribution curves for solid Diesel exhaust aerosol represented by lognormal curves with a geometric standard deviation (σ_g) of 1.6 and CMD ranging from 10 nm to 100 nm. Applying the size-based penetration fit of the R-95 and P-95 respirators to these curves, we obtain the overall

penetration of the respirators for each case of test aerosol size distribution. Figure 6.12 shows a plot of mass penetration versus D_g of solid Diesel exhaust size distribution. The R-95 respirator shows more variability in penetration with varying D_g of test aerosol compared to the P-95 respirator. Penetration is higher for the respirators when D_g of test aerosol is close to the MPPS of the respirators. However, respirator penetration is less than 1% for all cases and well within the maximum allowed penetration limit of 5%.

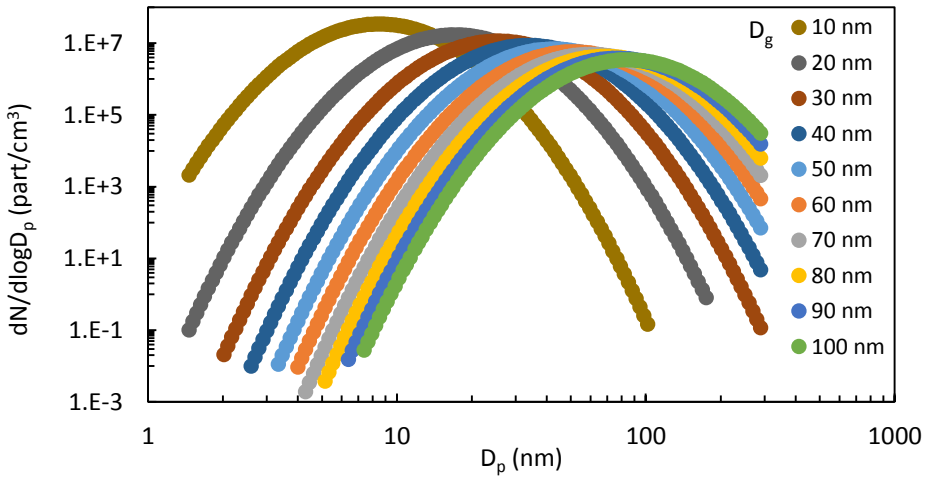

Figure 6.11 Possible solid Diesel exhaust number-based particle size distributions with D_g ranging from 10 nm – 100 nm

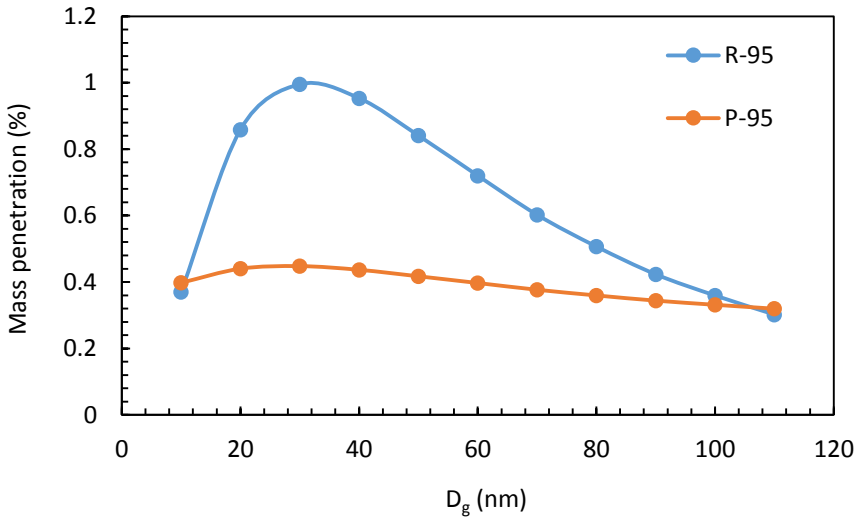

Figure 6.12 Influence of geometric mean diameter (D_g) of test aerosol on penetration of the R-95 and P-95 respirators

Another variability in solid Diesel exhaust aerosol generated is the particle morphology. According to Park et al. (2003), the mass mobility coefficient (fractal dimension) of soot (30 – 300 nm) generated from a Diesel engine similar to Engine 3 can vary from 2.3 to 2.4 with changes in load on the engine. Results from Kim et al. (2009) showing the dependence of filter penetration on particle morphology (Figure 6.13) were applied to three hypothetical cases of filters. Penetration can be calculated from single fiber efficiency by assuming certain filter parameters. According to Hinds (1999):

$$P = \exp\left(-\frac{4\alpha E_{\Sigma} t}{\pi(1-\alpha)d_f}\right) \quad (6\text{-a})$$

$$\text{or,} \quad P\,(\%) = \exp(-CE_{\Sigma}) * 100 \quad (6\text{-b})$$

$$\text{and} \quad C = \frac{4\alpha t}{\pi(1-\alpha)d_f} \quad (6\text{-c})$$

In the above equations, P denotes penetration, α denotes packing density, E_{Σ} denotes single fiber efficiency, t denotes the thickness of the filter or length of the fibers, d_f denotes fiber diameter and C represents a constant value. Filters A, B and C were assumed to have different properties, and hence different constant (C in 6-a) values. The constant (C) values assumed for filters A, B and C were 45, 35 and 15 respectively. The overall penetration of the three filters was calculated for particles with D_f 2.07, 2.25 and 2.95. These results were interpolated to calculate overall penetration for particles with D_f 2.3 to 2.4.

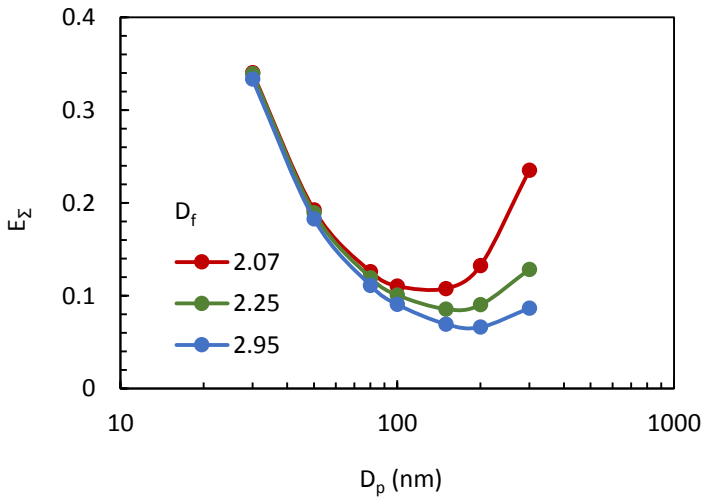

Figure 6.13 Results from Kim et al. (2009) relating particle fractal dimension (D_f) to single fiber efficiency

Figure 6.14 shows the variation in overall penetration for a range of particle fractal dimensions between 2.3 and 2.4 in the test aerosol for filters A, B and C. The changes in penetration with a change in fractal dimension was found to be trivial for all filters. Table 6.4 shows penetration for three filters for particles with fractal dimension 2.3 and 2.4. Filter penetration is lower for particles with a lower fractal dimension because they have greater interception length, resulting in better deposition efficiency.

Table 6.4 Filter penetration for particles of fractal dimension (D_f) 2.3 and 2.4

	Penetration (%)	
Filter	**D_f = 2.3**	**D_f = 2.4**
A	0.362	0.397
B	1.069	1.140
C	11.336	11.585

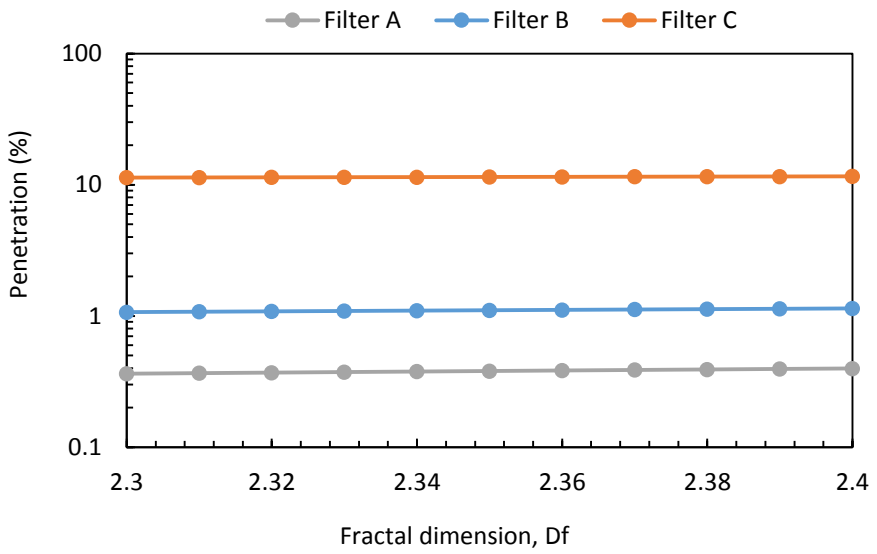

Figure 6.14 Variation of filter penetration for particles (30-300 nm) with a range of D_f from 2.3 to 2.4

6.6 Challenges and limitations

(i) Charge distribution of the test aerosol plays a major role in the deposition of particles on electret filters and respirators. In this study, the charge distribution of Diesel exhaust is not controlled. Results from a previous study indicate that accumulation mode particles (or soot particles) follow the Boltzmann charge distribution (Jung and Kittelson, 2007). But the total charge in the test aerosol varies from engine to engine and is different for different loads on the engine, which in turn influences respirator penetration.

(ii) The dilution ratio in the oxidation device should ideally be less than 6. For Diesel engines with a high exhaust particle concentration, higher dilution ratios are required. When the dilution flow rate is higher (> 75 L/min), the exhaust flow rate decreases and error in flow measurement becomes significant. A possible solution would be to use a dilutor before the inlet of the oxidation device.

(iii) The device can be used successfully to obtain solid Diesel exhaust aerosol with a controlled set of properties. However, experiments with introduction of OC into the device were not performed. It is extremely challenging to ensure that the required quantity of OC aerosol condenses onto the soot particles. Preliminary evaluations involving addition of OC into the device using a syringe pump indicated that OC should be added at 18 nL/min – this alone would take about 20 minutes to enter the device. After the addition of OC, losses within would have to be determined. It would also be challenging to determine what portion of OC has condensed onto the soot particles in the resulting aerosol and what portion is present independently.

Chapter 7

CONCLUSIONS

This study was performed with the objective of measuring the penetration of filtering facepiece respirators for Diesel exhaust using different methodologies and in the process, understand the various factors that influence penetration. Two models of respirators were used in this study: R-95 and P-95 particulate respirators which are certified by NIOSH to be at least 95% efficient for solid and oily aerosols. Penetration measurements were performed using two techniques: particle counting method with the SMPS, and gravimetric analysis with PP and PTFE analytical filters. As a precursor to experiments with Diesel exhaust, the test respirators were evaluated for NaCl and DOP aerosols. The SMPS was used to measure the size distributions of the aerosols upstream and downstream of the test respirators, which were then used to calculated penetration. Results showed that the R-95 and P-95 test respirators were more than 95% efficient for both NaCl and DOP aerosols.

SMPS measurements with Diesel exhaust aerosol from Engine 1 challenged on to the test respirators were made at two engine conditions – light load and heavy load. Results show that the respirators behave differently at light and heavy load. At light load, the penetration of the R-95 and P-95 respirators were found to increase rapidly with mass loaded on to the respirators and exceeded 5% after about 30 – 45 minutes. Whereas at heavy load, the penetration did not show any significant variation with mass loaded and was well within the maximum penetration of 5%. This difference could be due to the presence of a high concentration of OC vapor at light load - Engine 1 was found to have high OC emissions due to excessive consumption of lube oil, which is atypical for a commercial Diesel engine. This led to the hypothesis that the EC/OC ratio in Diesel exhaust influences respirator penetration to a great degree, although the exact processes that occur when OC vapor/particles interact with respirator fibers are not fully understood.

Gravimetric analysis was performed to measure penetration of the test respirators for Diesel exhaust generated from Engines 1 and 2. It was observed that gravimetric measurements with PP filters for Engine 1 resulted in an overestimated of penetration values when compared to SMPS measurements. This was attributed to the presence of artifacts due to adsorption of semi-volatile

material in Diesel exhaust by the PP filters. As a correction method for filter artifacts, tandem PP filters were placed upstream and downstream of the respirators following the assumption that the primary filter collects both particles as well as semi-volatile material in the gas phase, and the secondary filter collects only vapor-phase semi-volatile material. The tandem filters method was found to be more effective than using singular upstream and downstream filters, but it still did not agree closely with the SMPS results. Results from measurements with Engine 2 are similar. When PTFE filters were used, filter based penetration measurements were in much better agreement with SMPS measurements, but even with these filters there was evidence of some semi-volatile artifact. Therefore for penetration measurements using gravimetric analysis, PTFE or similar filters should be used with precautions taken to check for filter artifacts.

Penetration of respirators for Diesel exhaust depends on various operating and sampling parameters such as the EC/OC ratio, OC concentration, total mass flow rate of the challenged aerosol, etc. Standard testing aerosols NaCl and DOP aerosols are not representative of Diesel exhaust aerosol for measurement of respirator penetration – therefore, a methodology was developed to produce Diesel exhaust with a controlled set of properties that can be obtained using most commercially available Diesel engines, which led to the design of the oxidation-dilution tunnel. It is a hollow cylindrical device with an embedded DOC which removes all of the semi-volatile material from raw Diesel exhaust aerosol. A known quantity of organic carbon from an external source is added to the "dry soot" aerosol, which is ten diluted to obtain the required particle concentration. Dilution also facilitates the adsorption/condensation of OC on to the soot particles. The device facilitates the control of EC concentration, OC concentration, EC/OC ratio and total volume flow rate of the test aerosol. In this study, the respirators were evaluated using the oxidation-dilution tunnel only for solid Diesel exhaust aerosol. The device was calibrated for a total flow rate of 0.085 m^3/min and a total EC concentration of 176 $\mu g/m^3$. Results from one-hour tests show that the R-95 and P-95 test respirators are more than 95% efficient for solid Diesel exhaust aerosol. For more realistic penetration measurements, 8-hour tests with solid Diesel exhaust aerosol are planned. There are several challenges associated with the oxidation-dilution tunnel, of which the most important one is the process of re-introduction of OC into the device. This requires extensive analysis and testing and could be a possible project in the future. Controlling the vapor-phase and particle-phase OC concentrations in the test aerosol will definitely prove to be a useful tool in understanding the degradation of electret filters and respirators by semi-volatile material.

REFERENCES

Abdul-Khalek IS, Kittelson DB, Graskow BR, Wei Q, Bear F. (1998) Diesel Exhaust Particle Size: Measurement Issues and Trends. SAE J-Automot Eng; 980525.

Abdul-Khalek IS, Kittelson DB, Brear F. (1999) The influence of dilution conditions on diesel exhaust particle size distribution measurements. SAE J-Automot Eng; 991142.

Abdul-Khalek IS, Kittelson DB, Brear F. (2000) Nanoparticle growth during dilution and cooling exhaust: experimental investigation and theoretical assessment. SAE J-Automot Eng; 2000-01-0515.

Bardasz EA, Cowling S, Panesar A, Durham J, Tadrous TN. (2005) Effects of Lubricant Derived Chemistries on Performance of the Catalyzed Diesel Particulate Filters. SAE J-Automot Eng; 2005-01-2168.

Barrett LW, Rousseau AD. (1998) Aerosol loading performance of electret filter media. Am Ind Hyg Assoc J; 59, 532–539.

Baumgartner HP, Loffler F. (1986) The collection performance of electret filters in the particle size range 10 nm–10 µm. J Aerosol Sci; 17, 438–445.

Berardinelli S, Sandy M, Martin SB Jr, Moyer ES. (2001) Performance of N-, Rand P-Series Respirator Filters against Diesel Exhaust. Presented at the American Industrial Hygiene Conference and Exposition, New Orleans, La; Abstracts, p. 70.

Blackford DB, Bostock GJ, Brown RC, Loxley R, Wake D. (1986) Alteration in the Performance of Electrostatic Filters Caused by Exposure to Aerosols. Paper presented at the 4th World Filtration Congress, Royal Flemish Society, Belgium.

Boffetta P, Harris RE, Wynder EL. (1990) Case-control study on occupational exposure to diesel exhaust and lung cancer risk. Am J Ind Med 15:577-591, 108.

Castranova V, Ma JYC, Yang HM, Antonini JM, Butterworth L, Barger MW, Roberts J, Ma JKH. (2001) Effect of exposure to diesel exhaust particles on the susceptibility of the lung to infection. Environ Health Persp; 109, 609e612.

Chase RE, Duszkiewicz GJ, Richert JFO, Lewis D, Maricq MM, Xu N. (2004) PM Measurement Artifact: Organic Vapor Deposition on Different Filter Media. SAE J-Automot Eng; 2004-01-0967.

Eninger RM, Honda T, Adhikari A, Tanski H, Reponen T, Grinshpun SA. (2008) Filter performance of N99 and N95 facepiece respirators against viruses and ultrafine particles. Ann Occup Hyg; 52:385–396.

Fissan HJ, Neumann S, Schurmann G. (1984) Electrostatic enhanced filtration. Aerosols (Eds: Liu BYH, Pui DYH, Fissan HJ); Elsevier Science Publishing, pp. 581–584, New York.

Fujieda S, Diaz-Sanchez D, Saxon A. (1998) Combined nasal challenge with diesel exhaust particles and allergen induces in vivo IgE isotype switching. Am J Respir Cell Mol Biol; 19:507–512.

Garshick E, Laden F, Hart JE, Rosner B, Smith TJ, Dockery DW, Speizer FE. (2004) Lung cancer in railroad workers exposed to diesel exhaust. Environ Health Persp; 112, 1539e1543.

Hansen J, Sato M, Ruedy R, Lacis A, Oinas V. (2000) Global warming in the twenty-first century: an alternative scenario. Proceedings of the National Academy of Sciences of the United States of America; 97, 9875e9880.

Hinds WC. (1999) Aerosol technology: Properties, behavior and measurement of airborne particles (2nd ed). John Wiley & Sons, Inc.

Huang S-H, Chen C-W, Chang C-P, Lai C-Y, Chen C-C. (2007) Penetration of 4.5 nm to 10 μm aerosol particles through fibrous filters. J Aero Sci; 38: 719–27.

Jacobson MZ. (2001) Strong radiative heating due to the mixing state of black carbon in atmospheric aerosols. Nature; 409, 695e697.

Janssen L, Bidwell J. (2006) Performance of Four Class 95 Electret Filters Against Diesel Particulate Matter. Journal of the International Society of Respiratory Protection; Vol. 23, Spring/Summer.

Janssen L, Bidwell J, Mullins H, Nelson T. (2003) Efficiency of Degraded Electret Filters: Part I – Laboratory Testing Against NaCl and DOP before and after Exposure to Workplace Aerosols. Journal of the International Society of Respiratory Protection; Vol. 20 Pgs 71-80.

Jasper W, Hinestroza J, Mohan A, Thompson D, Baker R. (2005) Effect of toluene on filtration performance of electret filter media against di-octyl-phthalate aerosols. J Int Soc Res Prot; 22:97-105.

Jasper W, Hinestroza J, Mohan A, Kim J, Shields B, Gunay M, Thompson D, Baker R (2006) Effect of xylene exposure on the performance of electret filter media. J Aero Sci; 37:903-911.

Jasper W, Mohan A, Hinestroza J, Baker R (2007) Degradation processes in carona-charged electret filter-media with exposure to ethyl benzene. J Engineered Fibers and Fabrics; 2:1-6.

Jung H and Kittelson DB. (2007) Measurement of electrical charge on Diesel particles. Aerosol Sci Tech; 39:12, 1129-1135

Kanaoka C, Emi H, Ishiguro T. (1984) Time dependency of collection performance of electret filters. 1st AAAR Conference; pp. 613–616, Amsterdam: Elsevier.

Kittelson DB (1998). Engines and Nanoparticles: a Review. Journal of Aerosol Science; 29(5): 575-588.

Kittelson DB, Watts WF, Johnson JP. (2002) Diesel Aerosol Sampling Methodology - CRC E-43: Final Report, University of Minnesota, Report for the Coordinating Research Council.

Kittelson DB, Watts WF, Johnson JP. (2006) On-road and laboratory evaluation of combustion aerosols—part1: Summary of Diesel engine results. J Aerosol Sci; 37, 913–930.

Kittelson DB, Watts WF, Johnson, JP, Ragatz A. (2010) A New Method for the Real-Time Measurement of Diesel Aerosol. Contract Final Report, University of Minnesota, Minneapolis, MN. Available at http://www.me.umn.edu/centers/cdr/reports/nioshrealtime.pdf

Lee D, Miller A, Kittelson DB, Zachariah MR. (2006) Characterization of metal-bearing diesel nanoparticles using single-particle mass spectrometry. J Aerosol Sci; Vol.37(1), pp.88-110.

Liu Z, Swanson J, Kittelson DB, Pui, DYH. (2012) Comparison of Methods for Online Measurement of Diesel Particulate Matter. Environ Sci Technol; 46, 6127−6133.

Mader BT, Flagan RC, Seinfeld JH. (2001) Sampling atmospheric carbonaceous aerosols using a particle trap impactor/denuder sampler. Environ Sci Technol; 35 (2001) 4857.

Maricq MM, Chase RE, Xu N, Laing PM. (2002) The effects of the catalytic converter and fuel sulphur level on motor vehicle particulate matter emissions. Environ Sci Technol; 36: 283-289.

Martin SB Jr, Moyer ES. (2000) Electrostatic respirator filter media: filter efficiency and most penetrating particle size effects. Appl Occup Environ Hyg; 15: 609–17.

Moyer ES, Bergman MS. (2000) Electrostatic N-95 respirator filter media efficiency degradation resulting from intermittent sodium chloride aerosol exposure. Appl Occup Environ Hyg; Vol.15(8), pp.600-608.

Nel A. (2005) Air pollution-related illness: effects of particles. Science; 308, 804e806.

Niemi S, Ekman K, Nousiainen P. (2012) Particle number emissions of nonroad Diesel engines of various ages. J Eng Gas Turb Power; Vol. 134 / 092807-1.

Norris G, YoungPong SN, Koenig JQ, Larson TV, Sheppard L, Stout JW. (1999) An association between fine particles and asthma emergency department visits for children in Seattle. Environ Health Persp; 107:489–493.

Oberdorster G. (2001) Pulmonary effects of inhaled ultrafine particles. Int Arch Occ Env Hea; 74, 1e8.

Ohtoshi T, Takizawa H, Okazaki H, Kawasaki S, Takeuchi N, Ohta K, Ito K. (1998) Diesel exhaust particles stimulate human airway epithelial cells to produce cytokines relevant to airway inflammation in vitro. J Allergy Clin Immun; 101, 778e785.

Park K, Cao F, Kittelson DB, McMurry P. (2003) Relationship between Particle Mass and Mobility for Diesel Exhaust Particles. Environ Sci Technol; 37, 577-583.

Patel H, Eo S, Kwon S. (2011) Effects of diesel particulate matters on inflammatory responses in static and dynamic culture of human alveolar epithelial cells. Toxicol Let; 200, 124e131.

Penconek A, Drazyk P, Moskal, A. (2013) Penetration of Diesel Exhaust Particles Through Commercially Available Dust Half Masks. Ann Occup Hyg; Vol.57(3), pp.360-373.

Rengasamy S, Eimer BC and Miller A. (2010) Effects of Organic Solvents on the Laboratory Filtration Performance of Electret N95 and P100 Filtering Facepiece Respirators. J Int Soc Res Prot; Vol. 27, No. 1.

Rengasamy S, Eimer BC, Shaffer RE. (2009) Comparison of nanoparticle filtration performance of NIOSH-approved and CE-marked particulate filtering facepiece respirators. Ann Occup Hyg; 53(2):117-128.

Rengasamy S, King WP, Eimer BC, Shaffer RE. (2008b) Filtration performance of NIOSH-approved N95 and P100 filtering facepiece respirators against 4 to 30 nanometer-size nanoparticles. J Occup Environ Hyg; 5:556–564

Richardson AW, Eshbaugh JP, Hofacre KC, Gardner PD. (2006) Respirator filter efficiency testing against particulate and biological aerosols under moderate to high flow rates. U.S. Army Edgewood Chemical Biological Center Report for Contract No. SP0700-00-D-3180, Task No. 335, ECBCCR-085.

Salvi SS, Frew AJ. (1997) Diesel exhaust particles and respiratory allergy. Clin Exp Allergy; Vol.27(3), pp.237-239

Sappok A, Wong V. (2007) Detailed Chemical and Physical Characterization of Ash Species in Diesel Exhaust Entering Aftertreatment Systems. SAE J-Automot Eng; 2007-01-0318

Swanson JJ, Kittelson DB. (2009) Factors Influencing Mass Collected During 2007 Diesel PM Filter Sampling. *SAE Int J Fuels Lubr;* 2(1):718-729.

Swanson JJ, Kittelson DB, Pui DYH, Watts WF. (2010) Alternatives to the gravimetric method for quantification of diesel particulate matter near the lower level of detection; J Air Waste Manage; Vol.60(10), pp.1177-91.

Swanson JJ, Febo R, Satish S, Pui DYH, Kittelson DB. (2015). Solid particle emissions from small diesel generator engines. *Submitted.*

Teas C, Kalligeros S, Zanikos F, Stournas S, Lois E, Anastopoulos G. (2001) Investigation of the Effectiveness of Absorbent Materials in Oil Spills Clean Up. Desalination; 140, 3, 259-264.

Tennal KB, Mazumder MK, Siag A, Reddy RN. (1991) Effect of loading with an oil aerosol on the collection efficiency of an electret filter. Particul Sci Technol; 9, 19–29.

Turpin B J, Saxena P, Andrews E. (2000) Measuring and simulating particulate organics in the atmosphere: problems and prospects. Atmos Environ; 34(18), 2983-3013.

U.S. Environmental Protection Agency. (2002) Health Assessment Document for Diesel Engine Exhaust; U.S. EPA: Research Park Triangle, NC. Supplemental materials.

Vaaraslahti K, Keskinen J, Gieshaskiel B, Solla A, Murtonen T, Vesala H. (2005) Effect of lubricant on the formation of heavy duty diesel exhaust nanoparticles. Environ Sci Technol; 39: 8497-8504.

Vaaraslahti K, Virtanen A, Ristimaki J, Keskinen J. (2004) Nucleation mode formation in heavy-duty diesel exhaust with and without a particulate filter. Environ. Sci. Technol.; 38, 4884-4890.

Wei QF, Mather RR, Fotheringham AF, Yang RD. (2003) Evaluation of Nonwoven PP Oil Sorbents in Marine Oil-Spill Recovery. Marine Pollution Bulletin; 46, 6, 780-783.

APPENDIX I

Size-based penetration of R-95 and P-95 respirators when challenged with Diesel exhaust from Engine 1:

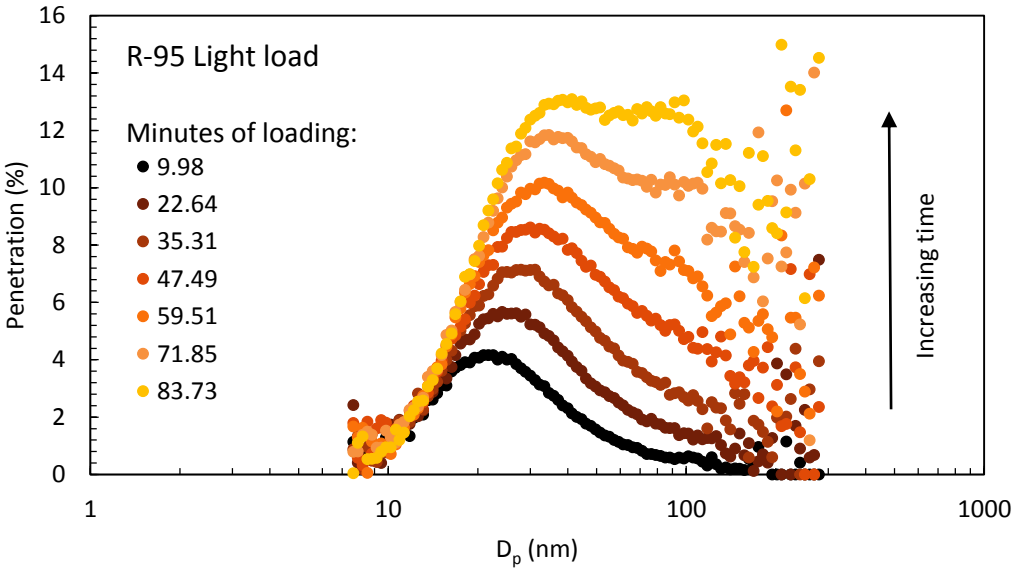

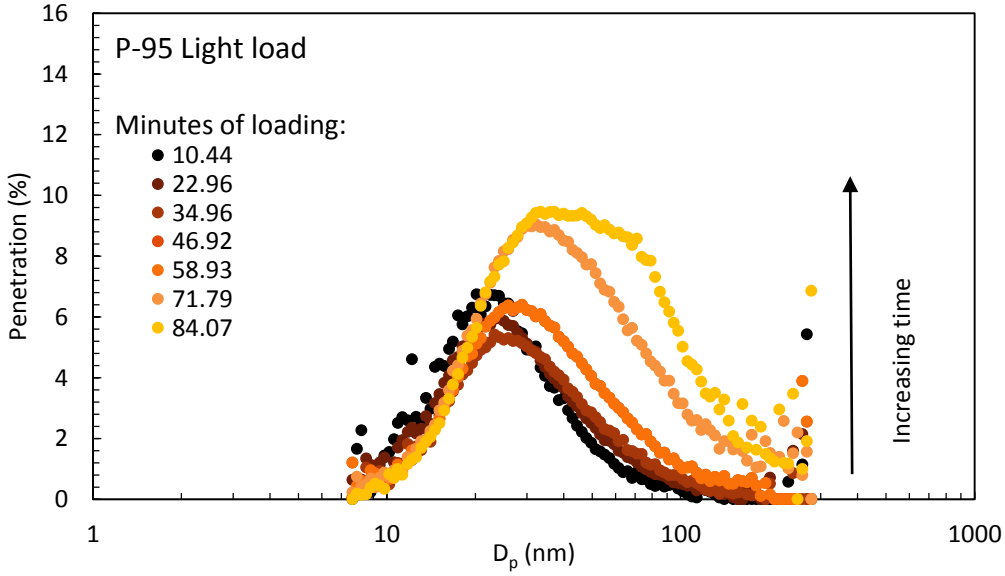

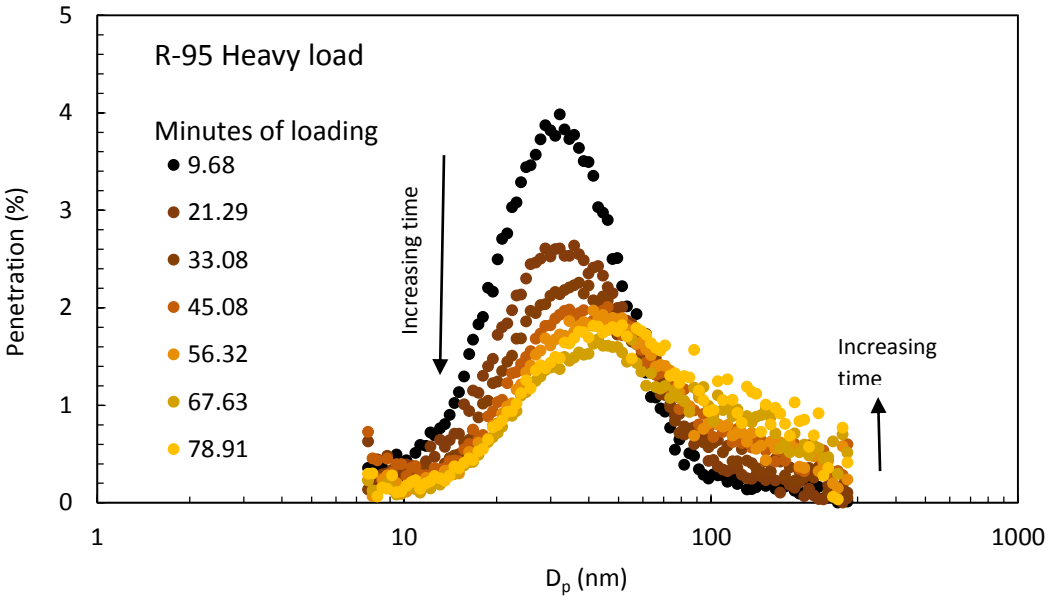
R-95 Heavy load
Minutes of loading
9.68
21.29
33.08
45.08
56.32
67.63
78.91
Increasing time
Increasing time
Penetration (%)
D_p (nm)
0
1
2
3
4
5
1
10
100
1000

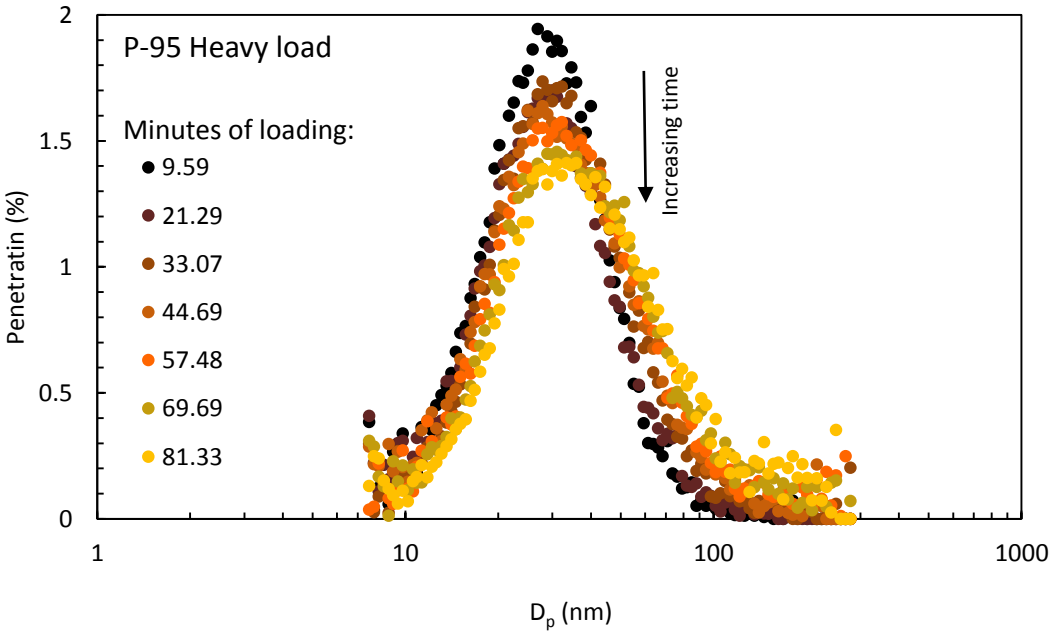
P-95 Heavy load
Minutes of loading:
9.59
21.29
33.07
44.69
57.48
69.69
81.33
Increasing time
Penetratin (%)
D_p (nm)
0
0.5
1
1.5
2
1
10
100
1000

APPENDIX II

Respirator test chamber:

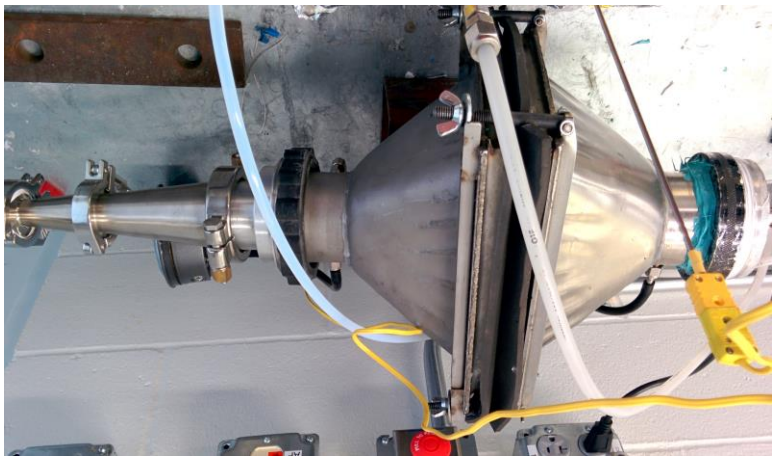

Glass plate with respirator:

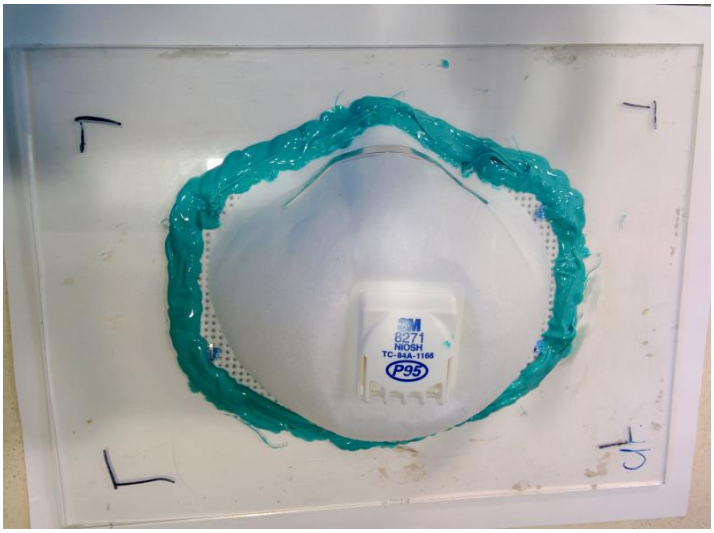

APPENDIX III

Images of the experimental setup for measurements with Engine 3 using the oxidation-dilution tunnel: